

Recent progress in organic solar cells (Part I material science)

Yahui Liu¹, Bowen Liu², Chang-Qi Ma², Fei Huang^{3*}, Guitao Feng⁶, Hongzheng Chen^{5*}, Jianhui Hou^{6*}, Lingpeng Yan², Qingya Wei⁷, Qun Luo², Qinye Bao⁸, Wei Ma⁹, Wei Liu⁷, Weiwei Li^{4*}, Xiangjian Wan^{10*}, Xiaotian Hu¹¹, Yanchun Han¹², Yaowen Li¹³, Yinhua Zhou¹⁴, Yingping Zou^{7*}, Yiwang Chen¹¹, Yongfang Li^{6,13*}, Yongsheng Chen^{10*}, Zheng Tang¹⁵, Zhicheng Hu³, Zhi-Guo Zhang^{16*} & Zhishan Bo^{1*}

¹College of Textiles & Clothing, State Key Laboratory of Bio-fibers and Eco-textiles, Qingdao University, Qingdao 266071, China;

²Suzhou Institute of Nano-Tech and Nano-Bionics, Chinese Academy of Sciences, Suzhou 215123, China;

³Institute of Polymer Optoelectronic Materials and Devices, State Key Laboratory of Luminescent Materials and Devices, South China University of Technology, Guangzhou 510640, China;

⁴Beijing Advanced Innovation Center for Soft Matter Science and Engineering & State Key Laboratory of Organic-Inorganic Composites, Beijing University of Chemical Technology, Beijing 100029, China;

⁵State Key Laboratory of Silicon Materials, MOE Key Laboratory of Macromolecular Synthesis and Functionalization, Department of Polymer Science and Engineering, Zhejiang University, Hangzhou 310027, China;

⁶Beijing National Laboratory for Molecular Sciences, Institute of Chemistry, Chinese Academy of Sciences, Beijing 100190, China;

⁷State Key Laboratory of Powder Metallurgy, College of Chemistry and Chemical Engineering, Central South University, Changsha 410083, China;

⁸School of Physics and Electronic Science, East China Normal University, Shanghai 200241, China;

⁹State Key Laboratory for Mechanical Behavior of Materials, Xi'an Jiaotong University, Xi'an 710049, China;

¹⁰State Key Laboratory and Institute of Elemento-Organic Chemistry, Key Laboratory of Functional Polymer Materials, College of Chemistry, Nankai University, Tianjin 300071, China;

¹¹College of Chemistry/Institute of Polymers and Energy Chemistry (IPEC), Nanchang University, Nanchang 330031, China;

¹²State Key Laboratory of Polymer Physics and Chemistry, Changchun Institute of Applied Chemistry, Chinese Academy of Sciences, Changchun 130022, China;

¹³Laboratory of Advanced Optoelectronic Materials, College of Chemistry, Chemical Engineering and Materials Science, Soochow University, Suzhou 215123, China;

¹⁴Wuhan National Laboratory for Optoelectronics, Huazhong University of Science and Technology, Wuhan 430074, China;

¹⁵Center for Advanced Low-Dimension Materials, State Key Laboratory for Modification of Chemical Fibers and Polymer Materials, College of Materials Science and Engineering, Donghua University, Shanghai 201620, China;

¹⁶State Key Laboratory of Chemical Resource Engineering, Beijing Advanced Innovation Center for Soft Matter Science and Engineering, Beijing University of Chemical Technology, Beijing 100029, China

Received December 8, 2021; accepted December 20, 2021; published online December 27, 2021

During past several years, the photovoltaic performances of organic solar cells (OSCs) have achieved rapid progress with power conversion efficiencies (PCEs) over 18%, demonstrating a great practical application prospect. The development of material science including conjugated polymer donors, oligomer-like organic molecule donors, fused and nonfused ring acceptors, polymer acceptors, single-component organic solar cells and water/alcohol soluble interface materials are the key research topics in OSC field. Herein, the recent progress of these aspects is systematically summarized. Meanwhile, the current problems and future development are also discussed.

*Corresponding authors (email: msfhuang@scut.edu.cn; hzchen@zju.edu.cn; hjhzl@iccas.ac.cn; liweiwei@iccas.ac.cn; xjwan@nankai.edu.cn; yingpingzou@csu.edu.cn; liyf@iccas.ac.cn; yschen99@nankai.edu.cn; zgzhang@mail.buct.edu.cn; zsbo@bnu.edu.cn)

organic solar cells, power conversion efficiency, photovoltaic materials, polymer solar cells

Citation: Liu Y, Liu B, Ma CQ, Huang F, Feng G, Chen H, Hou J, Yan L, Wei Q, Luo Q, Bao Q, Ma W, Liu W, Li W, Wan X, Hu X, Han Y, Li Y, Zhou Y, Zou Y, Chen Y, Li Y, Chen Y, Tang Z, Hu Z, Zhang ZG, Bo Z. Recent progress in organic solar cells (Part I material science). *Sci China Chem*, 2022, 65: 224–268, <https://doi.org/10.1007/s11426-021-1180-6>

1 Introduction

Solar cells that convert sunlight into electricity have obtained increasing interest from the academia and market in recent years, since they represent the most important way to use the renewable energy to meet the development of society and relieve the pressure of environmental pollution. In another aspect, flexible electronic devices have been recognized as the basic element in future daily life due to their light-weight, flexibility and portability. Therefore, organic solar cells (OSCs) that combine with the utilization of solar energy, electronics and flexibility have become a hot research field and attracted many researchers with the background of chemistry, physics, materials and even engineering. The multidisciplinary collaboration also enables OSCs to gain rapid development in recent years, providing the power conversion efficiency (PCE) over 18% and meanwhile realizing high thermal/light-stress stability and flexibility in large-area devices [1,2]. In this critical moment toward industry application for OSCs, we think that it is important to provide a universal review about the research history of OSCs so as to help this field enter a new stage.

Looking into the history of OSCs, although in 1960s there were a few reports about using single conjugated molecule as the photo-active layer in photovoltaic device, the small dielectric constant with strong binding energy between hole and electrons in the excitons prevents the photo-excited electrons to convert into free charges. This resulted in PCEs below 0.1% in OSCs at that time [3,4]. In 1977, it was found that the doping of polyacetylene with I₂ could switch the polymer from an insulator to an electron conductor [5]. In 1986, Tang C. W. for the first time reported a two-layer OSC with the p-type organic semiconductor (p-OS) copper phthalocyanine as the donor and the n-type organic semiconductor (n-OS) perylene diimide derivative as the acceptor with PCE of ~1% [6]. In 1992, Sariciftci *et al.* [7] found the fast photo-induced electron transfer from a conjugated polymer to fullerene, which brought about the innovation of bulk-heterojunction (BHJ) concept in 1995 [8]. Two soluble organic semiconductors, a p-OS poly(phenylene vinylene) derivative as a donor and an n-OS fullerene derivative as an acceptor, were physically mixed to form interpenetrated network. This pioneer work enabled OSCs to have the merits of (1) the soluble processing ability that can be easily converted into printing technique toward large-scale devices, and (2) the fast charge transfer from a donor to an acceptor to

tackle the strong binding energies and short diffusion length of excitons. Since then, the BHJ structure in OSCs was established, enabling OSCs to obtain fast development in the last two decades.

In general, a typical OSC contains a transparent conducting electrode (typically indium tin oxide (ITO)) and a metal top electrode, cathode and anode interlayers and photo-active layers with the donor/acceptor blend BHJ structure. The research of OSCs can be divided into the following section: (1) chemistry part, including the materials innovation of metal electrodes, interlayers and donor and acceptor materials of the photo-active layers that require the knowledge from inorganic to organic chemistry, the microstructure study by using many advanced analytical measurements, and the surface investigation; (2) physical part to understand the process of photo-conversion into free charges and resolve the mechanical properties of OSCs; (3) engineering part that is related to the fabrication process, such as doctor-blade coating, roll-to-roll printing technique, and sealing method. Beside these research fields, OSCs can also be related to the computer science (such as machine learning and simulation) [9,10] and biology (such as the assembly devices by using OSCs for supplying electricity, [11,12] and the application in greenhouse for planting [13]). In most cases, all these sections will entangle with each other, and hence, it also requires researchers to fully consider many aspects in order to realize the industry application of OSCs.

This review provides an overview about OSCs. We will start from introducing OSCs, including the device configuration, the working mechanism and the parameters. Besides, a relatively long section was organized to summarize the progress of organic semiconductors, including donor, acceptor and single-component materials. Subsequently, the research progress about device physics will be reviewed, especially focusing on the energy loss and small driving force for exciton separation. Then, the application of OSCs will be summarized, from indoor application to greenhouse, semitransparent windows and biological sensors. For better matching with various readers, this review is divided into two parts (material science and device engineering). This part is related to material science, including conjugated polymer donors, oligomer-like organic molecule donors, fused ring electron acceptors, nonfused ring electron acceptors, all-polymer solar cells, single-component organic solar cells and water/alcohol-soluble interface materials. We hope that this comprehensive review will inspire more deep

researches in this field and also promote the application of OSCs in our daily life.

2 Conjugated polymer donors for organic solar cells

MEH-PPV is the first polymer donor material with an optical bandgap of 2.1 eV in BHJ OSCs, which produced a power conversion efficiency (PCE) of 0.9% by blending with CN-PPV acceptor under the light of 20 mW/cm² [14]. However, the MEH-PPV:CN-PPV film exhibited a narrow photo-response region below ~600 nm, leading to a low solar photon utilization efficiency in a given device. To enhance solar photon utilization, a classic polymer donor of P3HT with an optical bandgap of 1.9 eV was employed and a PCE of 2.8% was achieved combining with PC₆₁BM as acceptor [15]. Subsequently, the PCE of this device was improved to 4.4% by morphological control using thermal annealing treatment [16]. When an electron acceptor (ICBA) with the up-shifting lowest unoccupied molecular orbital (LUMO) level was used, the PCE of the P3HT-based device was further increased to 7.4% due to the improvement of open-circuit voltage (V_{OC}) [17]. However, the PCEs of P3HT:fullerene analogue-based devices are still limited due to the poor light harvesting capability. Since the low bandgap nonfullerene acceptors (NFAs) were developed, P3HT obtained a new lease of life for pursuing high-performance OSCs due to the achievement of the broad absorption region and matched molecular energy levels in the blend film by NFA design. Up to now, P3HT-based device has achieved a PCE of 9.5% [18].

For the molecular design of the polymer donors used in the fullerene derivative-based OSCs, a key point is reducing bandgap of the polymers, because the fullerene derivative acceptors such as (6,6)-phenyl-C₆₁-butyric acid methyl ester (PCBM) are wide bandgap n-OS. To reduce the bandgap of the polymer donor, an alternating conjugated donor-acceptor (D-A) copolymer was designed by using a strong electron-donating fluorene as a D-unit and a strong electron-accepting benzothiadiazole (benzo[c][1,2,5]thiadiazole, BTZ) as an A-unit. Lower bandgap D-A copolymers were successfully applied in the PCBM-based BHJ OSCs [19]. For the polymer donors used in the nonfullerene OSCs with narrow bandgap small molecule acceptors, wide or medium bandgap is pursued and the wide bandgap D-A copolymers can also be realized by using weak electron-accepting A-unit [20]. Owing to their outstanding advantages in chemical and structural variety, molecular energy level and bandgap control, the D-A conjugated polymers have become the dominant donor materials in OSCs.

Up to now, a large number of D-A conjugated polymers were designed and synthesized, which made a highly im-

portant contribution to boost the PCEs of OSCs. Currently, there are many excellent reviews that summarize the polymer donor design, and the relationship between chemical structure of polymer donor and photovoltaic efficiency [21–34]. In this section, we first highlighted the methods in tuning molecular bandgap. Secondly, we summarized some fashionable electron-accepting unit-based polymer donors for achieving high-performance OSCs. Lastly, we discussed the challenges in designing polymer donors for high-performance OSCs.

2.1 Strategies for polymer bandgap control

For an ideal polymer donor, the primary principle of molecular design is to construct complementary absorption spectra against a given electron acceptor for maximizing solar photons utilization, so as to maintain a high upper limit of short-circuit current density (J_{SC}) in a photovoltaic device. Previous prediction indicates that a PCE over 20% within the onset absorption of 860±60 nm could be reached in a single-junction OSC [35]. On the other hand, some special applications in OSCs have strict requirements for the optical bandgap of the active layer. For example, a high-performance tandem OSC requires that the front cell and rear cell have the optical bandgaps of ~1.70 and 1.20 eV, respectively [36]; an OSC for indoor application highly requires an active layer that has an onset absorption wavelength below 700 nm [37]; the ideal semitransparent OSC requires an active layer that has high visible transmission values up to 50% (370–740 nm), while selectively harvesting light with the wavelength shorter than 435 nm and longer than 670 nm [38]. Overall, the bandgap control for polymer donors is highly important to meet applications of OSCs on different occasions.

There are two main contributions to tuning the bandgap of polymer donor: hybridization of frontier orbitals and delocalization of electrons along the conjugated backbone. First, the hybridization of frontier orbitals is frequently used to modulate the energy gap as shown in Figure 1. Once D and A units are combined by chemical bonding, their highest occupied molecular orbitals (HOMOs) and LUMOs will start to interact with each other. Then a new set of HOMO and LUMO levels with a smaller bandgap in D-A compound is formed due to the redistribution of electrons. The LUMO and HOMO levels of a D-A polymer are determined by the HOMO of the D moiety and the LUMO of the A moiety, respectively. They are directly related to the V_{OC} and charge-separation. That is why the control of energy levels of polymers is of crucial importance in improving photovoltaic efficiencies in OSCs. The rules of thumb in polymer donor design have been established based on this method. For example, the HOMO and LUMO levels of the polymer donor are downshifted simultaneously while keeping the same

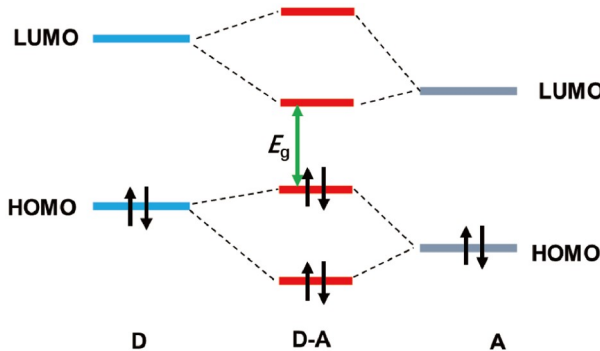


Figure 1 Orbital hybridization of the D and A units in a D-A conjugated polymer (color online).

optical bandgap; the HOMO level of the polymer donor is downshifted while maintaining the LUMO levels higher than that of the acceptor materials [39]. Second, delocalization of electrons along the conjugated backbone is an important tool in developing low bandgap polymers. Delocalization of the electrons along the conjugated backbone allows chemical bonds to convert between double bonds and single bonds, leading to the resonance structures between aromatic form and quinoid form [24]. The decrease of bandgap is proportional to the increase of quinoid structure in conjugated materials due to the destruction of its aromaticity and reduction of its stabilization energy. To better understand the influence of resonance structures of conjugated polymers on their bandgaps, herein, we only presented some homo-coupling polymers to exclude the disturbance of hybrid frontier orbitals between D and A units as shown in Figure 2. Poly(para-phenylene) (PPP) has a large bandgap of ~3.0 eV due to the weak quinoid character [40]. After condensed pyrazine in the perpendicular direction, the quinoid character of the benzene ring was enhanced in polyquinoxaline (PQX), thus yielding a lower bandgap of ~2.5 eV [41]. When the π conjugation of benzene was extended in the parallel direction, like isoindigo unit, the quinoid character of the benzene ring was further stabilized in polyisoindigo (PIID), and the

corresponding bandgap was reduced to ~1.7 eV [42]. Thiophene is a very important unit to construct high-performance polymer donors in OSCs, the polythiophene (PT) has a bandgap of ~2.0 eV [43]. One benzene and two thiophenes were fused to form the benzo[1,2-b:4,5-b']dithiophene (BDT) unit. Its homocoupling polymer (PBDT) or still-coupling with thiophene units exhibits bandgap of ~2.1 eV [44,45]. When the imide group was grafted onto thiophene or bithiophene to produce thieno[3,4-c]pyrrole-4,6(5H)-dione (TPD) and bithiophene imide (BTI) monomers, the electron-withdrawing ability of both units was significantly enhanced compared with thiophene unit. However, the imide group has a weak ability to stabilize the quinoid structure of thiophene in PTPD and s-BTI2-FT. That is why both polymers exhibit a similar bandgap to PT [46,47]. When the thiophene has fused another thiophene to form the thieno[3,4-b]thiophene (TT) unit, the top thiophene has a strong aromatic form to stabilize the quinoid structure of down thiophene in PTT. Thus this polymer exhibits a very low bandgap of ~1.2 eV [48]. As the top thiophene was changed into the stronger aromatic rings of benzene and pyrazine, the corresponding polymers of poly(isothianaphthene) (PITN) and poly(2,3-dihexylthieno[3,4-b]pyrazine) (PDHTP) gave the lower bandgaps of ~1.0 and 0.95 eV, respectively [49,50]. It should be noted that abovementioned two behaviors interact with each other in tuning the bandgap of polymer donors.

2.2 Key electron-accepting unit-based polymer donors

Up to now, a large number of conjugated polymer donors have been constructed by the combination of D and A units. Among these polymers, some building blocks have presented significant advantages in constructing high-performance polymer donors. Such as BDT [51], benzo[d][1,2,3]triazole (BTA) [20], BTZ [52], quinoxaline (QX) [53], TPD [54], TT [55], benzo[1,2-c:4,5-c']dithiophene-4,8-dione (BDD) [56]. Herein, we summarize the progress of some famous building block-based polymer donors according to the electron-

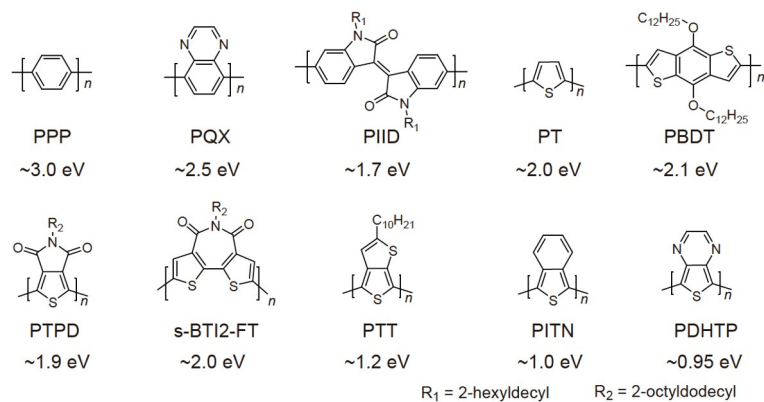


Figure 2 The conjugated homopolymers.

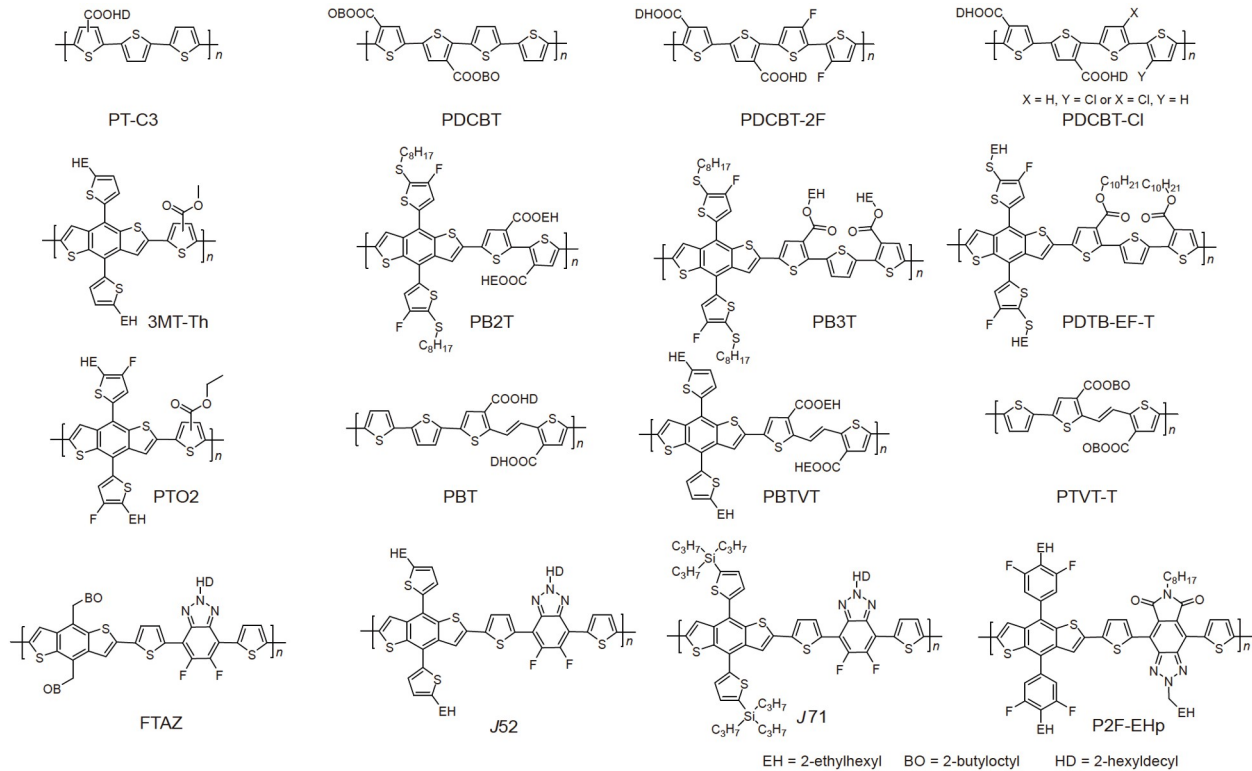


Figure 3 The TC- and BTA-containing polymer donors.

accepting units for application in OSCs. The chemical structures of the polymer donors are presented in Figure 3, and corresponding photovoltaic data are recorded in Tables 1–3.

Thiophene-3-carboxylate (TC) has a deeper HOMO level and stronger intermolecular interaction compared with 3-alkylated thiophene due to the existence of the ester group [57,58]. To overcome the low V_{OC} in P3HT-based photovoltaic cells, researchers tried to introduce TC units to build polymer donors with deeper HOMO levels. In 2011, Li *et al.* [59] reported a polymer PT-C3 with one TC unit and two thiophene units. PT-C3 showed a much deeper HOMO level of -5.10 eV than P3HT (~ 4.8 eV). Compared with P3HT-based OSCs, the PT-C3-based device exhibited a higher V_{OC} , but a lower fill factor (FF). The low FF could be attributed to the inferior charge carrier mobility due to the irregular conjugated backbone of PT-C3. Hou *et al.* [60] developed a regular TC-based polymer PDCBT, which exhibited a deeper HOMO level of -5.26 eV due to the increased proportion of TC in the polymer main chain. The PDCBT exhibited a smaller π stacking distance, which is beneficial for charge transport. The network morphological character in the PDCBT:PC₇₁BM film made this device achieve a PCE of 7.2% by improving V_{OC} and FF, simultaneously. When the low bandgap NFA of 3,9-bis(2-methylene-(3-(1,1-dicyano-methylene)-indanone))-5,5,11,11-tetrakis(4-hexylphenyl)-dithieno[2,3-d:2',3'-d']-s-indaceno[1,2-b:5,6-b']dithiophene

(ITIC) was used to fabricate OSCs, the PDCBT-based device showed a PCE of 10.16%, which was major attributed to the remarkably improved J_{SC} due to the broadening of photo-response region of blend film [61]. The PDCBT was further optimized by extending the side chain from 2-butyloctyl to 2-hexyldocyl, and introducing the Cl atoms into the conjugated backbone. After careful selection of electron acceptor, the PCE of this polymer reached 12.38% [62,63]. In 2017, Choi *et al.* [64] employed the BDT-TC-based polymer 3MT-Th to fabricate OSCs with ITIC using toluene as solvent. The devices gave a PCE of 9.73% with an excellent long-term performance stability. Since 2017, Hou *et al.* [65–67] also reported a series of TC-based polymer donors. They designed two polymer donors, PB2T and PB3T, which exhibited much different aggregation behaviors. The PB2T-based device only gave a PCE of 0.01% due to the highly twisted conjugated backbone. In contrast, the relatively planar polymer PB3T-based device produced a much higher PCE of 11.9% [65]. The aggregation ability and HOMO level of PB3T were optimized to produce a polymer PDTB-EF-T by introducing F atoms and employing the side chain strategy. The PDTB-EF-T-based device showed a more balanced hole/electron transport, yielding a higher PCE of 14.2% [66]. Additionally, they also reported a polymer PTO2 with the short synthetic route. This polymer gave an outstanding PCE of 14.7% by combining with the electron acceptor of IT-4F [67]. In 2018, Geng *et al.* [68] reported a

polymer PBT with TC and vinylene linker in the conjugated backbone, which exhibited a PCE of 6.25% by blending with PC₆₁BM. Bo *et al.* [69] used the BDT unit to replace the bithiophene group to prepare a new polymer PBTVT. This polymer possessed good solubility in halogen-free solvents and a deep HOMO level of -5.35 eV. The OSCs were fabricated with PBTVT as a donor and ITOIC-2F as an acceptor by *o*-xylene processing to produce a PCE of 11.04%. Recently, Hou *et al.* [70] reported a more easily prepared polymer PTVT-T with low cost using one thiophene to replace bithiophene in PBT. PTVT-T exhibited strong aggregation behavior, which makes it form nanoscale aggregations and face-on orientation. After blending with the electron acceptor of BTP-eC9, this polymer-based device showed the highest PCE of 16.2% among TC-based OSCs.

BTA is a weak electron-withdrawing unit for constructing wide or medium bandgap polymer donors [71,72]. You *et al.* [73] designed and synthesized two BTA-based polymer donors with or without fluorine atoms. Compared with fluorine atom-free BTA-based polymer donor, the fluorinated BTA (FBTA)-based polymer donor (FTAZ) exhibited similar optical and aggregation properties, but the deeper HOMO level and twenty times higher hole mobility. In PC₆₁BM-based OSCs, FTAZ showed an improved V_{OC} , J_{SC} , and FF, simultaneously, thus yielding a higher PCE (7.1%) than BTA-based counterpart (4.3%). Li *et al.* [74] employed FBTA-based polymer donor (J52) to fabricate NF OSCs by combining with low bandgap acceptor of ITIC and obtained a

PCE of 5.51%. Subsequently, the same group used trialkylsilylthiophene to replace alkylthiophene as a conjugated side chain to make a 2D-conjugated polymer donor (J71). This polymer possessed a deep HOMO level of -5.40 eV, and formed a favorable BHJ morphology to reduce charge recombination in the J71:ITIC-based device. This device gave a much higher PCE of 11.41% with the enhancement of V_{OC} , J_{SC} and FF compared with the J52-based device [75]. Lately, Zhan *et al.* [76] used the FTAZ to match a low bandgap acceptor of IDIC to fabricate OSCs. This device achieved a PCE up to 12.5% with an outstanding J_{SC} of 20.8 mA/cm² at that time. To develop deeper HOMO level BTA units, Huang *et al.* [77] designed and synthesized a novel acceptor unit of cyclic-imide substituted BTA, 4,8-di(thien-2-yl)-6-octyl-2-octyl-5H-pyrrolo[3,4-f]benzotriazole-5,7(6H)-dione (TZBI). The polymer based on TZBI and BDT unit showed a deep HOMO level of -5.34 eV. It was further optimized by tuning conjugated side chains and flexible alkyl chains to obtain a better polymer of P2F-EHp, which firstly achieved over 16% efficiency for single-junction OSCs [78]. The photovoltaic parameters of the TC- and BTA-containing polymer-based devices are summarized in Table 1.

Benzo[c][2,1,3]thiadiazole (BT) is a strong electron-accepting unit that has been used to construct medium or low bandgap polymer donors for OSCs. As shown in Figure 4, the BT-based polymer donors have been extensively studied due to their broad solar photon absorption, high mobility and

Table 1 The photovoltaic parameters of the TC- and BTA-containing polymer-based devices

Donor	Acceptor	V_{OC} (V)	J_{SC} (mA/cm ²)	FF	PCE (%)	Ref.
P3HT	PC ₆₁ BM	0.61	10.6	0.67	4.37	[16]
PT-C3	PC ₇₁ BM	0.78	9.68	0.51	3.87	[59]
PDCBT	PC ₇₁ BM	0.91	11.0	0.72	7.2	[60]
PDCBT	ITIC	0.94	16.50	0.66	10.16	[61]
PDCBT-2F	IT-4F	0.92	18.2	0.71	11.9	[63]
PDCBT-Cl	ITIC-Th1	0.94	18.50	0.71	12.38	[62]
3MT-Th	ITIC	0.95	17.01	0.60	9.73	[64]
PB2T	IT-M	0.56	0.08	0.26	0.01	[65]
PB3T	IT-M	1.0	18.9	0.63	11.9	[65]
PDTB-EF-T	IT-4F	0.90	20.60	0.70	13.0	[66]
PDTB-EF-T	IT-4F	0.90	20.73	0.76	14.2	[66]
PTO2	IT-4F	0.91	21.5	0.75	14.7	[67]
PBT	PC ₆₁ BM	0.83	11.21	0.67	6.25	[68]
PBTVT	ITPIC-2F	0.91	20.41	0.60	11.04	[69]
PTVT-T	BTP-eC9	0.79	26.22	0.78	16.20	[70]
FTAZ	PC ₆₁ BM	0.79	11.83	0.73	6.81	[73]
J52	ITIC	0.73	13.11	0.58	5.51	[74]
J71	ITIC	0.94	17.32	0.70	11.41	[75]
FTAZ	IDIC	0.84	20.8	0.72	12.5	[76]
P2F-EHp	Y6	0.81	26.68	0.74	16.02	[78]

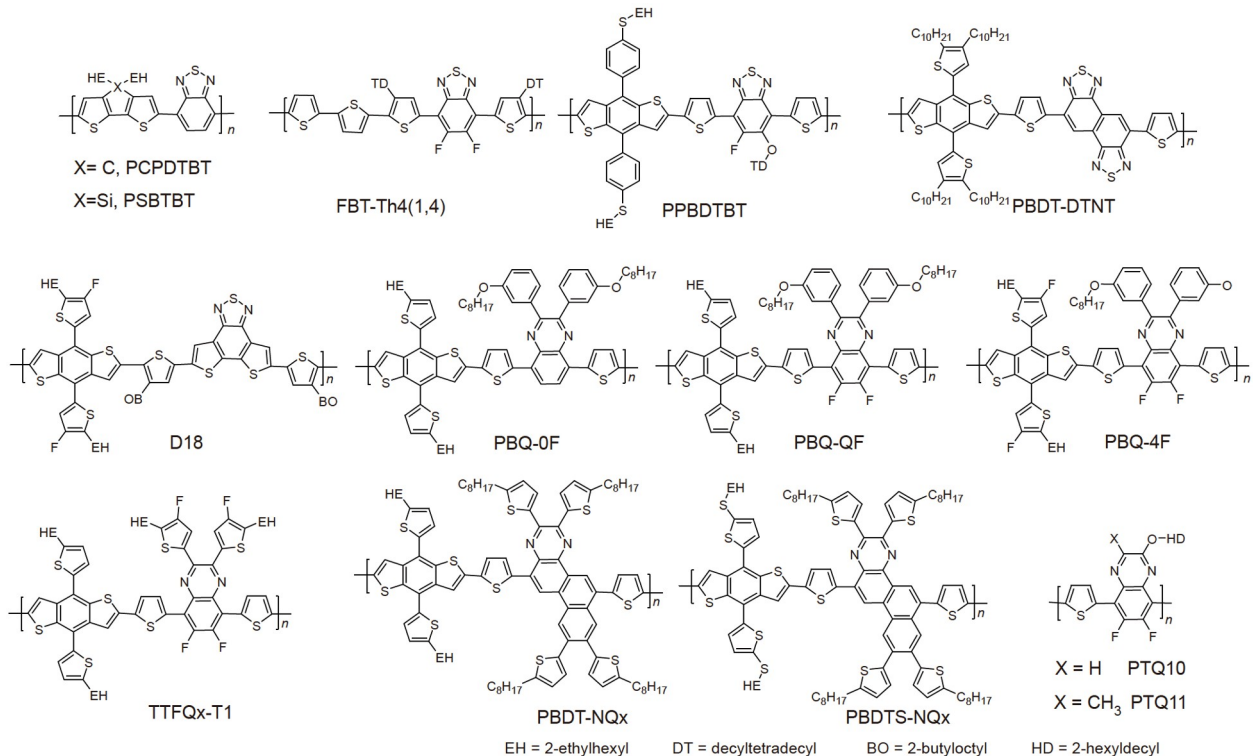


Figure 4 The BT- and Qx-containing polymer donors.

outstanding photovoltaic efficiency. In 2006, Brabec *et al.* [79] synthesized a polymer (PCPDTTB) with a bandgap of 1.40 eV by polymerizing between cyclopenta[2,1-b;3,4-b']dithiophene (CPDT) and the BT units. This polymer-based device showed a PCE of 3.2%. After the BHJ morphology was treated with 1,8-diiodooctane as the processing additive, the efficiency of this device was improved to 5.1% [80]. Replacement of the CPDT unit in PCPDTBT by a dithieno[3,2-b:2',3'-d]silole (DTS) to produce PSBTBT, the longer C-Si bond in PSBTBT could release some strain from the planar five-membered rings and thereby enhance polymer stacking. Therefore, the hole mobility of this polymer was three times higher than that of PCPDTBT. As a result, the PSBTBT-based device yielded a PCE of 5.1% without using solvent additives [81]. To downshift the HOMO level and enhance the interaction of BTZ-based polymer donor, Chen *et al.* [82] reported a fluorinated BT-based polymer (FBT-Th4(1,4)), which exhibited temperature-dependent aggregation property and deep HOMO level of -5.36 eV. This polymer gave a field-effect hole mobility up to $1.92 \text{ cm}^2/(\text{V s})$. In the PC₇₁BM-based device showed a PCE of 7.64% with a 230 nm thick active layer. The side chains of FBT-Th4(1,4) were optimized from 2-decyldodecyl to 2-nonyltridecyl, at the same time, the BHJ morphology was controlled using 1,2,4-trimethylbenzene and 1-phenylnaphthalene. A PCE of 11.7% was achieved [83]. Bo *et al.* [84] developed a 5-alkyloxy-6-fluorobenzothiadiazole-

based polymer (PPBDTBT) with a bandgap of 1.76 eV. Interestingly, the space charge limited current method measured that PPBDTBT:PC₇₁BM blend film exhibited a very high hole mobility of $0.06 \text{ cm}^2/(\text{V s})$ due to the formation of bi-continuous interpenetrating networks morphology even with an active layer thickness up to 500 nm. As a result, this polymer-based device showed a PCE of 7.7% with an active layer thickness of 250 nm. The ITIC was used to fabricate ternary OSCs with PPBDTBT:PC₇₁BM, and an over 10% efficiency was achieved [85]. Naphtho[1,2-c:5,6-c']bis[1,2,5]thiadiazole (NT) is a stronger acceptor and larger conjugation compared with BT, which was composed of doubly BT-fused heterocycle [86]. Huang *et al.* [87] used this acceptor to prepare PBDT-DTNT. Compared with the BT-based polymer, NT-based polymer had a lower bandgap and higher hole mobility. Thus, the NT-based polymer yielded a higher PCE of 6.0% than BT-based polymer (2.1%) by blending with PC₇₁BM. In 2012, Reynolds *et al.* [88] reported a method to produce a DTBT unit by fusing two thiophenes into the benzene ring of BTZ. Based on this unit, Ding *et al.* [1] designed a wide bandgap polymer with BDT and thiophene bridge. This polymer showed an outstanding PCE of 18.22% by blending with an electron acceptor of Y6.

Quinoxaline (Qx) is another popular A unit in developing high-performance polymer donors for OSCs. As shown in Figure 4, many state-of-the-art Qx-based polymer donors have been synthesized and applied in OSCs. Hou *et al.* [89]

designed and synthesized three polymer donors, PBQ-0F, PBQ-QF, and PBQ-4F, with different number of fluorine atoms on the conjugated skeleton. The HOMO levels of these polymers gradually downshifted with the increase of the number of fluorine atoms. PBQ-4F exhibited the deepest HOMO level of -5.05 eV compared with the other two polymers. Benefiting from the improvement of V_{OC} , PBQ-4F showed a PCE up to 8.55% by blending with PC₇₁BM. Afterwards, the same group used these three polymers to mix ITIC to fabricate photovoltaic devices. They found that although the PBQ-4F and ITIC had a small offset of ΔE_{HOMO} of 0.04 eV and ΔE_{LUMO} of 0.24 eV, the device of PBQ-4F:ITIC still produced a high PCE of 11.34% due to the efficient charge separation and low bimolecular recombination [90]. It is quite different with fullerene derivative-based OSCs, which need driving force (ΔE_{HOMO} and ΔE_{LUMO}) over 0.3 eV between donors and acceptors. The smaller driving force indicates that NF-based OSCs have a great potential for achieving higher photovoltaic efficiencies than fullerene-based OSCs. Zou *et al.* [91] also reported a Qx-based polymer donor (TTFQx-T1) with four fluorine atoms onto the Qx segment. TTFQx-T1 achieved a PCE of 13.1% by fabricating the device with Y5. To reduce the HOMO levels of Qx-based polymers, Peng *et al.* [92] used both fused-ring strategy and side chain engineering to prepare two NQx-based polymers, PBDT-NQx and PBDTS-NQx, which possessed deeper HOMO levels than Qx-based polymers even with the introduction of fluorine atoms. Thus, PBDTS-NQx:ITIC-based device gave a PCE of 11.47% with a high V_{OC} of 0.92 V. A low-cost polymer donor (PTQ10) was developed, which has a simple chemical structure with fluorinated Qx and thiophene unit. PTQ10 exhibited a deep HOMO level and complementary absorption spectrum with IDIC. The

favorable BHJ morphology with strong π stacking and the face-on arrangement were formed in the PTQ10:IDIC film. Thus, this device showed a PCE of 12.7% [93]. The PTQ10 was further optimized to prepare PTQ11 by introducing methyl group onto Qx for up-shifting HOMO level. Meanwhile, PTQ11 exhibited higher hole mobility and stronger crystallization than PTQ10. As a result, PTQ11:TPT10-based device achieved a PCE of up to 16.32%. The photovoltaic parameters of BT- and Qx-containing polymer-based devices are summarized in Table 2.

TPD is a promising candidate unit for constructing high-performance n-type polymers for electronics due to the advantages in its planarity, high electron affinity and strong π - π stacking, as shown in Figure 5. In 2010, Leclerc *et al.* [96] reported a polymer (PBDTTPD), which has a large bandgap of 1.81 eV and a deep HOMO level of -5.56 eV. After the combination with PC₇₁BM, the PBDTTPD-based device showed a PCE of 5.5% with a V_{OC} of 0.85 eV, a J_{SC} of 9.81 mA/cm², and an FF of 0.66. However, this blend film has a narrow photoresponse region from 300 to 700 nm, which limited their J_{SC} s. When a strong quinoid character of TT unit as the bridge was introduced into BDT and TPD units to make a new polymer donor (PBDT_{EH}-TBTT_{HD-i}), which has a bandgap of 1.56 eV, but an up-shifting HOMO level of -4.78 eV (measured by ultraviolet photoelectron spectroscopy). After blending with PC₇₁BM, although the PBDT_{EH}-TBTT_{HD-i}-based device showed a low V_{OC} of 0.63 eV, a remarkably high J_{SC} of 18.15 mA/cm² was obtained, thus yielding a PCE of 7.5% [97]. Hwang, *et al.* [98] developed a TPD-based polymer donor (PT-ttTPD) without BDT unit. This polymer possessed a bandgap of 1.75 eV, and a deep HOMO level of -5.65 eV. As a result, PT-ttTPD:PC₇₁BM-based device showed a much better PCE of 9.21%, with a

Table 2 The photovoltaic parameters of BT- and Qx-containing polymer-based devices

Donor	Acceptor	V_{OC} (V)	J_{SC} (mA/cm ²)	FF	PCE (%)	Ref.
PCPDTBT	PC ₇₁ BM	0.65	11.0	0.44	3.2	[79]
PCPDTBT	PC ₇₁ BM	0.61	15.73	0.53	5.1	[80]
PSBTBT	PC ₇₁ BM	0.68	12.7	0.55	5.1	[81]
FBT-Th4(1,4)	PC ₇₁ BM	0.76	16.2	0.62	7.64	[82]
PPBDTBT	PC ₇₁ BM	0.79	14.33	0.69	7.7	[84]
PBDT-DTNT	PC ₇₁ BM	0.80	11.71	0.61	6.00	[87]
D18	Y6	0.86	27.7	0.77	18.22	[1]
PBQ-0F	ITIC	0.69	16.16	0.60	6.68	[94]
PBQ-QF	ITIC	0.90	17.16	0.62	8.90	[94]
PBQ-4F	ITIC	0.91	17.87	0.67	11.34	[94]
TTFQx-T1	Y5	0.89	21.2	0.70	13.1	[91]
PBDT-NQx	ITIC	0.87	16.21	0.65	9.11	[92]
PBDTS-NQx	ITIC	0.92	17.86	0.70	11.47	[92]
PTQ10	IDIC	0.97	19.65	0.74	12.7	[93]
PTQ11	TPT10	0.81	24.79	0.75	16.32	[95]

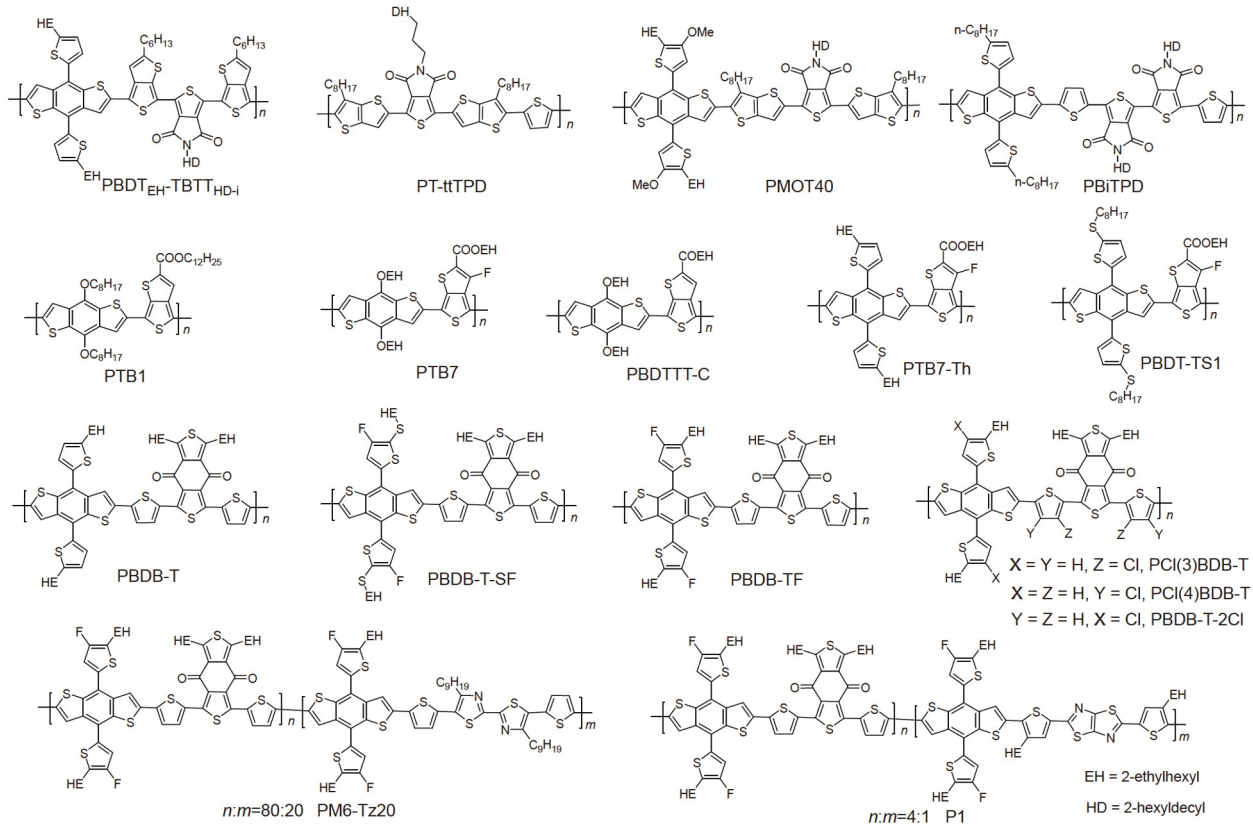


Figure 5 The TPD-, TT- and BDD-containing polymer donors.

V_{OC} of 0.86 eV, a J_{SC} of 15.30 mA/cm², and an FF of 0.70. Wu *et al.* [99] used a polymer donor PMOT40 and i-IEICO-4F to make an active layer, which forms complementary absorption spectra. This blend film exhibited a very low nonradiative recombination loss, but still achieved efficient charge separation and fast transport. As a result, this device yielded a PCE of 13%, with a J_{SC} over 20 mA/cm². Recently, Huang *et al.* [100] designed a bithieno[3,4-c]pyrrole-4,6-dione unit by bonding two TPD units and made a polymer PBiTPD. Compared with one TPD-based polymer donor, this polymer showed a lower bandgap of 1.75 eV, a deeper HOMO level of -5.20 eV. Using Y6 as an electron acceptor, the PBiTPD-based device showed an excellent PCE of 14.2% with a J_{SC} of 25.6 mA/cm², which was much higher than that of one TPD-based device (5.9%).

TT is a stable quinoid structure heterocycle, which was widely used to construct low bandgap polymers. The firstly alkylated TT was reported and constructed low bandgap semiconducting polymer in 1997 [48]. Until 2008, Yu *et al.* [55] prepared a PTB1 polymer with a bandgap of 1.6 eV, which exhibited a complementary absorption spectrum with PC₆₁BM. The PTB1:PC₆₁BM-based device showed a high J_{SC} of 12.5 mA/cm² at that time, but a quite low V_{OC} of 0.58 eV due to the high HOMO level of PTB1. Afterwards, this group developed a series of polymer donors based on PBT1 to downshift polymer HOMO levels and optimize BHJ

morphologies by introducing fluorine atom and tuning the side chains [101]. Finally, one of the polymer, PTB7, was developed to achieve a PCE of up to 7.4% [102]. Yang *et al.* [103] used carbonyl to replace the ester group onto the TT unit, which also achieved a lower polymer HOMO level. Thus the PBDTTT-C-based device gave a PCE of 6.58% with a higher V_{OC} than the PTB1-based device. Chen *et al.* [104] used BDT with conjugated thiophene as a side chain to make famous PTB7-Th with TT unit. Simultaneously, the inverted device was fabricated using fullerene derivative-doped zinc oxide nanofilm as the cathode. This device gave the best PCE of 9.35% at that time. In 2015, Hou *et al.* [105] employed side chain engineering to prepare PBDT-TS1 and carefully optimize BHJ morphology. Finally, over 10% efficiency of OSCs was certified by the National Institute of Metrology, China, which is the highest value for OSCs at that time. Currently, TT-based low bandgap polymer donors have been widely used in tandem solar cells as the rear-cell material and semitransparent organic solar cells [36,106]. The photovoltaic parameters of the TPD-, TT- and BDD-containing polymer-based devices are summarized in Table 3.

BDD is an exciting A unit in developing high-performance polymer donors. The first BDD-based polymer donor (PBDB-T) was synthesized by Hou *et al.* [115] in 2012. This polymer showed a strong temperature-dependent aggrega-

Table 3 The photovoltaic parameters of the TPD-, TT- and BDD-containing polymer-based devices

Donor	Acceptor	V_{OC} (V)	J_{SC} (mA/cm ²)	FF	PCE (%)	Ref.
PBDT _{EH} -TBTT _{HD-i}	PC ₇₁ BM	0.63	18.15	0.65	7.50	[97]
PT-ttTPD	PC ₇₁ BM	0.86	15.30	0.70	9.21	[98]
PMOT40	i-IEICO-4F	0.97	20.6	0.65	13.0%	[99]
PBiTPD	Y6	0.83	25.6	0.67	14.2	[100]
PTB1	PC ₆₁ BM	0.58	12.5	0.65	4.76	[55]
PTB7	PC ₆₁ BM	0.74	14.5	0.69	7.40	[102]
PBDTTT-C	PC ₇₁ BM	0.7	14.7	0.64	6.58	[103]
PTB7-Th	PC ₇₁ BM	0.80	15.73	0.74	9.35	[104]
PBDT-TS1	PC ₇₁ BM	0.84	17.62	0.69	10.2	[105]
PBDB-T	ITIC	0.90	16.81	0.74	11.21	[107]
PBDB-T-SF	IT-4F	0.88	20.88	0.71	13.1	[108]
PBDB-TF	IT-4F	0.87	20.38	0.77	13.7	[109]
PBDB-TF	BTP-eC9	0.84	26.2	0.81	17.8	[110]
PCI(3)BDB-T	IT-4F	0.88	0.88	0.24	0.2	[111]
PCI(4)BDB-T	IT-4F	0.84	20.60	0.71	12.3	[111]
PBDB-T-2Cl	IT-4F	0.86	20.80	0.77	14.4	[112]
PM6	Y6	0.85	25.6	0.72	15.7	[113]
PM6-Tz20	Y6	0.86	27.3	0.75	17.6	[113]
P1	Y6	0.87	25.9	0.78	17.6	[114]

tion property and good interpenetrating network morphology in neat film. In 2016, PBDB-T was combined with ITIC to form an active layer with matched energy levels and complementary absorption, which enhanced solar photon harvesting and reduced the energy loss at the same time, this active layer also formed a favorable nanoscale phase-separation morphology, thus producing an outstanding PCE of 11.21%. This is the first example to achieve over 10% efficiency for nonfullerene OSCs [107]. To improve J_{SC} at the same time, and maintain V_{OC} in the resulting device, Hou *et al.* [108] used fluorination strategy to develop a fluorinated polymer donor (PBDB-T-SF) and acceptor (IT-4F), simultaneously. Compared with the PBDB-T:ITIC blend, the PBDB-TSF:IT-4F blend showed similar energy offset between the HOMO of PBDB-T-SF and the LUMO of IT-4F, but a significant redshift of the absorption spectrum occurred. As a result, the PBDB-T-SF:IT-4F-based device showed a higher efficiency of 13.1% with an improved J_{SC} of 20.5 mA/cm² and similar V_{OC} of 0.88 V. The fluorinated PBDB-T (PBDB-TF, also namely PM6) exhibited a better phase-separation morphology with IT-4F to achieve higher charge mobilities than that of PBDB-T-SF. Thus, PBDB-TF-based device had a higher PCE of 13.7% due to the increase of FF [109]. Recently, a PBDB-TF-based device achieved a PCE of over 17% by employing the electron acceptor BTP-eC9 [110], and over 18% by using two acceptors and another donor of PBDB-T-2Cl [112]. Currently, PBDB-T and PBDB-TF have been widely used as donor materials to fabricate OSCs with new electron acceptors. The chlorine atom is also

an electron withdrawing atom. Compared with fluorinated polymers, chlorinated polymers have shorter synthetic route and deeper HOMO levels due to the empty d-orbitals for π -electron delocalization. However, the large van der Waals radius of the chlorine atom could also influence the molecular planarity and charge mobility. Hou *et al.* [111,112] reported three chlorinated polymers based on PBDB-T. When the thiophene-bearing Cl atom faces the BDD unit, the polymer (PCI(3)BDB-T) did not show charge mobility due to the strong twisted conjugated backbone, and thus this polymer gave an extremely low PCE of 0.2% with the acceptor of IT-4F. For PCI(4)BDB-T, the planarity of the conjugated backbone was significantly improved, and the blend film of PCI(4)BDB-T:IT-4F produced balanced hole/electron mobilities of 10^{-6} cm²/(V s). Thus, the corresponding device gave a PCE up to 12.3%. Furthermore, the chlorine atoms were introduced into the conjugated side chains, which did not impact the molecular planarity, so that this polymer-based blend showed charge mobilities up to the order of 10^{-4} cm²/(V s), and achieved an outstanding PCE of 14.4%. To further improve the PCE of OSCs by optimizing BHJ morphology, the PBDB-TF has been a key parent skeleton to make ternary copolymers. Recently, there have been two successful examples by using a 20% content of 5,5'-dithienyl-2,2'-bithiazole or thiophene-thiazolothiazole into PBDB-TF [113,114]. Compared with PBDB-TF:Y6-based device, both new polymers (PM-Tz20 and P1)-based devices showed increased V_{OC} , J_{SC} , and FF, simultaneously, thus giving higher PCE of 17.6%.

2.3 The challenge in designing polymer donors for high-performance OSCs

Conjugated polymer donors have been proven to be a type of BHJ materials in pursuing highly efficient single-junction OSCs. Meanwhile, they also exhibited great potential applications in tandem, ternary, semitransparent and indoor solar cells. However, they are still many challenges in further boosting device efficiency. (1) Most high-performance polymer donors have low hole mobilities (10^{-3} – 10^{-4} cm 2 /(V s) measured by the SCLC method), which is not beneficial for fabricating OSCs with thick active layer. The devices with an active layer thickness of ~250 nm would be an important way to achieve over 20% efficiency by improving J_{SC} in single-junction OSCs. (2) The BHJ morphology is highly dependent on interactions in the active layer, but the basic mechanism of the interactions between the polymer donor and NFA is still unclear. For example, some build blocks such as 2,5-dihydropyrrolo[3,4-c]pyrrole-1,4-dione (DPP) [117], isoindigo-based polymer donors [118] exhibited high hole mobilities. However, their photovoltaic efficiencies are quite poor with NFAs. Therefore, understanding the molecular interactions between the donor and acceptor is essential for the further guidance of polymer donor design. Once the challenges as above-mentioned were addressed, it will greatly promote the development of OSCs.

3 Oligomer-like organic molecule donors

Conjugated polymers have been in the dominant place as donor materials since the invention of BHJ device structure because their solution processing properties demonstrate the great potentials of OSC manufactured through large area printing. In contrast, in the early stage of OSC, nearly all the small molecule based OSCs were fabricated using the vacuum evaporation techniques, which demonstrated a higher cost than solution processable method. That is because common small molecule donors are hard to form good phase-separated mixture with PCBM owing to their rigid structures and generally bad film forming properties by solution process, and thus lead to low PCEs. However, with the further development of OSC, the disadvantages of polymers such as the batch to batch variation of synthesis and thus performance reproducibility and difficulty for purification cannot be omitted like before. Thus, more attentions have drawn on solution processed small molecules. Indeed, small molecules demonstrate many intrinsic advantages, *i.e.*, (1) no batch to batch variations for OSC device performance due to the defined molecular structure; (2) easily tuned absorptions and energy levels *via* delicate chemical structure design. With this, in recent years, many extensive studies have been conducted and rapid progress has been made on small mo-

lecle, especially oligomer-like molecules including donors and acceptors. In the past decade, there already have been some excellent and comprehensive reviews on this topic in OSCs [119–122]. Therefore, in this section, we focus on summarizing the most impactful progress of solution processed oligomer-like molecule donors, which are roughly categorized according to the representative building blocks in the molecule backbone. A short outlook will also be given for the future development of oligomer-like molecule donors.

3.1 Oligothiophene based donors

In the early years, Rocanli [123] reported a series of star or other branched oligothiophenes molecules for solution processed OSCs. However, PCEs below 2% were obtained owing to the limited absorption in visible and near-infrared region and unfavorable film forming properties of those molecules. Prompted by oligothiophene molecules for vacuum deposition devices [124], Chen *et al.* [125,126] reported a series of oligothiophene based molecule donors with acceptor-donor-acceptor (A-D-A) structures for solution processed OSCs (Figure 6). They have summarized the A-D-A molecule design rationale as follows. Firstly, the good film forming ability can be realized through introducing the alkyl side chains and oligomer like backbones. Secondly, the light absorptions and energy levels can be efficiently tuned by the end groups and central units since the LUMOs and HOMOs of those molecules are mainly determined by the end groups and central units, respectively. Lastly, efficient packing modes and high mobilities are expected owing to the planar molecular backbones and conformations. Through molecule engineering design from terminal electron withdrawing unit selection and conjugation length modification, together with device optimization, these A-D-A oligothiophene based small molecules achieved PCEs from the original value of 2.45% to record over 10%. It has demonstrated that the end groups play a great role in the absorptions, energy levels, mobilities, active layer morphologies for these A-D-A molecules. Molecule **DCAO7T** with alkyl cyanoacetate as end groups instead of dicyanovinyl had better solubility and film forming quality than **DCN7T** [127,128]. So, compared with **DCN7T** with a PCE of 2.45%, an impressive PCE of 5.08% was achieved for **DCAO7T** based devices. Later on, in order to get broader and stronger solar absorption and thus higher J_{SC} , Chen *et al.* [129] introduced a series of dye building blocks into the septithiophene backbone and synthesized a series of A-D-A donor molecules with oligothiophene backbone. Among them, the rhodanine based molecule **DRHD7T** showed a PCE of 6.10% with a high J_{SC} . With 2-(1,1-dicyanomethylene)rhodanine as end groups, molecule **DRCN7T** based device gave a record PCE of 9.30% with a V_{OC} of 0.91 V, a

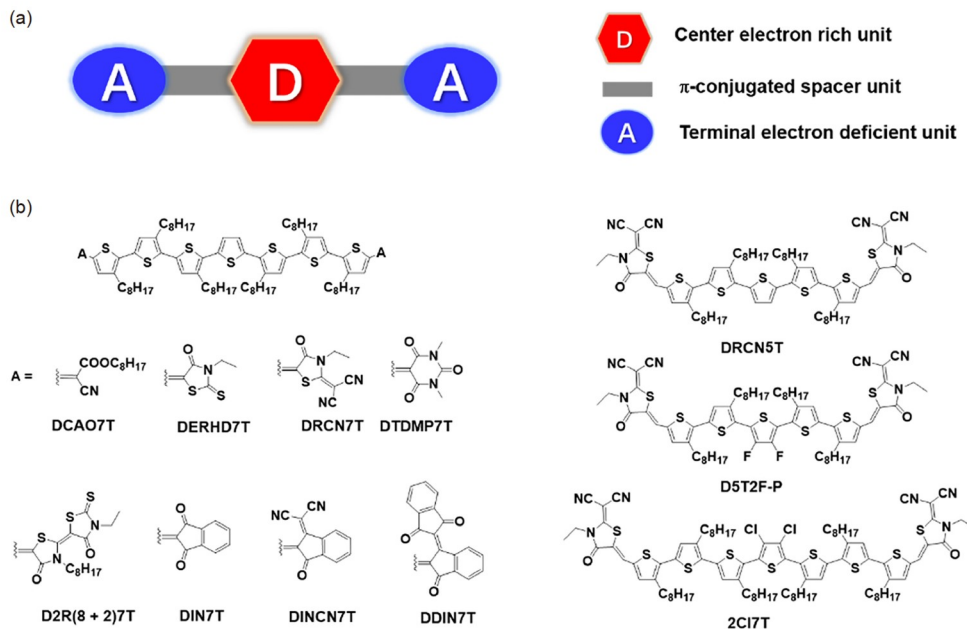


Figure 6 (a) Schematic diagram of general A-D-A molecules. (b) Chemical structures of some typical oligothiophene based molecule donors (color online).

J_{SC} of 14.87 mA/cm² and an FF of 0.687, which was mainly ascribed to the optimized morphology with an interpenetrating network consisting of ~10 nm diameter highly crystalline fibrils in their blending film [130]. The results indicate that solution processed small molecule OSCs can indeed attain comparable device performance with polymers through careful molecule chemical structure design. Molecules with other end groups such as indanedione and its derivatives also showed reduced bandgaps and wide absorption range owing to the strong electron withdrawing abilities of their end groups. However, relatively low PCEs were obtained owing to the unfavorable morphologies with large aggregation caused by the large and planar end groups. With strong intermolecular interaction, molecule **DINCN7T** using the 1,1-dicyano methylene-3-indanone (INCN), the famous end groups widely used in the later A-D-A acceptors, has poor solubility in common solvents and could not form decent films for device evaluation. Besides the 7T backbone molecules, Chen *et al.* [131] also synthesized quinqueithiophene derivatives with different end groups. Among them, a breakthrough PCE with value over 10% was achieved for **DRCN5T:PC₇₁BM** based devices. Meanwhile, molecules with the same end group and different thiophene numbers from 4 to 9 were synthesized and investigated comprehensively. An odd-even effect in J_{SC} and thus PCE was observed for **DRCN4T-9T**, which might be attributed to their different spatial symmetry and thus different dipole moment and packing modes.

Recently, promising device performances have also been achieved for oligothiophene donor based devices with NFAs. Using F-2Cl as an acceptor and **DRCN5T** as a donor, Chen

et al. [132] reported an all oligomer-like small molecule device with PCEs of 9.78%. Later on, Lu *et al.* [133,134] reported all oligomer-like small molecule OSCs by designing a series of oligothiophene based donors. Among them, D5T2F-P and 2Cl7T showed high PCEs of 9.36% and 11.45% using IDIC-4F and Y6 as acceptors, respectively, demonstrating the great potential of these oligothiophene based donors.

3.2 BDT-based donors

In 2011, BDT was firstly introduced by Chen *et al.* [135] as the central building block to synthesize oligomer-like donor **DCAO3T(BDT)3T** based on the above A-D-A molecule design strategy, as shown in Figure 7. Compared with its oligothiophene analogue **DCAO7T**, **DCAO3T(BDT)3T** showed higher hole mobility owing to its expanded coplanar chemical structure after introducing BDT unit. Thus, a PCE of 5.44% with a V_{OC} of 0.93 V, a J_{SC} of 9.77 mA/cm² and a notable FF of 0.599 was achieved. Before that, it had been regarded that low FF was a long term bottleneck for solution processed small molecule OSC. The work demonstrated that high FF could indeed be realized for solution processed small molecule OSC just by molecule design. From then on, lots of oligomer-like small molecules containing BDT unit have been designed and synthesized, most of which have utilized the above A-D-A strategy from the perspective of molecular engineering of BDT unit, end groups and linkers between the central BDT and end groups [136].

Following the work of **DCAO3T(BDT)3T**, Chen *et al.* [137] reporting a series of oligomer-like molecule donors by

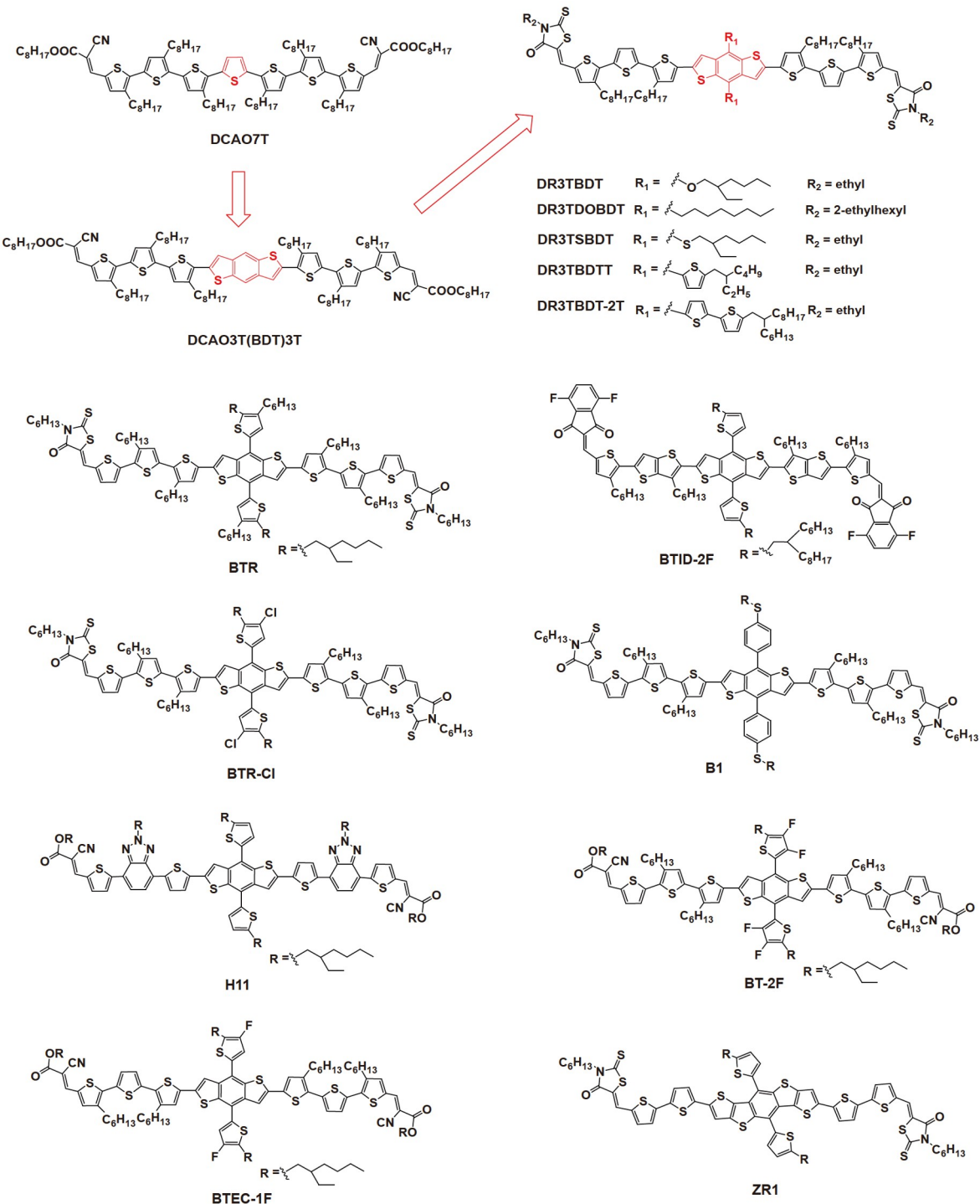


Figure 7 Chemical structures of some typical BDT based oligomer-like molecule donors (color online).

carefully modifying the BDT unit. Meanwhile, alkyl rhodanine was used as the end group to extend the absorption and an easier synthesized building block diethylterthiophene was introduced as linkers between the central BDT unit and terminal rhodanine group. Compared with their analogues with alkyl cyanoacetate as end group, these molecules showed red shifted absorption over 20 nm, and thus higher J_{SC} was expected. Importantly, their solid packing and active

layer morphologies can be modified by careful molecular design together with the device optimizations. With PDMS as an additive, **DR3TBDT:PC₇₁BM** based devices gave a high PCE of 7.38% with a V_{OC} of 0.93 V, a J_{SC} of 12.21 mA/cm² and an FF of 0.65. The results indicated that high performance solution processed oligomer-like OSCs could be realized by combination of delicate molecule design and device optimization. In the following work, molecule

DR3TSBDT with alkylthio-substituted BDT as the central building block was designed. It was demonstrated that alkylthio-substituted aromatic molecules could form better ordered packing in solid state. Using a two-step (thermal and solvent annealing, TSA) approach, device based on molecule **DR3TSBDT:PC₇₁BM** achieved a record PCE of 9.95% with a V_{OC} of 0.92 V, a J_{SC} of 14.61 mA/cm² and an FF of 74% [131]. Molecule **DR3TDOBBDT** with lower electron-donating octyl chain on BDT unit was also designed and demonstrated a PCE of 8.26% [138]. Meanwhile, in order to increase the intermolecular interaction, a series of molecules such as **DR3TBDDT** have been designed by introducing 2-dimensional BDT as the central unit, which showed slightly red shifted absorption and similar energy levels and band-gaps compared with that of molecule **DR3TBBDT**. Among them, **DR3TBDDT** showed a PCE of 8.12% [139]. Furthermore, a high PCE of 9.58% was achieved for **DR3TBDDT:PC₇₁BM** based device with solvent vapor treatment [140]. The above results opened an avenue for design of high efficiency BDT based oligomer-like molecule donors. After that, many other excellent oligomer-like molecule donors incorporating BDT units have been designed. In 2015, Jones *et al.* [141] reported the molecule **BTR**, which has the same backbone as **DR3TBDDT** except the position and length of alkyl chains on the BDT, linker and end groups. **BTR** exhibited the nematic liquid crystalline behavior and thus high hole mobility, demonstrating the importance of side chain on the molecule properties. A PCE of 9.3% was achieved for BTR based device with PC₇₁BM as acceptor. In 2016, Wei *et al.* [142] reported the molecule **BTID-2F**, which contained p-bridges with gradient-decreased electron density and end groups substituted with fluorine atoms. Devices based on **BTID-2F:PC₇₁BM** exhibited a high PCE of 11.08%, which was mainly attributed to the optimal active layer morphology with the fluorinated end groups.

With the excellent properties in PCBM based device, BDT based oligomer-like molecule donors have drawn great attention in nonfullerene acceptor (NFA) based device in recent years. Some representative BDT based molecule donors have been used to fabricate devices directly with NFAs. Furthermore, new BDT based oligomer-like small molecule donors have also been designed to pair with NFAs and much progress has been made in recent years. Some typical examples are discussed as below.

In 2016, Chen *et al.* [143] reported an all oligomer-like molecule device using **DR3TSBDT** as donor and **DTBTF** as acceptor, which showed a low PCE of 3.84% but a high V_{OC} of 1.15V, demonstrating a great potential for all small molecule OSCs. Beaujuge *et al.* [144] reported a ternary device using **DR3TBDDT** as donor, ICC6 and PC₇₁BM as acceptor. A PCE of 10.08% with active layer thickness >200 nm was achieved, which is attributed to the improved electron mobility, long carrier lifetimes and the reduced geminate re-

combination. Using **DR3TSBDT** as a donor, Y6 and PC₇₁BM as acceptors, Zhang *et al.* [145] reported a ternary device with a PCE of 10.53%, in which **DR3TSBDT** molecular aggregations could be tuned by incorporating PC₇₁BM to form 3D texture structure. Zhu *et al.* [146] constructed a high efficiency device using **BTR** as donor and NITI as acceptor. Compared with the binary device of **BTR:NITI** with PCE 6.82%, the ternary device of **BTR:NITI:PCBM** demonstrated a PCE of 13.63% with an improved J_{SC} of 19.50 mA/cm² and an FF of 73.8%, and retained a high V_{OC} of 0.94 V. The significantly improved device performance was attributed to forming a hierarchical morphology consisting of a PCBM transporting highway and an intricate nonfullerene phase-separated pathway network. Thus, an optimized balance could be realized for carrier generation and transport.

With the above promising results, new small molecule donors have been designed to pair with NFAs in order to get higher device performance. To create a well-matched donor-acceptor pair with low band gap nonfullerene acceptor, Hou *et al.* [147] reported a wide band gap donor molecule **DRTB-T**, which incorporates a two-dimensional trialkylthienyl-substituted benzodithiophene core building block. The device based on **DRTB-T:IC-C6IDT-IC** showed a PCE of 9.08% with a high V_{OC} of 0.98 V. By replacing the hexyl with Cl atom in the thienyl side-chain of **BTR**, Lu *et al.* [148] designed the molecule **BTR-Cl**. The device based on **BTR-Cl:Y6** showed a PCE of 13.61%. Furthermore, the ternary device using PC₇₁BM as the third component achieved a high efficiency of 15.34% (certified 14.7%) [149], which is attributed to the miscibility-induced active layer morphology optimization after introduction of PC₇₁BM. Later on, molecule **B1** incorporating phenyl-substituted benzodithiophene (BDT) central unit was designed by He and Hou *et al.* [150]. **B1** showed increased π - π stacking and enhanced crystalline property compared with BTR. The **B1:BO-4Cl**-based devices achieved an outstanding PCE of 15.3% (certified 15.1%). The results demonstrated that the active layer morphology optimization could be achieved through careful design of A-D-A type donor material.

Meanwhile, owing to the weak electron withdraw ability and good solubility compared with rhodanine, alkyl cyanoacetate has been used as end groups to design wide or medium band gap donor molecules to pair with low band gap acceptors. Molecule **H11**, **BT-2F**, **BTEC-1F** and **BTEC-2F** are the representative examples and have achieved promising PCEs 10%–14% through molecular engineering of the central BDT unit and alkyl chains on the bridge trithiophene building blocks. Wei *et al.* [151] reported a BDT analog, dithieno[2,3-d:2',3'-d']benzo[1,2-b:4,5-b']dithiophene (**DTBBDT**) based donor **ZR1**. With the extended conjugation length of **DTBBDT**, the single-crystal structure of **ZR1** showed the high planarity and compact molecular packing

with a short π - π stacking. The **ZR1:Y6** device reached a high PCE of 14.34% with a low E_{loss} of 0.52 eV. It is noting that there existed the hierarchical phase separation with the donor or acceptor rich domains with size up to ca. 70 nm, and the donor crystals of tens of nanometer.

3.3 Porphyrins based donors

With the large absorption coefficients and broad spectral response range, porphyrin derivatives have been widely used in the organic optoelectronic community. In the past decades, lots of porphyrin based donors have been reported, most of which have the A-D-A architecture with porphyrin unit as the central building block. In recent years, Peng and co-workers [152] have reported a series of porphyrin based donors with an A-D-A structure (Figure 8), in which two ethynylene bridges linked the porphyrin core to the two diketopyrrolopyrrole units. With the large planar and conjugation molecular backbone and the efficient intramolecular charge transfer (ICT) between porphyrin and DPP units, these molecules showed broad absorptions in the range from the ultraviolet (UV) to near-infrared (NIR) region with low band gap below 1.4 eV. Blending with PCBM as acceptor, DPPEZnP-TEH-based device showed a PCE of 8.08% with a high J_{SC} of 16.76 mA/cm² [152]. In their following work, two analogue molecules with different alkyl chains attached to the thiophene unit of the porphyrin core, DPPEZnP-TBO and DPPEZnP-THD were designed and the correlation of active layer morphology with device performances was thoroughly investigated [153]. Using pyridine and 1,8-diiodooctane (DIO) as the additives, impressive PCEs of 9.06% and 8.24% were achieved for DPPEZnP-TBO:PC₆₁BM and DPPEZnP-THD:PC₆₁BM based devices, respectively. The high device performances were attributed to forming a multi-length-scale morphology consisting of donor material crystalline domains and acceptor aggregate domains owing to the synergistic effect of two additives of pyridine and DIO. To pursue higher efficiency, ternary device using DPPEZnP-TEH and PTB7-Th as donors and PC₇₁BM as acceptor was fabricated and a high PCE of 11% was achieved with a high J_{SC} of 17.99 mA/cm² and an FF of 77.19% [154].

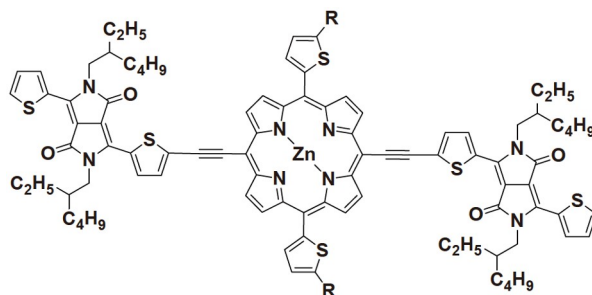


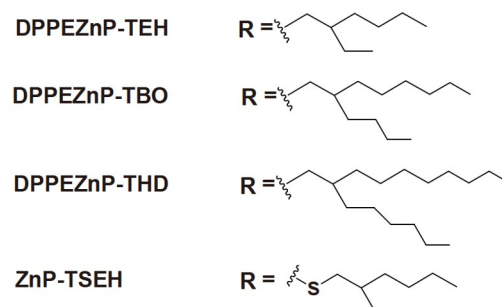
Figure 8 Chemical structures of some typical porphyrin based small molecule donors.

With the NIR absorptions for many porphyrin based donors, they are good candidates as rear cell materials for constructing tandem OSCs. Meanwhile, BDT based oligomer-like molecule donors generally show absorptions in the short wavelength region. With these, Chen and Peng *et al.* [155] reported a tandem device using DR3TSBDT as the front cell donor and DPPEZnP-TBO as the rear cell donor. A record PCE of 12.7% was achieved after device optimization, which is attributed to the complementary absorptions and highly balanced currents of the two subcells.

Recently, exciting device performance has been obtained for porphyrin donor based NFA devices. Using ZnP-TBO as a donor and 6TIC as an acceptor, the device delivered a remarkable efficiency of 12.08% with a J_{SC} over 20 mA/cm² and an FF near 74% [156]. With another acceptor 4TIC as the third component, a ternary device was fabricated with an impressive PCE of 14.73%, in which the crystallinity of the binary blend was improved with addition of 4TIC. Following this improvement, with an alkylthio substituted analogue ZnP-TSEH as a donor, an exciting and record result for all small molecule OSCs with a PCE of 15.88% was achieved, indicating the great potential of porphyrin based small molecule devices.

3.4 DTS based donors

Dithienosilole (DTS) is also a well-known building block widely used in OSC materials design. Bazan and co-workers [157] have reported a series of oligomer-like molecule donors with DTS as the core for solution processed OSC and comprehensively investigated photovoltaic properties of those molecules. Molecule **p-DTS(PTTh₂)₂** was their first DTS based oligomer-like molecule donor reported in 2012, as shown in Figure 9 [158]. The devices based on **p-DTS(PTTh₂)₂:PC₇₁BM** with 0.25% DIO additive yielded an impressive PCE of 6.7%. The 0.25% DIO additive could profoundly modify the active layer morphology with domain size reduced from 20–30 nm to 15–20 nm. Following this work, three isomeric molecules were reported to examine the correlations of the chemical structures to the packing modes and photovoltaic performances [159]. Active layer



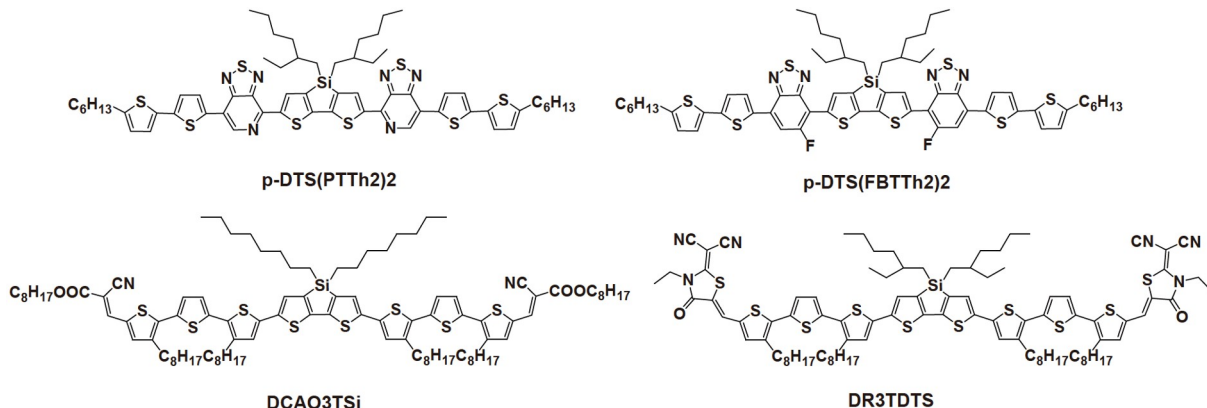


Figure 9 Chemical structures of some typical DTS based small molecule donors.

morphology study demonstrated that the difference of the packing modes and thus device performances were attributed to the influence of the acceptor component on the net dipole moment of the molecule. Considering that the lone pairs of electrons on the **p-DTS(PTTh₂)₂** might be prone to participate in acid/base reactions and lead to V_{OC} loss in devices with PSS:PEDOT, molecule **p-DTS(FBTTh₂)₂** using 5-fluorobenzo[c][1,2,5]thiadiazole (FBT) as the acceptor unit was designed [160]. Device with a structure of ITO/PEDOT:PSS/**p-DTS(FBTTh₂)₂**:PC_{7.1}BM/Ca/Al fabricated with DIO additive and thermal annealing, yielded a PCE of 7.0% with a V_{OC} of 0.809 V, a J_{SC} of 12.8 mA/cm² and an FF of 0.68. When barium (Ba) replaced by calcium (Ca) as the cathode interlayer between the aluminum and active layers, an improved FF of 0.75 and a high PCE of 9.02% were achieved [161].

Meanwhile, oligomer-like molecule donors with the A-D-A architecture containing DTS have been designed and demonstrated promising photovoltaic performances. In 2011, Chen *et al.* [162] reported molecule **DCAO3TSi** with DTS unit as the central building block and alkyl cyanoacetate as end groups. Device using **DCAO3TSi** and PC_{6.1}BM blend film yielded a PCE of 5.84%. Later on, **DR3TDTS** with rhodanine as end group was designed and gave a PCE of 8.02% with PC_{7.1}BM as acceptor after device optimization with the thermal and solvent annealing.

Compared with BDT based oligomer-like molecule donors, only a few studies on NFA devices have been conducted using DTS-containing donors. The two devices using **p-DTS(FBTTh₂)₂** as a donor and a perylene diimide and NIDCS-MO as acceptor only demonstrated PCEs of 3% and 5.44%, respectively [125,163]. Much effort is needed to be devoted to NFA devices using DTS-incorporating oligomer-like molecule donors.

3.5 Outlook in oligomer-like molecule donors

To date, lots of oligomer-like molecule donors with various

chemical structures have been designed and demonstrated promising device performance. The efficiencies of all oligomer-like molecule OSCs have achieved PCEs around 16%. In view of the advantages of oligomer-like small molecules including donors and acceptors, it is strongly believed that higher device performance can be obtained for oligomer-like molecule donor based devices through careful molecule design and device optimization. To this end, we think that some suggestions and opinions as below might be helpful for the future development of oligomer-like molecule donors and corresponding devices.

Firstly, synergistic design of oligomer-like molecule donors with NFAs. Currently, oligomer-like molecule donor based NFA OSCs, especially all oligomer-like molecule devices with A-D-A type donor and acceptor, have made much progress with PCEs near 16%. Wide bandgap oligomer-like molecule donors and low bandgap NFAs have proved to be the effective combinations for pursuing high efficiency OSCs. And oligomer-like molecule donors with deep HOMO are preferred to obtain high V_{OC} . With the comprehensive study in the past decade, the molecular level properties of oligomer-like molecule donors and acceptors such as absorption and HOMO/LUMO levels are relatively well understood. But, the miscibility and interaction between the donor and acceptor materials still need to be well investigated, which are directly correlated with the active layer morphology and significantly impact the device performance.

Secondly, understanding the correlation between molecular structure and morphology. The control of active layer morphology is one of the most important issues for OSCs. Unlike polymers, oligomer-like molecule donors can hardly form pre-aggregation state in the solution, which bring the difficulty to produce nanoscale phase separation with acceptors, especially with oligomer-like molecule acceptors. Generally, even a little change in the chemical structure on oligomer-like molecule materials can give a large difference in the morphology and device performance. It is important

and urgent to investigate the intrinsic determining factors that impact the packing modes and phase separation behavior in the active layer. The understanding of the correlation between molecular structure and morphology can provide valuable hints for the design of new molecules to realize better phase separation. In fact, oligomer-like molecule materials, especially A-D-A type molecules including donors and acceptors have the advantage to conduct this investigation owing to their defined chemical structures and superior properties.

4 Fused ring electron acceptors

Electron acceptors are key component for the active layer of organic solar cells. From the view of the development of electron acceptor materials, the fused-ring electron acceptor (FREA) materials, which mainly include fused aromatic diimide derivatives (*e.g.*, perylene diimides (PDIs) and naphthalene diimides (NDIs)), fullerene acceptors, A-D-A type fused-ring electron acceptors and A-DA'D-A type fused-ring electron acceptors, have played a great role in promoting the progress of the OSCs. In the early time of OSCs, fullerene derivatives and fused aromatic diimide acceptors were widely used as the electron acceptors. However, these two kinds of acceptors have inevitable drawbacks. Fullerene acceptors possess weak absorption in the visible and near-infrared region, unstable morphology, and difficulties in molecular modification and purification [164]; fused aromatic diimide acceptors have relatively narrow absorption range and difficulty in adjusting the energy levels [165]. Therefore, these two kinds of acceptors limit the PCE to a moderate level no more than 13%. Since the invention of A-D-A type fused-ring electron acceptors in 2015 by Zhan *et al.* [166] and A-DA'D-A type fused-ring electron acceptors in 2017 by Zou *et al.* [167], the PCE of OSCs has been rapidly boosted to ~19%. In this part, we will focus on A-D-A type and A-DA'D-A type fused-ring electron acceptors and figure out the relationship between molecular structure and device performance.

4.1 A-D-A type fused-ring electron acceptors

In 2015, the emergence of the FREA ITIC, as shown in Figure 10, with a typical A-D-A structure shed new light on OSCs [166]. As the most promising acceptors at that time, ITIC and its derivatives have the distinctive and important molecular structure, which leads to a great superiority in photoelectric and photovoltaic performance [167–170]. The important features from the chemical structure point of view are: (1) ITIC and its derivatives consist of two electron-deficient end groups (A) and one electron-rich central core (D, fused backbone). A strong push-pull electronic effect

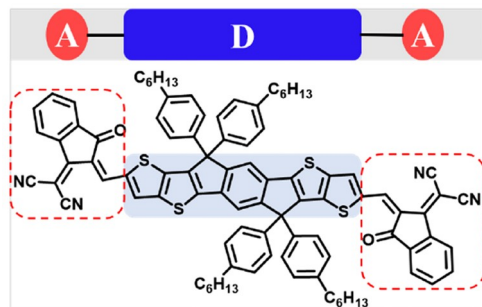


Figure 10 The structure of the representative A-D-A type acceptor ITIC (color online).

resulting from these A and D units was generated, and the photoelectric properties such as absorption and energy levels could be easily regulated. Besides, the rigid and planar backbone as well as strong inter/intramolecular interactions was beneficial to the charge transfer. (2) The attached side chains could modulate the molecular solubility and the miscibility with the donors to form a favorable blend with a desired nanometer-scale interpenetrated network. (3) The A-D-A molecules possessed several reaction positions where some functional atoms and groups could be introduced to finely tune the molecular structure and thus the molecular properties. Here, we will summarize the development of A-D-A type acceptors centered on the star ITIC and focus on the modification of fused-ring core, end groups and side chains.

4.1.1 Fused-ring core engineering

The fused-ring core (D) of ITIC is comprised of a central benzene and two flanking thieno[3,2-b]thiophene (TT') that are bridged by two cyclopentadiene units [166]. Modification on the electron-rich fused-ring core mainly includes replacing the benzene and thiophene units, expanding the conjugated backbone length, isomerization, asymmetry and introducing heteroatoms, as shown in Figure 11. Zhan *et al.* [171] reported a typical benzene-centered FREA IDTIC with pentacyclic indaceno[1,2-b:5,6-b']dithiophene (IDT) as the backbone. When blended with polymer donor PDBT-T1, PDBT-T1:IDTIC based device could achieve a PCE of 7.39% with a high V_{OC} of 0.9 V. Then, IHIC1 with replacing the central benzene in IDTIC with naphthalene showed more co-planar backbone, larger π -conjugation, and thus higher electron mobility (3.0×10^{-4} and $1.5 \times 10^{-4} \text{ cm}^2/(\text{V s})$ for IHIC1 and IDTIC, respectively). Due to the higher LUMO energy level of IHIC1, the device with FTAZ donor could achieve a higher V_{OC} . Combined with the simultaneously improved J_{SC} and FF, the FTAZ:IHIC1 based OSC realized a higher PCE of 9.21% (FTAZ:IDTIC, 7.13%). To further expand the π -conjugation of fused-ring core, pyrene was used to replace the benzene in ITIC to synthesize FPIC with fluorinated IC (2FIC) as the end group [172]. Blending with

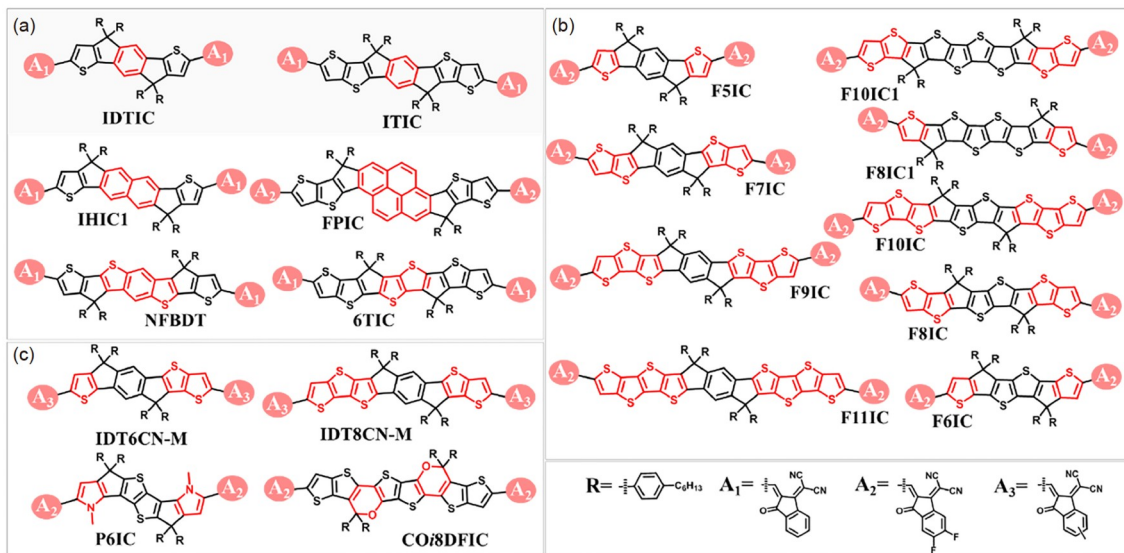


Figure 11 The structure of A-D-A type acceptors with fused-ring core engineering. (a) Replacing the central benzene of the fused-ring core; (b) expanding the conjugated length of the fused-ring core; (c) introducing asymmetric backbone and heteroatoms to the fused-ring core (color online).

PTB7-Th, the FPIC based OSC obtained a moderate efficiency of 8.45%. It is worth noting that the larger π plane (central benzene, naphthalene and pyrene) led to a blue-shifted absorption. Therefore, FPIC showed a medium optical bandgap of 1.63 eV, which had the potential in ternary OSCs. BDT as an electron-rich and highly planar unit was also widely introduced to FREAs to improve the light absorption and charge transfer properties. A substitution of benzene in IDTIC by BDT unit gave a heptacyclic acceptor, NFBDT [173], which is also an isomer of ITIC. NFBDT showed a strong absorption at the range of 600–800 nm with a narrow optical bandgap of 1.56 eV. Blending with a wide bandgap polymer donor PBDB-T, a high efficiency of 10.42% was achieved. Meanwhile, OSCs with BDT-centered FREAs usually obtained efficiency over 10%, demonstrating the great potential of BDT units in electron acceptor materials. Besides the BDT, TT' and derivatives are also popular electron-donating moieties. Introducing TT' units in central of FREAs could not only enhance the intramolecular D-A effect, but also strengthen the intermolecular packing. From this viewpoint, Jen *et al.* [174] synthesized a TT'-centered FREAs, 6TIC, by replacing the benzene in ITIC with TT' units. 6TIC had a red absorption onset of 905 nm much more than that of ITIC (730 nm). Blending with PTB7-Th, 6TIC based device achieved a high efficiency of 11.07% with a high J_{SC} over 20 mA/cm². Expanding the conjugated backbone length was another efficient strategy to improve the photoelectric properties of photoactive materials. Zhan *et al.* [175] adjusted the number of fused thiophene in ITIC and employed the 2FIC end group to synthesize four acceptors with symmetric thiophene, thieno[3,2-b]thiophene, dithieno[3,2-b:2',3'-d]thiophene and thieno[2',3':4,5]thieno[3,2-b]thieno[2,3-d]thiophene units, respectively (four acceptors:

F5IC, F7IC, F9IC, F11IC). As expected, with the increasing fused rings, the four acceptors showed upshifted HOMO (from -5.82 to -5.44 eV) and LUMO (from -4.05 to -3.94 eV) energy levels, as well as a decreased E_g^{opt} (from 1.64 to 1.47 eV). Besides, the electron-donating ability of the fused-ring core and intermolecular packing were enhanced, and thus electron mobilities of pure films were also increased from 8.1×10^{-4} to 1.4×10^{-3} cm²/(V s). Consequently, PCEs of FTAZ:F5IC, FTAZ:F7IC and FTAZ:F9IC based OSCs were also increased from 5.6% to 11.7%. However, the 11 fused rings-centered F11IC showed no photovoltaic effect when blended with FTAZ due to the poor solubility. When the benzene in the center of F5IC, F7IC and F9IC was replaced by TT', Zhan *et al.* [176] synthesized F6IC, F8IC and F10IC. These three acceptors had similar performance tendency, further confirming the importance of expanding the thiophene units at the flanks of the core. In addition, Zhan *et al.* [177] expanded the central TT' moiety in the core of F6IC and F8IC to thieno[2',3':4,5]thieno[3,2-b]thieno[2,3-d]thiophene to obtain F8IC1 and F10IC1, respectively. The energy levels were upshifted, the E_g^{opt} was narrowed, and the PCE was promoted using PTB7-Th as the donor. Isomerization can also broaden the core variety. Chen *et al.* [173] moved the cyclopentadiene moiety in ITIC to the flanking direction and synthesized NFBDT. The absorption was redshifted by 15 nm, the HOMO was upshifted and the efficiency was advanced to 10.42% with simultaneously improved V_{OC} , J_{SC} and FF. Asymmetric backbone showed large dipole moments and enhanced intermolecular interaction, which would benefit the carrier mobility and blend morphology, thus promoting the FF. Yang *et al.* [178,179] designed and synthesized systematically asymmetric FREAs. When using T, TT' and TTT as the flanking groups and methylated IC

(IC-M) as the end groups, two asymmetric acceptors IDT6CN-M and IDT8CN-M were reported. Using PBDB-T as the donor, IDT6CN-M and IDT8CN-M based OSCs achieved high FF of ~0.77 and 0.79, respectively. Besides, other reported asymmetric cores-based FREAs by their groups also showed high FFs over 0.7, revealing the great importance of symmetric strategy in designing high performance FREAs. Heteroatoms with strong electronegativity and special electronic orbit arrangement (*e.g.*, oxygen, nitrogen and selenium) were popular in FREAs. For example, Zhan *et al.* [180] changed the flanking thiophene of F6IC to pyrrole unit for P6IC. The E_g^{opt} was decreased from 1.37 to 1.3 eV and the HOMO and LUMO levels were both raised. As a result, PTB7-Th:P6IC based OSC realized an outstanding PCE of 12.2% with a high J_{SC} of 25 mA/cm² and an FF of 0.7 which was higher than that of PTB7-Th:F6IC based analogs (a PCE of 5.57% with a J_{SC} of 18.2 mA/cm² and an FF of 0.51). Moreover, Ding *et al.* [181] inserted an oxygen atom into the bridging group of cyclopentadiene and designed series of carbon-oxygen-bridged (CO-bridged) A-D-A type acceptors. Compared with F8IC, the corresponding CO-bridged CO₈DFIC obtained redshifted absorption and raised energy levels, thus the PCE, V_{OC} , J_{SC} and FF were simultaneously improved.

4.1.2 End group engineering

End groups (A) with strong electron-accepting ability play a great role in enhancing the intra/intermolecular interactions and packing effects, charge transfer, and thus the photovoltaic performance, as shown in Figure 12. IC and its derivatives are the most commonly used end groups, because their electron-accepting ability is strong enough and can be delicately controlled by substituting the H atoms with halide atoms or alkyl groups. Here, all the highlighted acceptors are based on the fused-ring core of the typical ITIC. In order to

investigate the halogenation effect on the A-D-A type acceptors, Li *et al.* [182] designed and synthesized four ITIC-analogs, naming X-ITIC (F-ITIC, Cl-ITIC, Br-ITIC, I-ITIC) with single F, Cl, Br, I atom on the IC end groups, respectively. Compared with ITIC, the halogenated X-ITICs possessed redshifted absorption, deeper energy levels and enhanced crystallinity due to the heavy atom effect and strong electronegativity. Using PTPDBDT as the donor, the X-ITIC based OSCs showed higher efficiencies (~9%) than that of ITIC counterpart (~6%). Hou *et al.* introduced more F and Cl atoms to ITIC to obtain IT-4F [108,109] and IT-4Cl [169]. Compared with the di-halogen atoms-substituted IT-2F and IT-2Cl, IT-4F and IT-4Cl exhibited redshifted absorption and deeper energy levels, leading to a decreased V_{OC} but improved J_{SC} and FF, when blending with PBPD-TF. Both the IT-4F and IT-4Cl based OSCs achieved over 13% efficiency [168,169]. Apart from the electron-withdrawing halogen atoms, electron-donating methyl and methoxy groups were also attached to IC. Hou *et al.* [183] synthesized a new methyl-substituted ITIC analog, IT-M. The absorption was slightly blue-shifted and the energy levels were slightly elevated. Blending with PBDB-T, the device efficiency was boosted from 11.22% to 12.05% due to an increased V_{OC} . Yang *et al.* [184] introduced fluorine atom and methyl to IC at the same time for a new CFDCI end group. Combined with IDTT core, the new synthesized ITCF showed moderate absorption and energy levels compared with IT-DM and IT-4F, thus medium J_{SC} and V_{OC} . Nevertheless, an outstanding FF (78.8%) of J71:ITCF was achieved, leading to a high PCE of 13.2%. Hou *et al.* [185] also employed series of alkoxy with different length to IC and synthesized a series of ITIC-based acceptors (IT-O1 to IT-O4 with methoxy, ethoxy, propoxy and butoxy groups, respectively). With the increasing alkyl length, both molecular solubility and electron mobility were improved. However, a larger domain size was

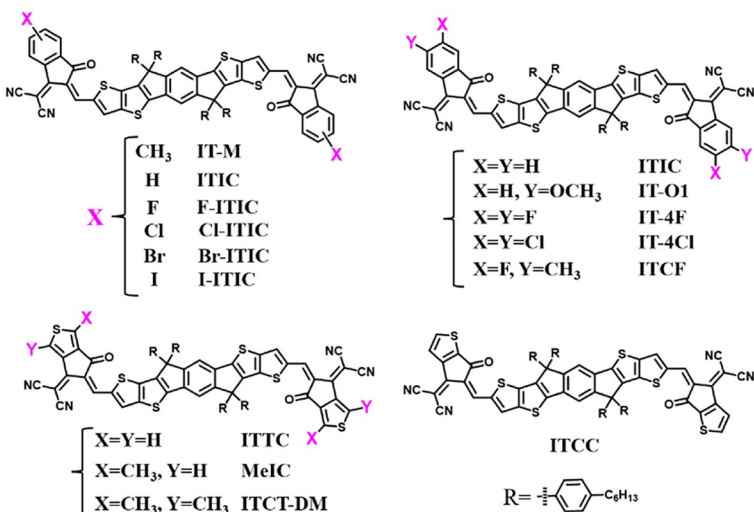


Figure 12 The structure of A-D-A type acceptors with end groups engineering (color online).

found in the blend with bulkier alkoxyl, leading to worse morphology and thus lower J_{SC} and FF. As a result, IT-O1 with the small methoxy group had the favorable blend morphology and the highest PCE of 11.6%. When taking the place of benzene in IC by thiophene, a new TC end group and its derivatives were synthesized. Zou *et al.* [186] designed and synthesized a TC end group. Connected with the IDTT core, a new TC based acceptor of ITTC was synthesized. Compared with ITIC, ITTC exhibited narrowed E_g^{opt} and upshifted energy levels. The HFQx-T:ITTC performed a high PCE of 10.4%. To the thiophene α -position of TC, Yang *et al.* [187] and Zhan *et al.* [188] introduced one or two methyl groups. MeIC and ITCT-DM were obtained with similar absorption and lifted energy levels. As a result, J71:MeIC and PBDB-T:ITCT-DM performed 12.54% and 10.56% efficiencies, respectively. An isomerization of TC was devoted to CC end group. Based on CC, Hou *et al.* [189] synthesized a new ITCC acceptor. PBDB-T:ITCC device obtained a high PCE of 11.4% with an outstanding V_{OC} over 1 V due to the upshifted LUMO.

4.1.3 Side chains engineering

Side chains engineering plays an important role in controlling the solubility and photo-electrochemical properties. The positions at the fused-ring core where the side chains can be attached could be classified into three categories: the cyclopentadiene, the central benzene and the β -site of the flanking thiophene, as shown in Figure 13. Taking ITIC as an example, attaching side chains onto the sp^3 -hybridized carbon of the bridged cyclopentadiene was the widest, easiest and most efficient method. The two sp^3 -hybridized carbons were centrosymmetric and located at the opposite of the fused core, as a result, the four *p*-hexylphenyl chains pointed to different directions in the space. Based on ITIC, Li *et al.* [190] changed the position of hexyl at the *p*-hexylphenyl chains to obtain m-ITIC. The isomeric m-ITIC showed an increased film absorption coefficient, a stronger crystallinity and a higher electron mobility. Consequently, J61:m-ITIC

achieved a higher performance of 11.7% than the ITIC counterpart. Meanwhile, Zhan *et al.* [191] replaced the benzene at the *p*-hexylphenyl chains with thiophene to synthesize ITIC-Th. Due to the σ -inductive effect of thiophene side chains, ITIC-Th showed a downshifted energy level than ITIC. The intermolecular interaction was enhanced due to the introduction of sulphur, resulting in an enhanced charge transfer. Therefore, a high PCE of 9.6% was obtained in PDBT-T1:ITIC-Th device. In addition to aryl side chains, alkyl chains were also widely employed. Heeney *et al.* [192] synthesized C8-ITIC by replacing the *p*-hexylphenyl in ITIC with octyl. The E_g^{opt} was reduced and the crystallinity was enhanced. As a result, a high PCE of 13.2% was achieved when blending C8-ITIC with polymer donor PFBDB-T. Side chains onto the central benzene usually occurred in the BDT-based FREAs. Zhan *et al.* [193] introduced thiophenyl to the central benzene of NFBDT (ITIC1) to obtain ITIC2. The side-chain conjugation provided ITIC2 with an absorption redshift and a higher energy level. Using FTAZ as the donor, ITIC2-based device showed a higher efficiency of 11% than ITIC1 analogs (8.54%). Besides, Chen *et al.* employed octyl and octyloxy substituents BDT and fluorinated IC-F end group to synthesize NCBDT [194] and NOBDT [195]. The energy levels were finely controlled by the enhanced electron-donating ability of D units and the electron-withdrawing ability of A units. The E_g^{opt} 's were reduced to 1.45 and 1.39 eV, respectively. And the PBDB-T:NCBDT and PTB7-Th:NOBDT based OSCs obtained high efficiencies of 12.12% and 10.55%, respectively. Different from much attention on the above two categories of side chains, only a few side-chain investigations on the β -site of the flanking thiophene were reported. Tang *et al.* [196] reported an ITIC derivative, ITC6-IC, by introducing hexyl to the terminal of the fused-ring core. ITC6-IC showed a better solubility in common solvents and an elevated LUMO energy level. And the molecular conformation was stabilized by steric hindrance caused by the long alkyls. As a result, OSCs based on PBDB-T:ITC6-IC had a PCE of 11.61% with a high V_{OC} of

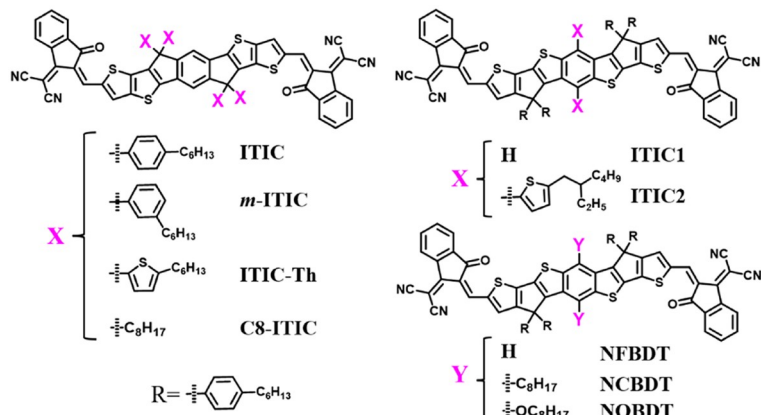


Figure 13 The structure of A-D-A type acceptors with side chains engineering (color online).

0.97 V.

4.2 A-DA'D-A type fused-ring electron acceptor

As mentioned above, as an epoch-making type of acceptor, A-D-A type acceptors have attracted great attention in recent years. Special fused-ring formation is endowed with strong and broad absorption, tunable molecular structure inter-relating physical and chemical properties. Based on the dominant formation of A-D-A type acceptors and structural diversity of polymer donors, Zou *et al.* [167] designed and proposed an original fused-ring acceptor, BZIC, exhibiting the conjugated backbones with A-DA'D-A structure, as shown in Figure 14. Unique design characters of such molecules are: First, a deficient electron unit is introduced into the fused-ring molecular skeleton to improve the luminescent efficiency; Second, DA'D unit containing pyrrole rings with electron-donating ability and chemical modification site, which is conducive to adjust molecular crystallinity and packing.

With further molecular structure modification and device optimization, the PCE of OSCs based on A-DA'D-A type acceptors is already close to 20%. The rapid progress of A-DA'D-A type materials are focused on the fused-ring molecular structure; central electron-deficient core (A'); end groups and side chains on pyrrole rings, D and A' units.

4.2.1 Fused-ring molecular skeleton engineering

In 2017, Zou *et al.* [167] designed and synthesized the first A-DA'D-A type acceptor, BZIC, with a ladder-type electron-deficient-core-based five-number fused-ring structure. Compared with the classical A-D-A type acceptor ITIC, BZIC showed a significant red-shift absorption of approximately 90 nm. Longer conjugation length and stronger ICT are conducive to the broad absorption and the improved J_{SC} . Therefore, Zou and Yang [197] replaced thiophene (T) units with TT' units and synthesized Y1, as shown in Figure 15.

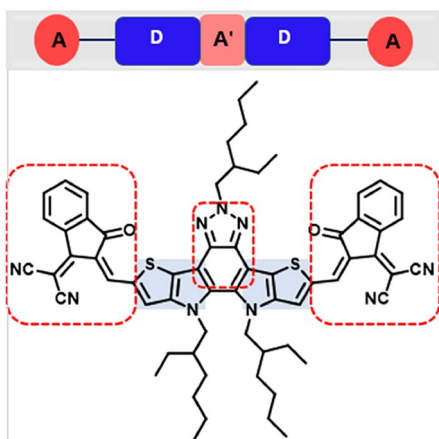


Figure 14 The structure of the first A-DA'D-A type acceptor, BZIC (color online).

With molecular skeleton extended to heptacyclic, Y1 exhibited a narrow bandgap of 1.44 eV. As a result, the PBDB-T:Y1 solar cell achieved a high PCE of 13.40% with an impressive J_{SC} of 22.44 mA/cm², a V_{OC} of 0.88 V and an FF of 69.1%. Instead of increasing the fused ring numbers, Jen *et al.* [198] replaced sulfur with selenium on TT' units and synthesized CH1007, the introduction of Se strengthened the intra- and intermolecular interactions and expanded π -core to broad photon absorption, thus significantly increasing the J_{SC} to 27.48 mA/cm². The PM6:CH1007 based OSC afforded a high PCE of 15.9%, and the ternary device achieved one of the highest PCE of 17.08% using PC₇₁BM as the third component. However, when Se was introduced into the inner thiophene units adjacent to pyrrole rings, the isomer of CH1007, Y6-2Se was obtained. The OSC based on Y6-2Se yielded a poor PCE of 14.61% with reduced J_{SC} and FF. The differential photovoltaic properties may be ascribed to the tighter intermolecular packing of CH1007, which was induced by the non-covalent inter-actions between Se and O. To further optimize molecular structure and nourish the DA'D species, Zou *et al.* [199] reported the first asymmetric A-DA'D-A type acceptor Y21 with hexacyclic structure. The device based on PM6:Y21 showed an excellent PCE of 15.4 % with a high J_{SC} of 24.9 mA/cm², which ranks with the heptacyclic fused-ring acceptors ever made. Asymmetric molecule design strategy provides more potential to develop high-performance A-DA'D-A type acceptors. Seven, eight and nine-number fused-ring symmetric A-DA'D-A type acceptor, BDTP-4F, ABP4T-4F, BTDTDP-4F and BP5T-4F have also been reported [200,201]. The different numbers of fused rings not only influences photon absorption and energy level, but also changes molecular conformation. Even though octacyclic S-shaped BTDTDP-4F exhibited broader absorption and lower LUMO energy level than heptacyclic C-shaped BDTP-4F, FF of BTDTDP-4F was inferior to BDTP-4F, which mostly results from the stronger crystallinity and self-assembly trend. Besides, BTDTDP-4F based device showed faster and more balanced charge dissociation and transport, owing to the more suitable pure phase separation length and suppressed bimolecular recombination. Similarly, octacyclic Z-shape BP5T-4F showed a higher dielectric constant with reduced geminate/nongeminate recombination compared with heptacyclic W-shape ABP4T-4F. Besides, owing to the favorable face-on orientation and molecular stacking, OSCs fabricated with PM6:BP4T-4F showed higher PCE (16.7%) than PM6:ABP4T-4F. These studies illustrate the importance of asymmetric molecule design strategy and molecular conformation, which induces significant effect on the molecular dielectric constant, charge recombination and morphology in OSCs, and thus the eventual device properties.

4.2.2 Central electron-deficient core engineering

The advent of A-DA'D-A type acceptors undoubtedly

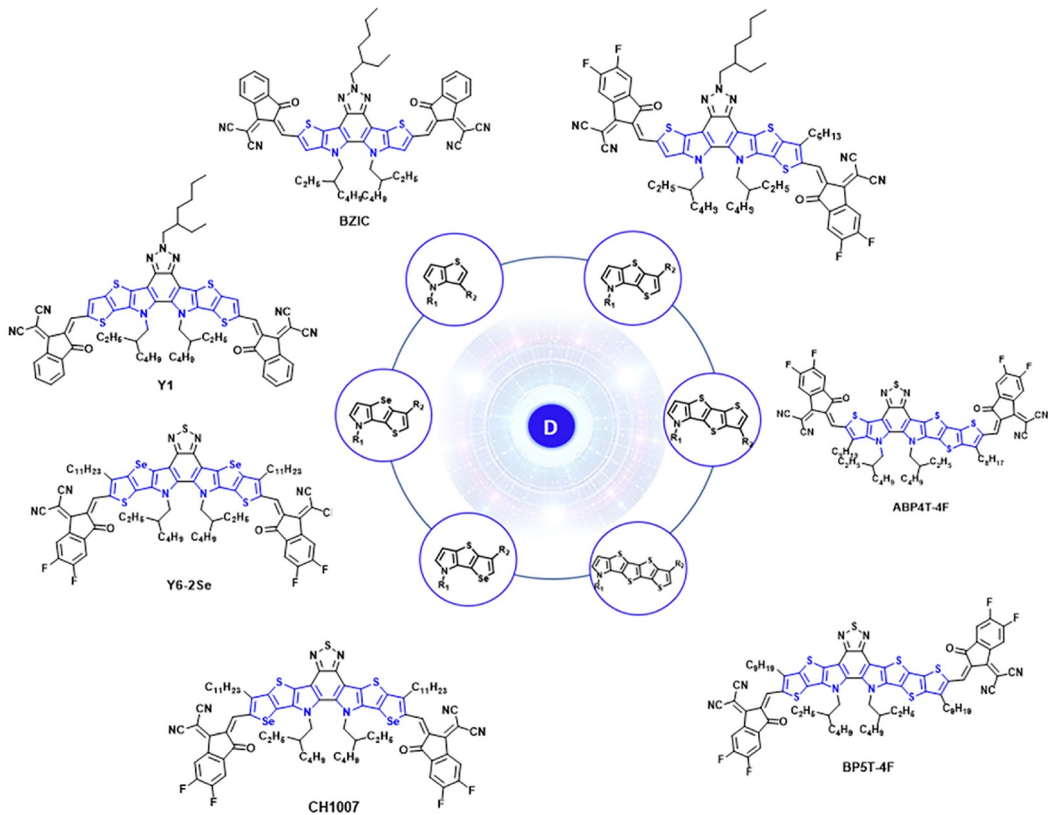


Figure 15 The structure of A-DA'D-A type acceptors with fused-ring molecular skeleton engineering (color online).

opened the new door of high-performance OSCs. The alternation of A' unit can slightly adjust chemo-physical properties of SMAs and affect the intermolecular interaction, stacking and orientation. Based on the in-depth research of photoelectric material, researchers developed more and more suitable A' unit to optimize the molecule and device performance. Considering that BT moiety can strengthen the intermolecular interactions, Zou *et al.* [91] substituted BT unit for benzotriazole (BTz) unit, and synthesized Y5. Compared with a fused BTz-containing NFA Y9, as shown in Figure 16 [202], Y5 shows deeper HOMO energy level, more balanced electron/hole transport and higher FF. Moreover, OSCs based on Y5 achieve a high PCE over 10% with several donors, which shows Y5 is universal acceptor to fabricate efficient OSCs. Qx as an electron-deficient unit can deliver quinoid-resonance effect and possess two modified sites to flexibly adjust molecular structures and properties. Zhu and Liu *et al.* [203] applied Qx as the A' segment and reported a novel electron acceptor AQx-2. The device based on PM6:AQx-2 showed an outstanding PCE of 16.68%. Such high performance benefited from the introduction of Qx into AQx-2 which efficiently reduced charge recombination, and thus facilitated electron transport and intermolecular packing. High Urbach energy of semiconductors leads to nonradiative recombination, and then causes big energy loss. Lin *et al.* [204] adopted sele-

nium substitution to reduce the Urbach energy of acceptors and then synthesized Y6-Se with a facile method using 2,1,3-benzoselenadiazole (BSe) as the central core. Y6-Se showed a relatively low Urbach energy of 20.4 meV, providing broad absorption and higher electron mobility. As a result, OSCs based Y6-Se presented an impressive PCE of 17.7%. The useful way of changing central electron-deficient core (A') can inspire the development of acceptors for high-performance OSCs.

4.2.3 End groups engineering

In the A-DA'D-A type molecules, electrophilic end group, namely A unit plays important role in the intermolecular stacking, absorption, energy levels and other chemo-physical properties of materials. End group engineering is also an easy and feasible design method to adjust molecular structure to achieve ideal results, as shown in Figure 17. In 2019, Zou *et al.* [205] reported a star NFA Y6, which achieved a remarkable PCE of 15.7% and made a great breakthrough in the development of OSCs. Y6 was effectively modified by fluorination of end groups based on BT core-based fused-ring A-DA'D-A type NFA Y5. Y6 shows improved intermolecular interactions through noncovalent F-S and F-H bonds between the end-groups, and thus more balanced and faster electron/hole mobility. This work also illustrated that halogenation of end groups on the A-DA'D-A type NFAs is

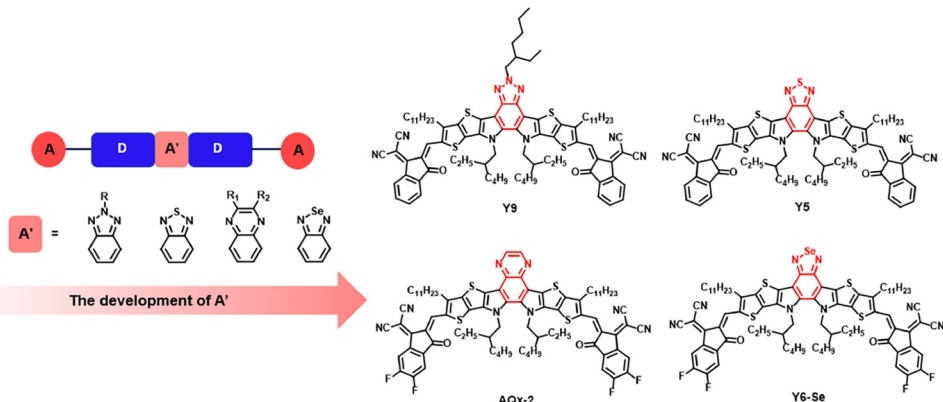


Figure 16 The structure of A-DA'D-A type acceptors with central electron-deficient core engineering (color online).

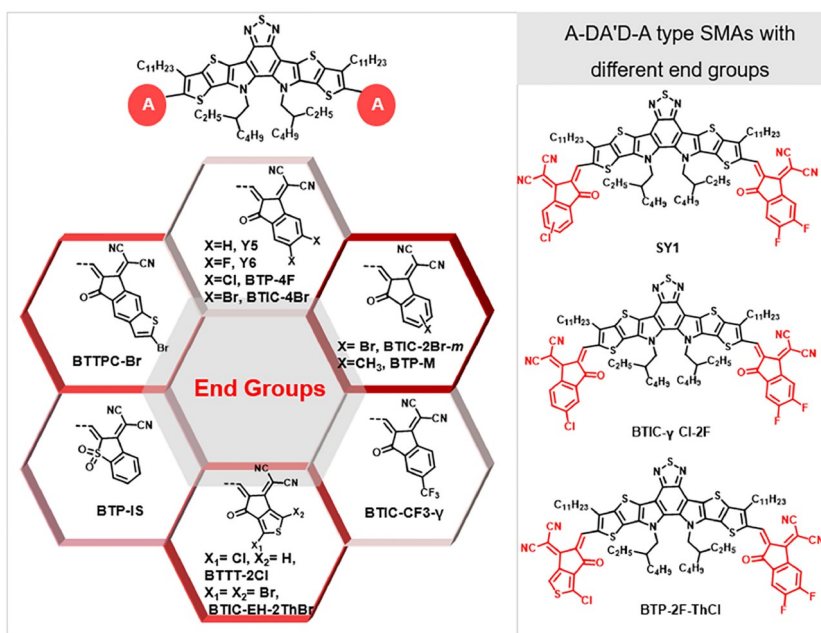


Figure 17 The structure of A-DA'D-A type acceptors with end group engineering (color online).

an efficient and rational approach to broadening absorption, lowering energy level and increasing the intra- and intermolecular interactions. Subsequently, numerous studies about end group engineering for A-DA'D-A type NFAs have been reported, which have driven the research and development of OSCs dramatically. A series of functional units such as Cl, Br, -CH₃, -CF₃ are introduced into the IC, TC and TPC end groups. Compared with Y6, BTP-4Cl [206] and BTIC-4Br [207] with IC-2Cl and IC-2Br as end groups, respectively, showed significant redshifts, related to the corresponding stronger intermolecular π - π packing. It was found that the chlorination of molecules can also lower non-radiative energy loss. Therefore, the OSCs based on PM6: BTP-4Cl exhibited high J_{SC} and V_{OC} with a relatively low non-radiative energy loss of 0.206 eV. Also, Hou *et al.* [208] investigated the impact of number of F atoms attaching to the

IC units on intermolecular interactions. As the number of F atoms increased, the resulting molecular surface electrostatic potential (ESP) difference between donors and acceptors was enhanced. This work revealed that large ESP difference by changing the number of F atoms will increase the hybridization of charge-transfer (CT) and local exciton (LE) state, resulting in an increased non-radiative energy loss. When -CF₃ group was introduced into IC units, an ultra-narrow band-gap (1.3 eV) acceptor BTIC-CF₃-γ was synthesized [209]. BTIC-CF₃-γ possessed multiple intermolecular interactions and close π - π packing; besides, the single-crystal analysis of BTIC-CF₃-γ delivered a 3D interpenetrating network structure which helps charge transport in multiple directions for improved electron mobility. Electron-donating functional groups like -CH₃ make opposite effects on the electro-chemical properties of acceptors

compared with electron-withdrawing ones. The SMA BTP-M showed blue-shifted absorption and higher energy levels [210]. Due to the mismatched energy level alignment with PM6, the obtained PCE of the device is only 4.26% eventually. Applying new TC units as the end groups, an A-DA'D-A type NFA, Y10, reported by Zou *et al.* [211] showed a lifted LUMO energy level compared with Y6 end-capped by IC-2F units. It indicated that TC units as end groups are expected to increase the V_{OC} of OSCs. Similarly, the halogenation of TC was also applied to synthesize the corresponding SMAs, such as BTIC-EH-2ThBr [212] and BTTC2Cl [213]. Especially, as a medium bandgap NFA, BTIC-EH-2ThBr exactly served as the third component of PM6:Y6 blend. Owing to the weaker crystallinity and molecular packing, BTIC-EH-2ThBr promoted the blend to obtain a better phase separation structure. As a result, a high PCE of 17.5% was achieved. Other modification of end groups for A-DA'D-A type acceptors was also investigated. The ketone groups in IC units were substituted by sulfonyl, and the relevant acceptor BTP-IS showed red-shifted absorption and lower LUMO energy levels compared with Y5 [214]. The sulfonyl-based end group can be a potential building block for high-efficient OSCs. And BTTPC-Br using TPC-Br with extended conjugation as end group exhibited closer “face-on” oriented π - π stacking [215]. Thus, vertical charge transport was improved with inhibited charge carrier recombination, which facilitated the performance of OSCs. Moreover, the asymmetric A-DA'D-A type acceptors flanked with two different ending groups offered a new idea for the exploration of OSCs. The asymmetric acceptor BTP-2F-ThCl and its symmetric counterpart Y6 maintained an adjacent optic-electrochemistry, and crystallinity properties [216]. Besides, BTP-2FThCl ensured sufficient charge separation despite existing a small HOMO energy offset, and

the final device obtained high J_{SC} and V_{OC} simultaneously. Other A-DA'D-A type SMAs with different end groups like BTIC- γ Cl-2F [217] and SY1 [218] played their unique role in the corresponding device, and showed excellent performance. These works indicated a more sophisticated structure-property relationship that incorporating two different end groups which can be finely modified to shape NFAs can effectively control the molecular photo-electrochemical properties, crystallinity and π - π stacking. Finally, the morphology and charge transport can be controlled rationally.

4.2.4 Side chains engineering

Both in A-D-A and A-DA'D-A type acceptors, side chains make a significant influence on the solubility, crystallinity, inter-/intra-molecular interaction and other properties. As a special molecular structure, A-DA'D-A type acceptors possess more positions for functional chain modification, as shown in Figure 18. Compared with other chain on the D and A', the side chains on the pyrrole rings are more alternatively adjusted, and the research of them is more now, as well. The typical N3 selecting 3rd-position branched alkyl chains on the pyrrole rings showed the optimal face-on/edge-on orientation compared with the Y6 and N4 with 2nd and 4th-position branched on the pyrrole motif [219]. Usually, the increasing length of alkyl chains can improve the solubility of molecules and lower crystallinity. Accordingly, BTP-4Cl-12 exhibited better morphology than BTP-4Cl when blended with PM6 [220]. Thus, charge recombination was effectively suppressed in PM6:BTP-4Cl-12, which achieved a high PCE of 17%. On the contrary, although modified by longer alkyl chains, BTP-4F-12 presented stronger crystallinity than Y6 [221]. Owing to the better solubility and crystallinity of BTP-4F-12, it exhibited tighter π - π stacking and lamellar packing, favoring the charge transport. Interestingly, when

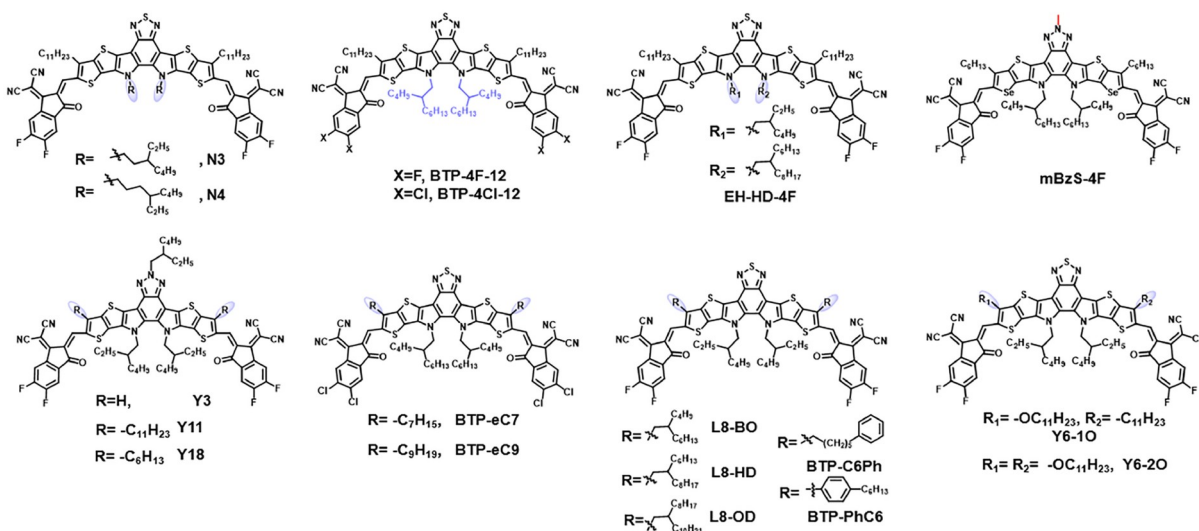


Figure 18 The structure of A-DA'D-A type acceptors with side chains engineering (color online).

two different alkyl chains, 2-ethylhexyl (EH) and 2-hexyldecyl (HD) were introduced in the pyrrole rings together, high-efficient SMA EH-HD-4F was obtained, which got one of the best PCE (18.38%) [222]. Such a high performance was attributed to the more suitable face-on orientation and well blend phase separation morphology. Some electron-deficient units used as A' core are also available for the appropriate site of alky/arene chains modification. Jen *et al.* [223] cut the length of *N*-alkyl EH chain on the BTz core to get a methyl-substituted BTz central unit-based acceptor, mBzS-4F. The blend based on PM6:mBzS-4F delivered more balanced and higher charge carrier mobilities, and give an obviously increased FF of 76.35% than its counterpart, EHBzS-4F's FF (70.07%). mBzS-4F with shorter chains indicated a smaller steric hindrance and more favorable morphology, which manifested that shortening the length of side chains on the A' is a feasible method to gain closer molecular stacking and higher FF of OSCs. Previously mentioned work about AQx-1 also reflected such design strategy, which provides a great potential to synthesize pretty acceptor materials. In addition, it was discovered that optimizing the alkyl chain on the edge of the A-DA'D-A type acceptors can also greatly influence the molecular crystallinity and ordered stacking related to Urbach energy. Zou *et al.* [224] proposed a rational molecular structure-properties relationship of regulating the side chains attached on the TT' units to reduce energy disorder and improve the FF. First, the introduction of side chains into the TT' units of Y3 effectively reduced the structure and energy disorder as well as Urbach energy, which made a faster and more balanced electron/hole transport. Then, tailoring the length of alky chains on TT' units can also reduce the steric hindrance and increase molecular stacking. Accordingly, the obtained Y18 acquired a higher FF than Y11. BTP-eC9 reported by Hou *et al.* [110] also possessed good solubility and enhanced intermolecular ordering to get the best morphology features compared with its counterpart, BTP-eC7 and BTP-eC11 with poorer properties. Recently, a series of branched side chains with different length have been introduced into the TT' units of A-DA'D-A type acceptors. Three new acceptors L8-BO, L8-HD, L8-OD with 2-butyloctyl (BO), HD and 2-octyldodecyl (OD) substitution at the beta position of thiophenes were reported by Sun and Liu *et al.* [225]. Molecular stacking and phase separation morphology were regulated by the rational design of alternating branched chains with linear ones and changing the alkyl chains length. This research showed that those branched side chains modified molecules pack in rotational symmetry, while Y6 in mirror symmetry, which caused different molecular packing motif. Additionally, the OSCs based on three new acceptors all exhibited small non-radiative recombination energy loss (ΔE_3), among which the L8-BO and L8-OD presented reduced ΔE_3 compared with Y6-based OSCs. As a result, the OSC based on L8-BO

achieved an unprecedented PCE of 18.32% due to the superior molecular properties, structure order and morphology. Surprisingly, the ΔE_3 decreased as the branched alkyl chains length increased, which showed a little difference from the work about Y18 and Y11. Some other reported work about side chains engineering on the TT' unit such as BTP-C6Ph and BTP-PhC6 designed by Zhan *et al.* [226] and Y6-1O and Y6-2O reported by Yan and Liu *et al.* [227] all showed the effects of side-chains at such position on their molecular and photovoltaic properties. Also, it indicated that the extended exploration of side chains on the beta position of thiophenes is a plausible avenue to manipulate the molecular structure and properties, and a great potential to improve the OSC performance as well.

It can be concluded that fused-ring electron acceptors have injected new energy to the development of photovoltaic materials, and also made a great contribution to the rapid progress of OSCs. With the continuous growing of device fabrication technologies, the further investigation and optimization of photovoltaic materials is also needed in the future.

5 Nonfused ring electron acceptors

Relative to acceptor-donor-acceptor (A-D-A) type fused-ring electron acceptors (FREAs), nonfused ring electron acceptors (NFREAs) are molecules with nonfused backbone in the electron-donating part, which were widely developed and studied in Chen's group, Bo's group and so on [228]. For the intentions of designing nonfused acceptors, there mainly existed the following considerations: (1) simplifying the synthetic routes for lower material costs, (2) enriching the structure tunability for unique features, and (3) releasing surface tension for better device stability. For NFREAs, to realize high efficiencies, noncovalent interactions, like F···H, O···H, and S···N are usually essential to lock the molecular backbones for planar geometries more or less. Till now, numerous NFREAs have been developed and reported by modifying molecular structures. Among them, small fused ring building blocks such as indacenodithiophene (IDT) and cyclopentadithiophene (CPDT) are the most widely used in the construction of nonfused ring electron acceptors (NFREAs). Further, fully nonfused ring electron acceptors are also developed by researcher in recent several years. In this section, NFREAs will be discussed in two parts: (1) Core engineering, (2) Terminal engineering.

5.1 Core engineering

IDT units with pentacyclic fused core structures exhibit low degree energetic disorder, high charge carrier mobility, etc, which can be utilized to fabricate A- π -D- π -A type NREAs as

the donor units, as shown in Figure 19 [229]. The sp^3 hybridization side chain in IDT core units could suppress the molecular aggregation and ensure the solubility of molecules in common organic solvent. The aromatic π bridge units could adjust the photophysical property. The electron-withdrawing end groups can form strong intramolecular charge transfer effect on the central electron-donating groups, and thus broaden the absorption of the molecules. Moreover, some researches indicate that the intermolecular electrostatic interactions between end groups and central units play a vital role in the formation of charge transport channels.

In 2017, two NFREAs (IDT-BOC6 and IDT-BC6) are purposefully designed and synthesized with 2,5-dihexylphenylene and 2,5-bis(hexyloxy)phenylene as the π -bridge units [230]. According to theoretical calculation, the intramolecular noncovalent interaction in IDT-BOC6 can force the molecule to form planar conformation, whereas the counterpart IDT-BC6 displays a twisted molecular backbone. Thus, IDT-BOC6 exhibits red-shifted optical absorption, enhanced transport mobility and reduced nonradiative energy loss. A PCE of 9.6% is achieved based on IDT-BOC6, which is much higher than that of IDT-BC6 (2.3%). Subsequently, a series of A- π -D- π -A type NREAs with IDT as the core unit are designed and synthesized according to the concept of intramolecular noncovalent interactions. The similar acceptor ITOIC with 2,5-bis(hexyloxy)phenylene replaced by 4,4-bis(hexyloxy)thiophene gives a PCE of 8.87% [231]. Furthermore, the fluorinated counterparts ITOIC-F and ITOIC-2F could achieve much higher PCE of 10.65% and 12.17%, respectively, which can be mainly ascribed to the enhanced intermolecular interactions and improved charge transport mobilities. Similarly, IDT-EDOT with 3,4-ethylenedioxythiophene as the π -bridge unit could generate a high PCE of 11.32%, which is much higher than IDT-PDOT with 3,4-propylenedioxythiophene as the bridge unit (2.18%) [232]. However, IDT-PDOT-C6 with 3,4-propylenedioxy-

thiophene bearing two hexyl side chains could enhance the solubility of the small molecular acceptors and give a higher PCE of 11.08%. Furthermore, the ternary devices display an improved PCE of 13.04% with IDTT-OB introduced to the binary blends (PBDB-T:IDT-PDOT-C6) [233]. Especially, IEICO [234] exhibits small optical bandgap of 1.34 eV by employing alkoxy substituted thiophene units, which is smaller than that of IEIC (1.50 eV) [235]. Further, the optical bandgap of IEICO-4F reduces to 1.24 eV with the introduction of fluorinated end groups, which can be ascribed to the enhanced ICT effect, optimal ternary OSCs based on IEICO-4F give a high PCE of 10.9% with an impressive J_{SC} of 25.3 mA/cm² [236]. The chlorinated counterpart IEICO-4Cl is used to construct semitransparent OSCs, which could give a PCE of 8.38% with an average visible transmittance (AVT) of 25.7% [237]. Bo and Liu *et al.* [238] reported a novel IDT derivative (IDTO) with the introduction of two alkoxyl side chains, which can be used to fabricate A- π -D- π -A type acceptors with different π bridge units. The photovoltaic devices based on the acceptor with thiophene as the electron-donating π -spacer demonstrate a high PCE of over 12.5%, which is much higher than the ones with selenophene and thieno[3,2-b]thiophene as the π bridge units [239]. Bazan *et al.* [240] reported the substitution of bulky phenylhexyl for linear octyl chains on the central IDT core and replacing bisalkoxy for alkyl-alkoxyl combination on the π -bridge units, which could manipulate the optoelectronic properties and intermolecular organization of the acceptors. Among them, o-IO1 could achieve a PCE of 13.1% with a J_{SC} of 26.3 mA/cm² and an energy loss of 0.54 eV. Besides, varied IDT cores, π -bridge units and end groups are used to construct A- π -D- π -A nonfullerene acceptors. The chemical structures, fundamental properties and photovoltaic parameters of these acceptors are shown in Figure 19 and Table 4, respectively.

CPDT is a commonly used electron-donating building

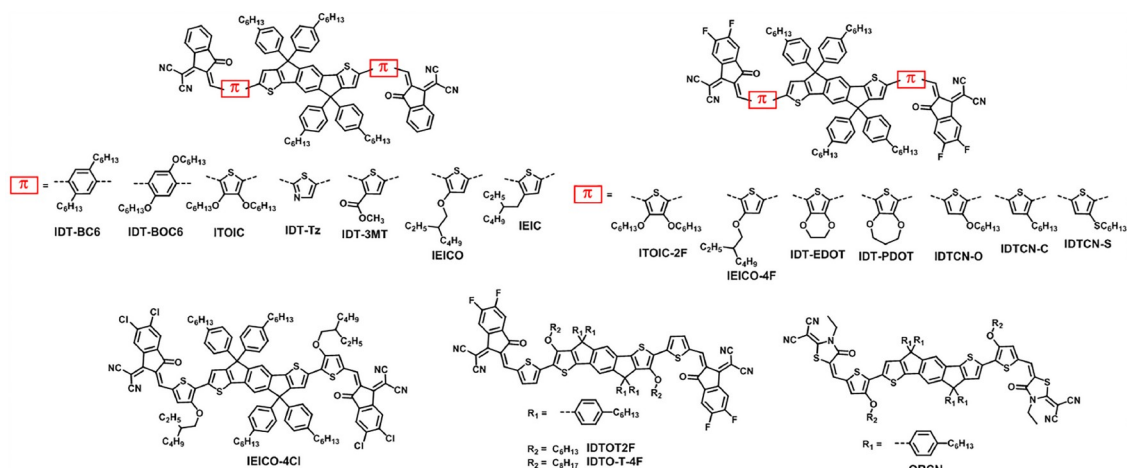


Figure 19 Nonfused electron acceptors based on IDT units (color online).

block consisting of carbon bridged bithiophene, which can be used to construct low bandgap polymers and small molecules, as shown in Figure 20. With the rapid development of nonfullerene acceptors, researchers also tried to use this building block to fabricate NFAs. Most of these acceptors adopt acceptor-donor-core-donor-acceptor (A-D-C-D-A) type structure, where C and D represent central linkers and CPDT units, respectively. Chen *et al.* [241] studied the effects of introducing four noncovalent interactions between the “C” and “D” parts, and found that more noncovalent interactions (OF-PCIC and HFO-PCIC) might disturb the ordered molecular packing and result in severe face-to-face arrangement, finally leading to unfavorable morphology. Bo *et al.* [242] replaced F···H noncovalent interaction with O···S noncovalent interaction and obtained DOC2C6-2F. Due to the enhanced ICT effect, the absorption was red-shifted to around 900 nm. Although energy levels were lifted, it was still enough for pairing with PBDB-T. The optimized OSCs based on PBDB-T:DOC2C6-2F showed an optimal PCE of 13.24% with a high photocurrent of 21.35 mA/cm². By altering the positions of alkoxy substituents from *para*-position to *ortho*-position (*o*-DOC6-2F) on the phenylene core, molecular shape would be converted from C_{2h} to C_{2v} symmetry [243]. The benefits of such arrangement were enlarging dipole moment, increasing solubility and tuning molecular packing. However, the absorption of C_{2v} molecule would be blue-shifted. After optimization, a PCE of 11.87% was achieved for *o*-DOC6-2F-based devices. Bo *et al.* [244] also reported NFREAs (FOC2C6-2FIC) with fluorine and alkoxy on the phenylene core, and found that π - π stacking was existing not only between two IC terminals but also between the IC terminal and phenyl core. Besides using alkoxy substituents, applying thiophene-based core was also effective in extending the absorption to near-infrared ranges. Chen *et al.* [245] replaced 2,5-difluorobenzene with 2,3-difluorothiophene and synthesized HF-TCIC. The absorption of HF-TCIC was extended to around 900 nm and a PCE of 9.40% was presented for HF-TCIC-based devices.

Although enhancing ICT effect was able to red-shift the absorption, energy levels would inevitably be uplifted. Maintaining a deep HOMO level could provide more space for selecting donors to pair with. The solution was adopting electron-withdrawing units with quinoid resonance effect as the “C” part, since quinoid resonance effect could help extend the absorption and electron-withdrawing ability could help deepen the HOMO level. For the above purpose, Chen *et al.* [246] developed NFREAs (X-PCIC) with near-infrared absorption up to 900 nm by using benzobis(thiazole) as the “C” part. In this work, S···N noncovalent interaction was proven existing in the molecule from the single crystal result. In addition, efficient *J*-aggregation (or head-to-end arrangement) was maintained in the solid state of X-PCIC.

Finally, OSCs based on PBDB-T:X-PCIC blend exhibited a PCE of 11.50% with a low energy loss of 0.53 eV. Since IC terminal could also be in contact with the “C” part in non-fused acceptors, using units with very strong electron-withdrawing ability as the core might help form an extra charge transport channel between the IC terminal and “C” part. Then, electron deficient cores (bezothiadiazole derivatives) are used as the “C” part to fabricate acceptors. The alkoxy substituted one can not only lock the molecule as a planar geometry, but also large improve the solubility of the acceptors. As a result, Bo *et al.* [247] achieved a high PCE of 11.48% with BTOR-IC4F as the acceptor. By using a chlorinated IC terminal, the obtained BCDT-4Cl could exhibit better molecular packing with stronger *J*-aggregation, and finally lead to a high PCE of 12.10% for BCDT-4Cl-based OSCs. Similarly, Huang *et al.* [248] used alkoxy-substituted benzotriazole as the “C” part and synthesized BTzO-4F. There was an extra alkyl chain on the benzotriazole, which could help lock the molecular geometry as a C_{2v} symmetry more tightly. Indicated by the shape of absorption, a large proportion of *J*-aggregation between two IC terminals was kept both in solution and thin film. Due to the above benefits, the optimal OSCs based on PBDB-T:BTzO-4F blend showed a high PCE of 13.80%. All in all, the diversity of “C” part indeed provided infinite possibility and unlimited imaginary space for NFREAs.

To further lower the material costs and simplify the molecular structures, researchers also developed fully nonfused ring electron acceptors, as shown in Figure 20. Chen *et al.* [249] reported a very simple NFREA (ICTP) composed of alkoxy-substituted phenyl, thiophene and IC terminal. It could be synthesized in three feasible steps. After blending with PBDB-T, a PCE of 4.43% was achieved. To further improve the efficiencies, ICTP was optimized on two aspects: IC terminal and thiophene unit. By introducing fluorine atoms on the IC terminals, PTICH was obtained [250]. Based on the molecule of PTICH, PTIC and PTICO were further synthesized by introducing a 3-hexyl or 3-hexyloxy substituent. Due to the deepening of energy levels, PTIC-series molecules were able to pair with fluorinated polymer donor, like PBDB-TF. The introduction of alkyl chain could not only increase the solubility of NFREAs, but also lock the orientation of IC terminals, thus enhancing the molecular ordering in the solid state. However, inserting an oxygen atom between thiophene and 3-hexyl played a negative role in the absorption and blend morphology. Finally, PTIC-based OSCs exhibited the best PCE of 10.27%, which was outstanding for such a simple NFREA. More importantly, excellent light stability was demonstrated for PTIC-based OSCs, significantly better than OSCs based on FREAs. Later, Bo *et al.* [251] also reported fully non-fused electron acceptors (*o*-4TBC-2F and *m*-4TBC-2F) by using four thiophene units as the main backbone. Molecular geo-

metry could be significantly tuned by regulating the location of hexyloxy chains on the phenyl substituents. When the hexyloxy chain was in *ortho*-position, the obtained molecule of *o*-4TBC-2F demonstrated a planar geometry. When hexyloxy chain was in meta position, the obtained molecule of *m*-4TBC-2F showed a twisted geometry. What's more, *J*-aggregation of *o*-4TBC-2F could be significantly enhanced after thermal annealing, thus leading to obvious absorption red-shifting. Finally, optimized OSCs based on PBDB-T:*o*-4TBC-2F blend exhibited a high PCE of 10.26%, better than *m*-4TBC-2F-based OSCs (2.63%), indicating the importance of maintaining a planar geometry and strong *J*-aggregation. Subsequently, a series of tetrathiophene-based fully nonfused acceptors are designed by tailoring the lateral chains, which can tune the molecular solubility and stacking in pure and blend film. Among them, PCEs of 10.15% and 12.04% for PBDB-T:4T-3 and D18:4T-3 are achieved, respectively, which is the champion PCE for fully nonfused acceptors at that time [252]. Recently, Hou *et al.* [253] developed a series of fully nonfused ring electron acceptors (A4T-16, A4T-21

and A4T-23) *via* regulating side chains. Among them, A4T-16 with 2,4,6-trimethylphenyl groups can enhance the conformational stability of the planar backbone and provide large steric hindrance to induce favourable intermolecular packing model. Thus, a champion PCE of 15.2% based on fully nonfused ring electron acceptors is achieved; moreover, the acceptors display good universality matched with various polymer donors and the corresponding photovoltaic devices display excellent long-term stabilities under continuously simulated 1-sun-illumination. Above results present that fully NFREAs could also show good efficiencies, and further improved performances could be expected by modulating the molecular backbones.

Very recently, triarylamine (TAA) units are used in the design of nonfused ring electron acceptors [254,255]. The natural three-dimensional molecular configuration and electron-donating feature can restrain the molecular aggregation and enhance the ICT effect to broaden the absorption. Moreover, the side chain substitution investigation reveals that $\text{CH}_3\text{-}2\text{F}$ displays an obvious face-on molecular

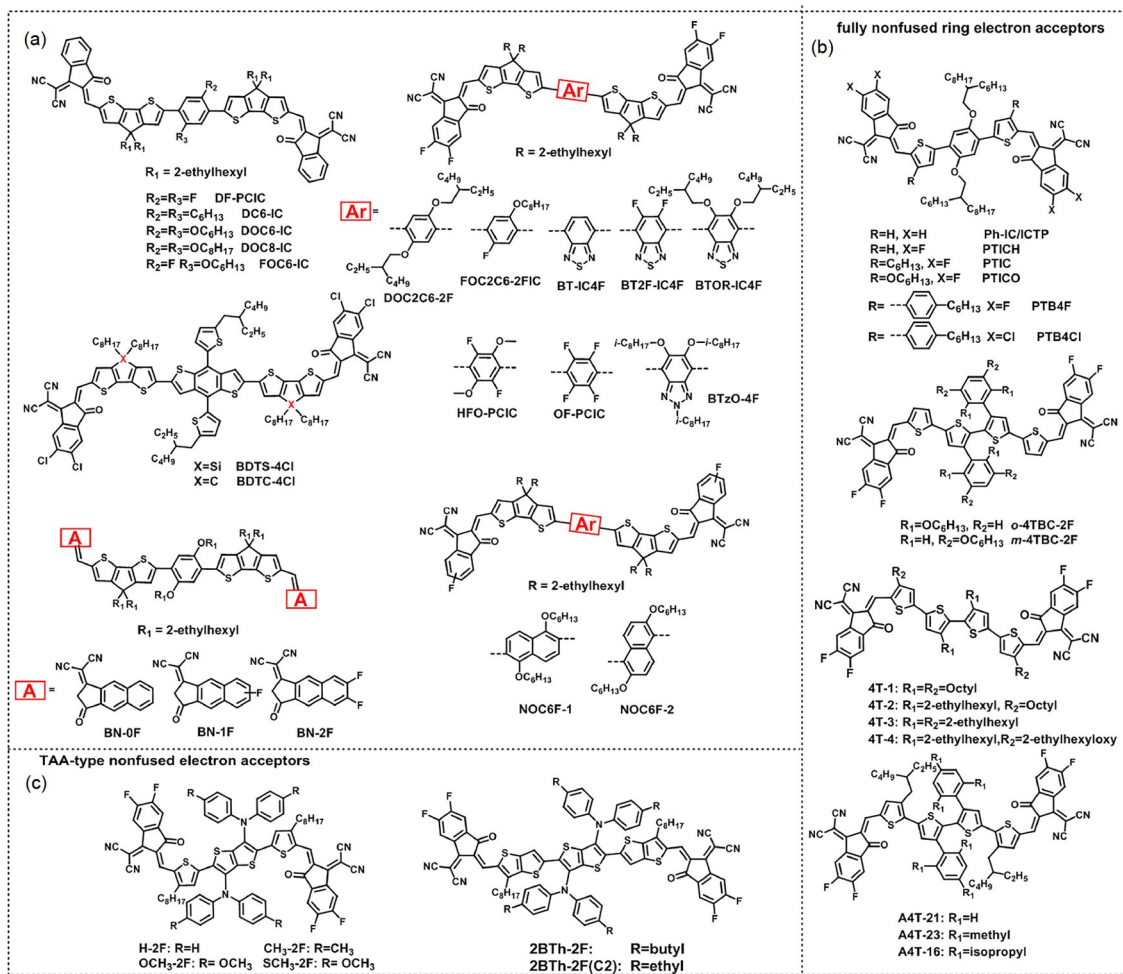


Figure 20 (a) Nonfused electron acceptors based on CPDT units; (b) fully nonfused electron acceptors; (c) TAA-typed nonfused electron acceptors (color online).

orientation, more ordered molecular stacking, and better miscibility with polymer donor. Thus, $\text{CH}_3\text{-}2\text{F}$ based device gives the highest PCE of 12.28% [255]. Further, 2BTh-2F with extended π -bridge units was also developed by Bo *et al.* [256]. The π -bridge variation from thiophene to thieno[3,2-b]thiophene could extend the absorption spectrum, enlarge the molar absorption coefficient, and enhance the order molecular packing. More importantly, the molecular packing model is converted from 2D to 3D, which is beneficial for the isotropic charge transport. Due to these comprehensive benefits, 2BTh-2F derivatives-based device can generate a champion PCE of 15.44%. All in all, core units engineering can much influence the properties of acceptors and is the main research topic in the design of nonfused ring electron acceptors.

5.2 Terminal engineering

For acceptors with electron-withdrawing groups (“A” part) exposed at terminals, efficient charge transport channels are mainly formed between the terminals. Therefore, modifying the “A” part is an effective way to enhance the device performances. Due to the multi-functions of halogen atoms, including enhancing intermolecular interaction, adjusting molecular polarity or modulating energy levels, halogenation of “A” part has proven to be efficient. Hence, Chen *et al.* synthesized HF-PCIC [241] and HC-PCIC [257] by introducing four fluorine or chlorine atoms at the terminals. With the deepening of LUMO and HOMO levels caused by the electronegativity of fluorine and chlorine atoms, to maintain a high V_{OC} , fluorinated polymer donor PBDB-TF (or PM6) was picked to pair with HF-PCIC and HC-PCIC. It was found that significant enhancement in J_{SC} was observed, thus leading to improved PCEs of 11.49% for HF-PCIC-based OSCs and 11.75% for HC-PCIC-based OSCs, when compared with DF-PCIC-based OSCs. If both electron-withdrawing and electron-donating units were introduced at the terminals, the properties of resulting molecule, FO-PCIC, was similar to those of DF-PCIC, so as for the efficiencies. Besides halogenation, extending conjugation of IC terminal was another method for enhancing terminal packing. For example, by extending one phenyl at the IC terminal, the resulting NFREA (DF-PCNC) not only showed red-shifted absorption, but also enhanced molecular packing, when compared with DF-PCIC. As a result, OSCs based on PBDB-T:DF-PCNC exhibited an enhanced PCE of 11.63% [258]. In a word, above works presented that, by modifying the “A” part of UAs, absorption, energy levels and molecular packing could all be regulated, finally leading to efficiency improvements. Among different kinds of IC terminals, halogenated IC terminals were found to be the best choices. The photovoltaic parameters of typical nonfused ring electron acceptors are also summarized in Table 4.

6 All-polymer solar cells

In 1995, Friend *et al.* [269] and Heeger *et al.* [14], independently proposed the concept of all polymer solar cells (all-PSCs), in which, an n-type polymer acceptor CN-PPV (see Figure 21) was blended with a p-type polymer donor MEH-PPV to form the bulk heterojunction layer. As compared with its counterpart of PSCs with small molecular acceptor (SMA), all-PSCs show pronounced advantages of superior mechanical flexibility/stretchability and improved device stability. In this section, with the brief introduction on its history, recent research progress of all-PSCs was provided.

High-performance *n*-type polymer semiconductors are the bottleneck for efficient all-PSCs. In the early stages, besides cyano-substituted polyphenylenevinylene (such as CN-PPV [14,269] in Figure 21 and DOCN-PPV [269–271]), benzothiadiazole-based polyfluorenes [272,273] (such as F8TBT in Figure 21) are also explored as polymer acceptors. However, those two-type polymers suffer from considerably lower electron mobilities ($10^{-5}\text{--}10^{-7}\text{ cm}^2/(\text{V s})$) [272–274] than fullerene acceptors and cause electron accumulation inside the active layer. Thus the as-fabricated devices usually have low FF and J_{SC} .

From 2007, rylene diimide-based polymer acceptors, bearing key building block of naphthalene diimide (NDI) or perylene diimide (PDI) were explored as polymer acceptors [274–278]. Those polymer acceptors have high electron mobility (comparable to those of fullerenes) and broad absorptions from the visible to the NIR region. An important breakthrough work is that Zhan *et al.* developed rylene diimide-based polymer acceptors, poly(perylenediimide-alt-dithienothiophene) (PDI-DTT [275], Figure 21), which is a pioneering rylene diimide-based polymer acceptor for all-PSCs with an initially reported PCE of 1.0% and increased to 3.45% by binary additives [279]. The success of fused rylene diimides as acceptors in organic solar cells also triggered their use as building blocks in polymer acceptors [280–282].

In 2008, with NDI as the key building block, Guo and co-workers [283] synthesized a series of n-type copolymers containing thienyl comonomers, including NDI-bithiophene copolymer (P2a) with 2-decyldodecyl side chain. In 2019, Yan *et al.* [284] reported the application of NDI-bithiophene copolymer (with 2-octyldodecyl chain, named as NDI2OD-T2 or N2200, Figure 21) in organic field-effect transistor. Inspired by its high electron mobility ($0.85\text{--}6.4\text{ cm}^2/(\text{V s})$) and good ambient stability, N2200 attracted substantial interest as polymer acceptor in all-PSCs [285], which enable N2200 as the most representative and widely used polymer acceptor before 2017. Although the initial PCE is less than 0.20% in 2011 [286,287], the PCE of the N2200-based all-PSCs steadily increased to over 5% before 2015, mostly benefited from new polymer donors and the morphology

Table 4 The photovoltaic parameters of typical nonfused ring electron acceptors

Acceptors	Donors	E_g (eV)	V_{OC} (V)	J_{SC} (mA/cm ²)	FF	PCE (%)	Ref.
IDT-BOC6	PBDB-T	1.63	1.01	17.52	0.54	9.60	[230]
IDT-BC6	PBDB-T	1.75	0.92	5.63	0.44	2.30	
ITOIC	PBDB-T	1.55	1.02	15.73	0.55	8.87	[231]
ITOIC-F	PBDB-T	1.50	0.95	18.60	0.61	10.65	
ITOIC-2F	PBDB-T	1.45	0.90	21.04	0.65	12.17	
IEICO		1.34	0.82	17.70	0.58	8.40	[234]
IEICO-4F		1.24	0.74	22.80	0.59	10.00	[236]
IEICO-4Cl		1.23	0.73	22.80	0.62	10.30	[237]
IDTOT2F	PBDB-T	1.44	0.85	20.87	0.72	12.79	[238]
IDTO-T-4F		1.45	0.86	20.12	0.73	12.62	[239]
IDT-Tz		1.53	0.88	13.67	0.71	8.52	[259]
IDT-EDOT	PBDB-T	1.63	0.86	21.34	0.62	11.32	[232]
IDT-PDOT	PBDB-T	1.62	0.85	5.26	0.49	2.18	
IDTO-Se-4F		1.40	0.83	18.55	0.69	10.67	[239]
IDTO-TT-4F		1.38	0.86	17.21	0.69	10.21	
IDT-3MT		1.52	0.95	14.43	0.61	8.40	[260]
ORCN		1.64	0.87	11.50	0.62	6.40	[261]
DF-PCIC		1.59	0.91	15.66	0.72	10.14	[262]
DC6-IC	PBDB-T	1.69	0.99	11.19	0.62	6.87	[242]
DOC6-IC	PBDB-T	1.43	0.91	19.21	0.60	10.52	
DOC8-IC	PBDB-T	1.39	0.92	17.74	0.57	9.41	
DOC2C6-IC	PBDB-T	1.44	0.93	18.85	0.63	11.10	
DOC2C6-2F	PBDB-T	1.42	0.85	21.35	0.73	13.24	
BCDT-4Cl	PBDB-T	1.59	0.76	23.77	0.67	12.10	[263]
NOC6F-1	PBDB-T	1.58	0.95	17.08	0.66	10.62	[264]
NOC6F-2	PBDB-T	1.68	0.96	13.21	0.53	6.74	
FOC6-IC	PBDB-T	1.51	0.93	17.64	0.66	10.80	[244]
FOC6-FIC	PBDB-T	1.47	0.89	19.18	0.71	12.08	
FOC2C6-FIC	PBDB-T	1.43	0.87	19.66	0.72	12.36	
BT-IC4F	PBDB-T	1.37	0.69	21.40	0.66	9.83	[247]
BT2F-IC4F	PBDB-T	1.38	0.67	19.43	0.65	8.45	
BTOR-IC4F	PBDB-T	1.37	0.80	20.57	0.70	11.48	
BDTS-4Cl		1.46	0.83	9.80	0.46	3.73	[265]
BDTC-4Cl		1.42	0.86	18.56	0.60	9.54	
OF-PCIC		1.59	0.91	13.76	0.73	9.09	[241]
HFO-PCIC		1.48	0.93	12.62	0.71	8.36	
DF-PCNC		1.54	0.86	18.16	0.73	11.63	
NoCA-5	J52		0.814	26.02	0.699	14.82	[266]
BN-0F	J52	1.41	0.835	21.91	0.601	11.00	[267]
BN-2F	J52	1.40	0.813	25.25	0.708	14.53	
BN-4F	J52	1.38	0.792	25.76	0.649	13.24	
PTIC	PBDB-TF	1.53	0.93	16.73	0.66	10.27	[250]
PTB4Cl	PBDB-TF	1.58	0.93	19.01	0.722	12.76	[268]
<i>o</i> -4TBC-2F	PBDB-T	1.37	0.76	20.48	0.657	10.26	[251]
<i>m</i> -4TBC-2F	PBDB-T	1.66	0.84	7.90	0.400	2.63	
4T-3	PBDB-T	1.52	0.81	17.27	0.725	10.15	[252]
	D18		0.93	18.28	0.710	12.04	
CH ₃ -2F	PBDB-T	1.42	0.77	22.76	0.6985	12.28	[255]
A4T-16	PBDB-TF	1.45	0.86	21.8	0.798	15.2	[253]
2BTh-2F	D18	1.43	0.90	23.61	0.723	15.44	[256]

optimization of active layer [288–290].

In 2016, Li *et al.* [291] promoted the efficiency of the N2200-based all-PSCs from 5% to 8.27% by using medium bandgap polymer J51 as donor that provided a complementary absorption and suitable phase separation with N2200 acceptor. In 2019, PCE of the N2200-based all-PSCs reached over 11.5% [292,293] with the tailor-made medium bandgap polymer PTzBI-Si [294] (with an imide group fused BTA unit as A-unit) as donor. Despite the great success for N2200 and other rylene diimides-based polymer acceptors, the weak absorption coefficient of N2200 in the NIR region limited its photo current.

In the exploration of alternative polymer acceptor to those rylene diimide-based polymer, polymer acceptors with a variety of electron-deficient units, including diketopyrrolo-pyrrole [294,295], isoindigo [42], thieno[3,4-c]pyrrole-4,6-dione [296], bithiophene imides, [297] B←N bridged unit [298–300] and cyanobenzothiadiazole (DCNBT) [301,302] based n-CPs have also been explored. Among them, polymer acceptors based on B←N bridged bipyridine [303] and DCNBT [301] are more impressive with PCE over 10%.

Liu and coworkers [303] designed B←N bridged unit to construct *n*-type polymer acceptor with a large V_{OC} (>1 V) and a high absorption coefficient in the visible-light range. With structure optimization, their PCEs have improved substantially from 0.12% to over 10.0%. The latter PCE was obtained for the polymer PBN-12 (Figure 21), based on a double B←N bridged bipyridine, and benzothiadiazole unit as the second electron deficient unit. By co-polymerizing DCNBT with IDT, DCNBT-IDT (Figure 21) was obtained with a deep LUMO (-3.75 eV), narrow band gap (1.42 eV), and high absorption coefficient [301], and achieved a respectable PCE of 8.32% in all-PSCs. To further narrow the bandgap, DCNBT-TPIC was designed with carbon-oxygen bridged units as highly electron-rich donor building blocks [302], yielding a bandgap of 1.28 eV and a PCE of

10.22%.

In order to overcome the weak NIR absorbance problem of N2200 and other rylene diimide-based polymer acceptors, Zhang and Li *et al.* [304,305] proposed a new strategy of polymerizing SMA (PSMA) with aromatic thiophene unit (L1) to construct a polymer acceptor PZ1 in 2017 with those SMA as the key building block (Figure 22). The PSMA strategy maintains the virtues (see Figure 22) of SMAs (narrow bandgap, strong absorption, and suitable electronic energy levels) as well as the good film-forming property, outstanding morphology stability and mechanical robustness from the polymers. With PBDB-T as donor, the PZ1-based all-PSCs achieved a high PCE of 9.19% with a V_{OC} of 0.83 V. By replacing of PBDB-T with a lower E_{HOMO} polymer donor of PM6, the PZ1-based all-PSC demonstrated an increased V_{OC} of 0.96 V together with a further increased PCE of 11.2% [306]. One advantage for PMSA strategy is that the physicochemical and photovoltaic properties of the PSMAs can be easily tuned by using different SMA building blocks (Figure 22b, c) as well as the copolymerized linkage units (Figure 22d). Now, the PSMA *n*-type conjugated polymers (*n*-CPs) have received increasing attentions, and many SMAs-building blocks and different conjugated linkage units were used for constructing the high performance PSMAs.

Figure 22 shows the building block of the PSMA that have been reported in literatures. With IDIC (D1) or ITIC (D2 and D3) based SMA building blocks, the resulting PSMA approach enabled PCEs of all-PSCs ranging from 9%–12%. Generally, the extension of conjugation of the SMA unit from tetracyclic core (D1) to pentacyclic core (D2 or D3) results in PSMAs with slightly red-shifted absorption [307,308]. With D1 (Figure 22) as the same building block, the thiophene linkage (denoted as L1) in PZ1 was replaced with bithiophene (BT, L4) [309], bridged BT (L7–L10) [310] and flexible chain tethered thiophene (L3) [311] in synthesizing the PSMAs, producing different photophysical prop-

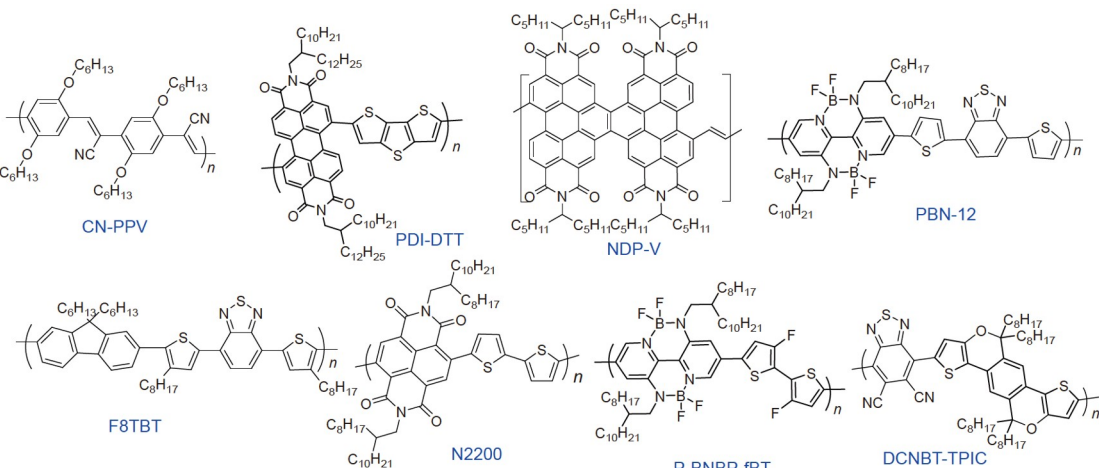


Figure 21 Representative polymer acceptors for all-PSCs (color online).

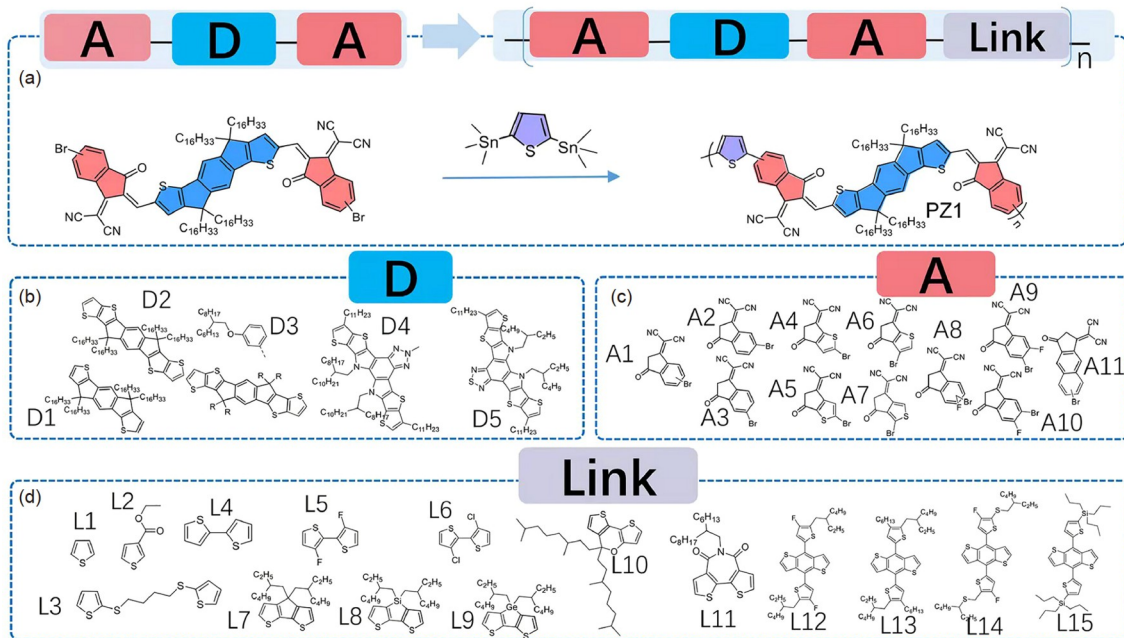


Figure 22 (a) Schematic illustration of the strategy for polymerized SMAs along with (b–d) the building blocks used to construct PSMAs (color online).

erties. Notably, benzodithiophene (BDT) derivative linkages were used (L11–14), showing efficiency in the range of 9%–10% depending on the conjugated side chains attached [312,313].

Recently, inspired by the distinctive advantage of the Y6-type SMAs [205], PSMAs with Y6-type SMA as the key building block were designed by several groups [314–321]. For example, with a bulky 2-decytetradecyl functionalized Y6 derivative as building block, Jia *et al.* [314] reported PJ1 with a high PCE of 14.4% and a low voltage loss of 0.5 V. Independently, Min *et al.* [315] reported PYT with the same conjugated backbone as PJ1 but a slightly shorter side chain, which afforded a PCE of 13.44% in all-PSCs. Specifically, both of their studies highlighted the important role of proper molecular weights of PSMA in achieving high-efficiency all-PSCs. Notably, an approach based on random ternary copolymerization is also effective in synthesizing high performance Y6-based PSMAs [316].

By replacing the commonly used linkage of thiophene (L1) with electron-deficient bithiophene imide (L11, shown in Figure 22d), L14 was obtained with improved *n*-type characteristics and suitable low-lying frontier molecular orbital levels [322]. A high efficiency of 14.3% with a V_{OC} of 0.96 eV was achieved with PM6 as a donor. Fluorination of end groups has been proved to be a great success in developing efficient SMA [323]. By developing a new dihalogenated linkage (A6), PYF-T was designed with the same polymer backbone as PY-T but with an additional F atom on the linkage. This strategy enables PYF-T with stronger and red-shifted absorption spectra, and higher electron mobility, thus a higher efficiency 14.1% than that of PY-T (11.1%)

with PM6 as a donor.

Despite the remarkable progress, regioisomeric issue of the polymer chain is a limitation for better device performance [324]. This issue is brought by the SMA-based dibromide monomer (containing Br group at either 5- or 6-position on the SMAs terminal unit as shown in A1, Figure 22c), which is unfavorable for the crystallinity and the electron mobility of the polymers [325]. Luo *et al.* [326] successfully separated two isomeric end groups (A2 and A3 from A1), and constructed regioregular PSMA (Figure 23) of PY-OT with A2 as a linkage and PY-IT with A3 as a linkage. It shows that from PY-IOT, PY-OT (regiorandom analogue) to PY-IT, and the absorption edge gradually redshifts and electron mobility progressively increases. PM6:PY-IT system achieved an excellent PCE of 15.05%, significantly higher than those for PY-OT (10.04%) and PY-IOT (12.12%). The success of this approach is also demonstrated by Min and co-workers [327] in addressing the regioisomeric issue in PYF-T as mentioned above by developing fluorolinkage groups (A9 and A10), and corresponding PSMAs of PYF-T-o and PYF-T-m. PYF-T-o exhibits stronger and bathochromic absorption and more ordered inter-chain. Devices based on PM6:PYF-T-o can yield a PCE of 15.2%, dramatically higher than that of PM6:PYF-T-m (1.4%). Another high performance regular PSMA is reported by Fu *et al.* by using A3 as the linkage and *N*-methyl-benzotriazole (BTz)-core fused SMA [328], the less-electron deficient BTA [329] as the core of the donor unit. This approach renders PZT- γ a red-shifted absorption, up-shifted energy levels and thus a high PCE of 15.8% with a small E_{loss} of 0.51 eV and a high J_{SC} of 24.7 mA/cm².

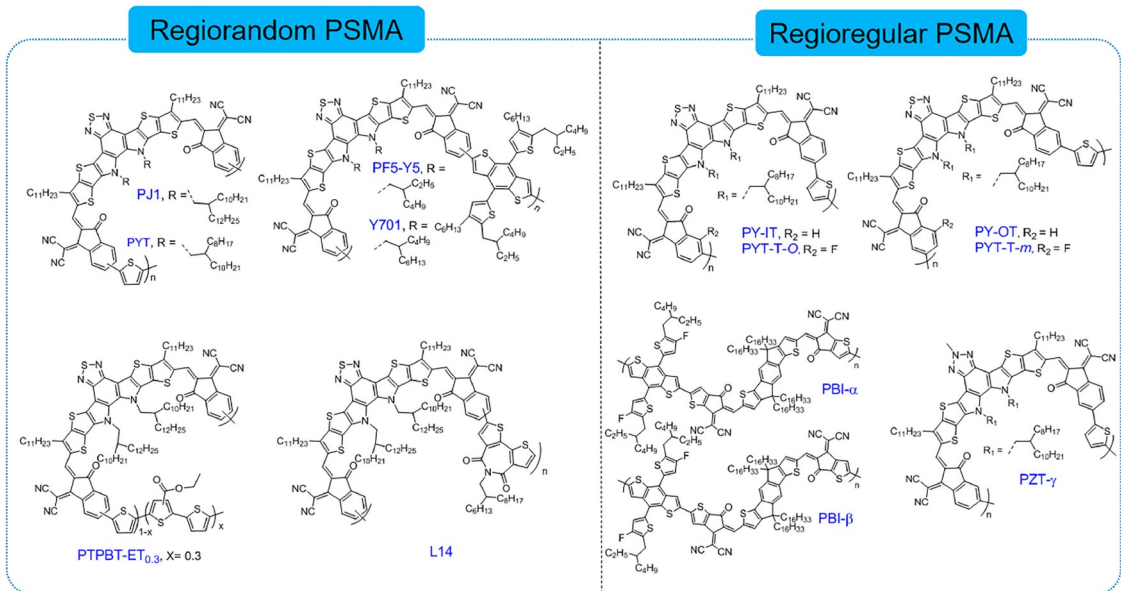


Figure 23 Representative PSMAs for all-PSCs (color online).

Besides developing new PSMAs, there are also a variety of strategies suggested to be effective in improving the performance of all-PSCs, such as molecular weight control of donor [330], stepwise optimization strategy [331,332] and ternary blend. Notably, the morphology control and ternary blend strategies have resulted in the PCE of the all-PSCs over 16% [321,333].

7 Single-component organic solar cells

Single component organic solar cells (SCOSCs) contain only one material in their active layers and get high expectation because of their potential high-stability. Although the BHJ-OSCs with blended D and A materials have higher PCEs that are more than twice of SCOSCs in a long period [1,334,335], some groups around the world still put their efforts into the SCOSCs, mainly focusing on three types of materials: D-A molecular dyads, D-A block copolymers (BCPs) and D/A double-cable conjugated polymers (DCPs). These works enabled the PCEs of SCOSCs to gradually increase to over 8% in the past years. To realize efficiencies as high as BHJ-OSCs, the single-component materials need to be multifunctional with both electron donor parts and electron acceptor parts in one material and bipolar charge-transport property, to simultaneously produce excitons with broad absorption of sunlight, promote the exciton separation with enough donor/acceptor interface and transfer the free charges to the electrodes [336,337]. Therefore, the molecular dyads, BCPs, and DCPs emerged with preeminent performance in SCOSCs caused by different advantages.

For the molecular dyads, fullerenes-like C₆₀, C₇₀, or PCBM

were used as the acceptor part and oligomers such as phenylenevinylene and thiophene segments acted as the donor part in the early years. However, these dyads always showed poor photovoltaic performance with PCEs below 2% because of the unbalanced content of D/A part with narrow absorption spectrum and disadvantaged morphology [336]. Afterwards, electron-deficient units like diketopyrrolo-pyrrole, benzothiadiazole and rhodanine and electron-donating units such as benzodithiophene, dithiafulvalene and fluorene were introduced into the molecular dyads to broaden the photoabsorption region and to tune the energy level and crystallinity of the donor part, and PCEs of the SCOSCs fabricated by these molecule dyads were optimized to 4.26% [338,339]. PDI is an electron-deficient conjugated unit with high crystallinity and commonly used to build electron acceptors in organic solar cells, as well as the molecular dyads for SCOSCs. In 2009, Geng *et al.* [340] used oligo(fluorene-alt-biothiophene)s with liquid crystal properties as donor segment, PDI units as the acceptor part and synthesized a series of linear molecular dyads with different molecular length, as shown in Figure 24. SCOSCs based on these dyads had the highest PCE up to 1.5% and external quantum efficiencies (EQE) up to 0.46 at 410–500 nm as highly ordered films can be obtained with comprising alternating D-A lamellar nanostructures in their active layers. Through the transmission electron microscopy (TEM) measurements, when dyad films were annealed at 210 °C for 2 min, all the three molecule films could get dark-bright stripes (Figure 25d), while ordered structures can be found only in F5T8-hP system. Interestingly, the order degree could be enhanced by vapor annealing with CH₂Cl₂. As shown in Figure 25d, the solvent-vapor annealed films showed much

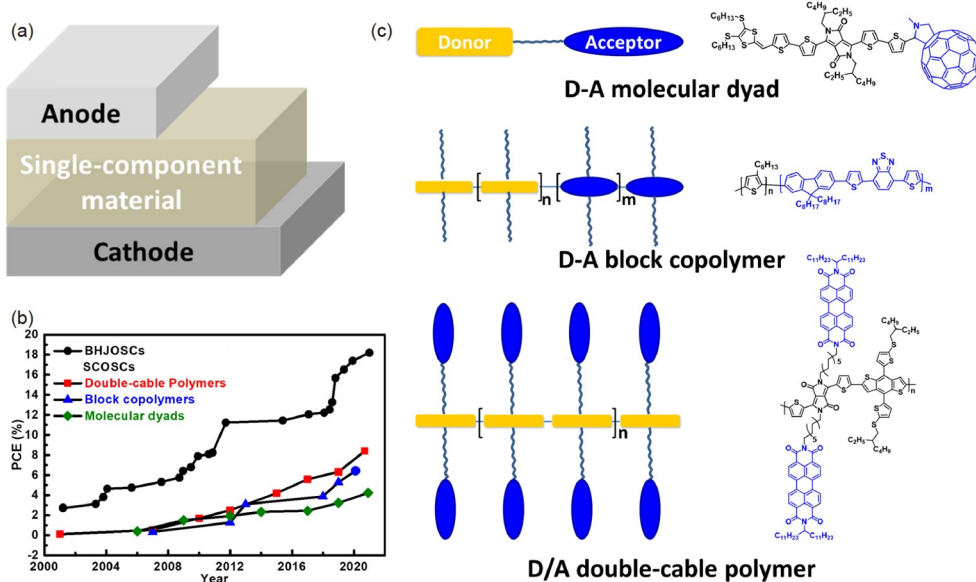


Figure 24 (a) Illustration of SCOSCs, (b) PCEs of different types of OSCs since 2000 and (c) schematic diagram of different material concepts and represented examples for SCOSCs (color online).

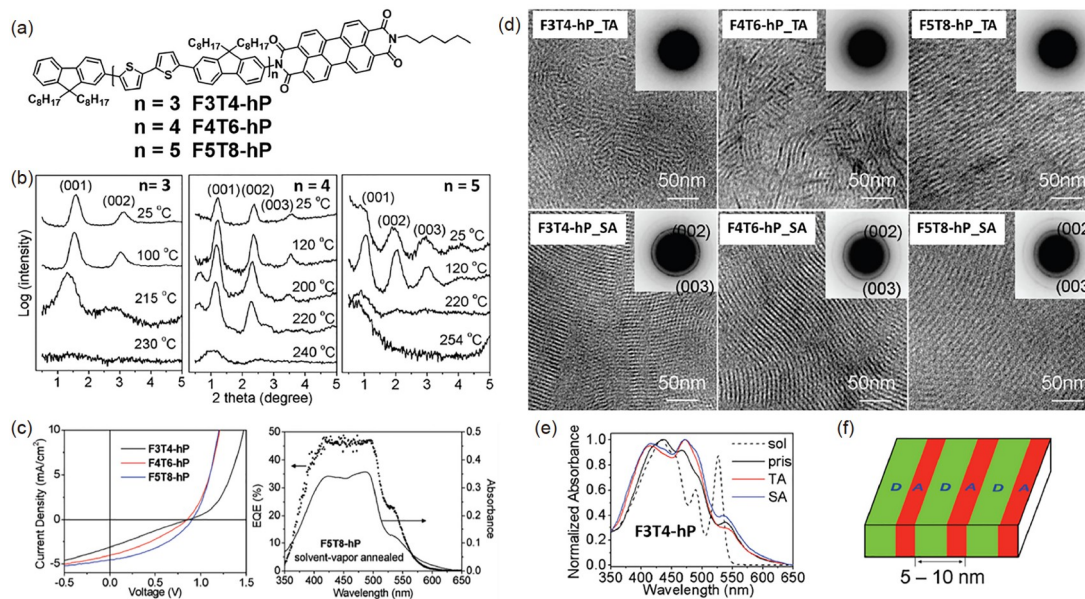


Figure 25 (a) Chemical structures, (b) SAXS of the powders at different temperatures, (c) current density-voltage ($I-V$) characteristics and EQE spectra, (d) TEM images and selected area electron diffraction (SAED) patterns (e) absorption spectra, and (f) schematic illustration of the lamellar nanostructures [340] (color online).

longer persistent lengths (100–400 nm) of the lamellae than the thermally annealed films (50–150 nm), and bigger crystalline sizes of the lamellae (5.6, 7.4, and 8.9 nm for F3T4-hP, F4T6-hP and F5T8-hP respectively). As shown in Figure 25e, f, the UV-vis absorption spectra of the molecular dyads showed that the PDI units in the films are face-to-face stacked (H-aggregation), and the authors concluded these films had alternating D-A lamellar nanostructures with the period varying from the molecular length. These results indicated that the D-A type molecular dyads could be a good

choice to design high-performance materials for SCOSCs [341,342].

In high-performance BHJ-OSCs, polymers were commonly used as donors, and in the SCOSCs, BCPs and DCs were the two main types of polymers. As their self-assembly characteristics, BCPs were widely studied to obtain multi-function. In the early time, oligo phenylenevinylene and oligothiophenes were commonly used as donor segment, while PDI and benzothiadiazole-based blocks were chosen as acceptor segment. However, the related SCOSCs always

showed low PCEs [343]. In 2013, Verduzco *et al.* [344] reported a new BCP (P3HT-*b*-PFTBT) with alternating P3HT donor part and PFTBT acceptor part, which could self-assemble into in-plane lamellar morphologies. SCOSCs based on P3HT-*b*-PFTBT showed a PCE of 3.1% with a high V_{OC} of 1.2 V. Besides, N2200 and its derivatives were widely studied in organic field-effect transistors, photodetectors and OSCs because of their near-infrared absorption, low-lying energy levels, high crystallinity with good solubility in common solvents [284,345–349]. Therefore, Nakabayashi *et al.* [350] and Choi *et al.* [351–354] introduced N2200 or its derivatives as acceptor segment to the BCPs, reported a lot of work on SCOSCs and improved the PCE step by step since 2012. Especially, Choi *et al.* [353,354] have reported a new polymerization method that can synthesize a new BCP by performing the entire reaction in one-pot from start to completion, which can reduce the synthesis time and lower the cost. As shown in Figure 26, it is a new BCP (named PBDT2T-*b*-N2200) with a record PCE in SCOSCs. They started with the synthesis of the acceptor block of N2200 by adding the monomers M1 and M2 into the reaction system after a period of time, the monomers M3 and M4 were added and reacted to form the donor part from the tail of N2200. The entire synthesis process was done through the typical Stille coupling reaction with a palladium catalyst and the molecular weight of the polymer was controlled by the reaction time. As a result, PBDT2T-*b*-N2200 possessed a complementary absorption from 300 to 800 nm. When the film was thermally treated for 10 min, the SCOSCs showed a record PCE of 6.43% among the BCP-based SCOSCs [354]. Furthermore, the devices of the high-performance SCOSCs showed excellent stability with the PCE decreasing less than 10% under ambient conditions for 1,020 h, which was much better than the related BHJ devices. Such a work indicated the advantage of the BCPs in the application of SCOSCs.

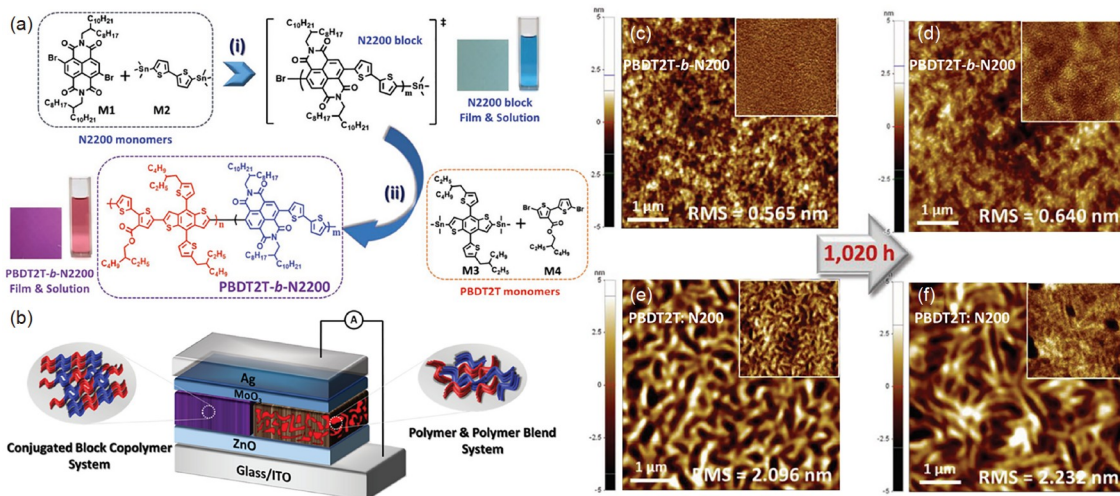


Figure 26 (a) Synthesis procedure of PBDT2T-*b*-N2200, (b) device structures, (c–f) atomic force microscopy (AFM) of the films before aging and after aging under ambient conditions in the dark [354] (color online).

Double-cable polymers are another type of polymers for SCOSCs. The first DCP, a polythiophene with pendant C₆₀ was reported by Benincori *et al.* [355] in 1996 and synthesized *via* electrochemical polymerization. However, the poor solubility in common solvents prevented it from being applied in solution-processed OSCs. In 2001, Janssen *et al.* [356] and Zhang *et al.* [357] simultaneously reported solution-processed SCOSCs with poly(*p*-phenylenevinylene) or polythiophene as the conjugated backbone as a donor and fullerene derivatives as the pendant acceptor. After that, DCP based on polythiophene with pendant fullerenes became the main materials that were applied in SCOSCs, and most of these DCPs were synthesized by a strategy of “polymerization-post functionalization”. The PCE of these DCP-based SCOSCs can also be up to 5% recently by tuning the content ratio, linkages of the donor and acceptor part, or refining the chemical structures.

Since 2017, Li *et al.* [334,337] have developed a synthetic method of “functionalization-polymerization” and reported a series of double-cable polymers with PDI or its derivatives as pendant acceptor. By such an effective method, several high performance donor polymers were successfully introduced to the DCPs. As a result, the record PCE of SCOSCs was broken repeatedly by fine regulation of the chemical structures (including the conjugated backbone, linkers, and acceptor units) and the nanophase separation of the donor and acceptor pairs in the films. The design of linear backbone facilitated a nanophase separation of about 5 nm between the donor and acceptor parts, and in DCP SF-PBDTPBI (Figure 27a), it further promoted high EQE up to 0.65 [358]. When the electron-deficient unit 5,7-bis(2-ethylhexyl)benzo[1,2-*c*:4,5-*c'*]dithiophene-4,8-dione was introduced into the backbone, they obtained a new DCP PBDBPBI-Cl with broader absorption. Surprisingly, the film of PBDBPBI-Cl could self-organize to well-ordered D/A lamellar nanos-

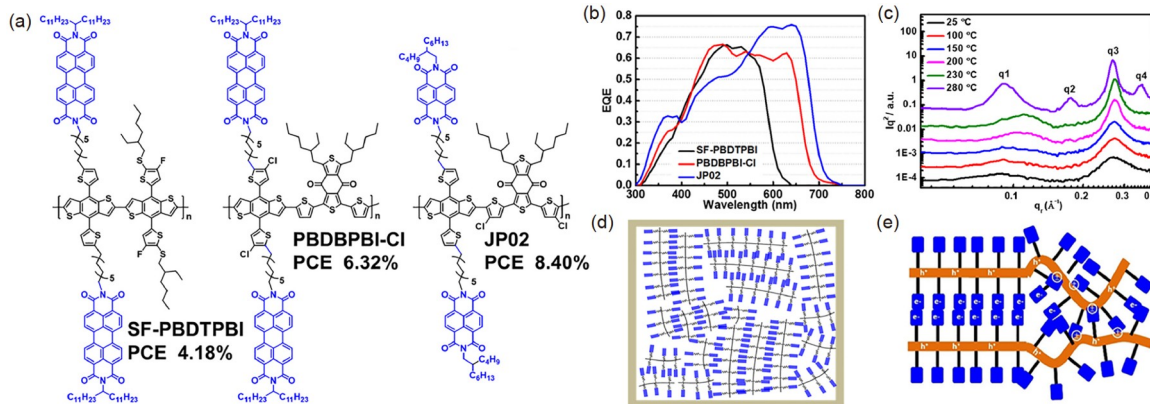


Figure 27 (a) Chemical structure and (b) EQE of the DCPs, (c) GIMAXS scattering curves and (d) the proposed illustration of the ordered film of PBDBPBI-Cl, (e) the idealized model to illustrate the crystalline region and amorphous regions of JP02 [358–360] (color online).

ture after thermal annealing under a high temperature, as shown in Figure 27c, leading to a high-performance SCOSC with PCE up to 6.32% [359]. Recently, they used naphthalenediimide (NDI) to replace the PDI as an acceptor and fine-tuned the backbone with Cl atoms on different positions of the backbone. Their studies on the morphology and crystallinity of the films revealed that the miscibility of the donor and acceptor parts were important to charge generation, and consequently they obtained a record PCE of 8.4% with the highest EQE over 0.75 in the SCOSCs based on JP02 where the Cl atoms were on the main chain of the backbone, as shown in Figure 27. This work expressed a new stage of controlling the miscibility of the D/A parts in DCP to optimize the performance of SCOSCs [360].

Above all, SCOSCs performed a great potential to get high PCEs *via* chemical structure engineering, morphology controlling, and tuning the nanophase separation. The proven excellent stability [361] also demonstrated the SCOSCs' capability of practical application.

8 Water/alcohol soluble conjugated polymers for the interface engineering of organic solar cells

Typical BHJ OSCs usually use a multilayer device architecture (Figure 28a), including the active layer, the hole and electron collecting electrodes and corresponding interlayers. The interlayers between the active layer and electrodes aim to facilitate hole and electron transport/collection, which are crucial to achieve high-performance OSCs [362–364]. The interlayers are capable of changing polarity of electrodes and minimizing energy barrier to collect charge selectively. Besides, the interlayers can also tune surface property, protect organic layer and modulate the optical field, which synergistically promote the device performance [363,364]. In the past two decades, a variety of anode interlayers (such as PEDOT:PSS [365] and its derivatives [366,367], p-type

conjugated polymers [368,369], and inorganic oxide semiconductor [370]) and cathode interlayers (small molecules and polymers [362–364,371,372], ZnO [373], etc.) were reported and exhibited great promise to improve the photovoltaic performance.

The most widely studied interlayers for the cathode modification are water/alcohol soluble conjugated polymers (WSCPs) due to their advantages of semi-conductivity and excellent processability from environmentally-friendly solvents. This kind of materials shares polar side chains such as ionic groups, making them soluble and processable in water/alcohol-like polar solvents. Combining with non/low-polar solvents soluble active materials and WSCPs, the multi-layer OSCs could be prepared *via* successive solution processing from orthogonal solvents without interface mixing between different layers. The insertion of such a thin-layer WSCP can form dipole interactions with the metal electrode and enhance the electron collection efficiency of the high work function metal electrode. For example, the polyfluorene-based WSCPs, such as PFN and PFN-Br (Figure 28c) are widely used as cathode interlayers to improve electron collection of OSCs [374,375]. A thin layer of cathode interlayer can reduce the work function of the metal electrode, block holes to the cathode, optimize the active layer morphology, etc [375–377]. Moreover, it was found that side chains in PFN and PFN-Br are capable of doping PCBM in the interface, resulting in improved electron collection in the cathode [376].

In recent years, the rapid improvement in the PCE of OSCs implies the great potential for commercial application. Large-scale OSC modules employ a scalable roll-to-roll processing protocol, which requires high-mobility active layer/interlayer that works well in a wide thickness range. Although non-conjugated molecules (such as PEIE and PEI [371]) and polyfluorene-based WSCPs are widely used to achieve high efficiency; however, they can only work well in a small thickness range of 5–10 nm due to their low electron

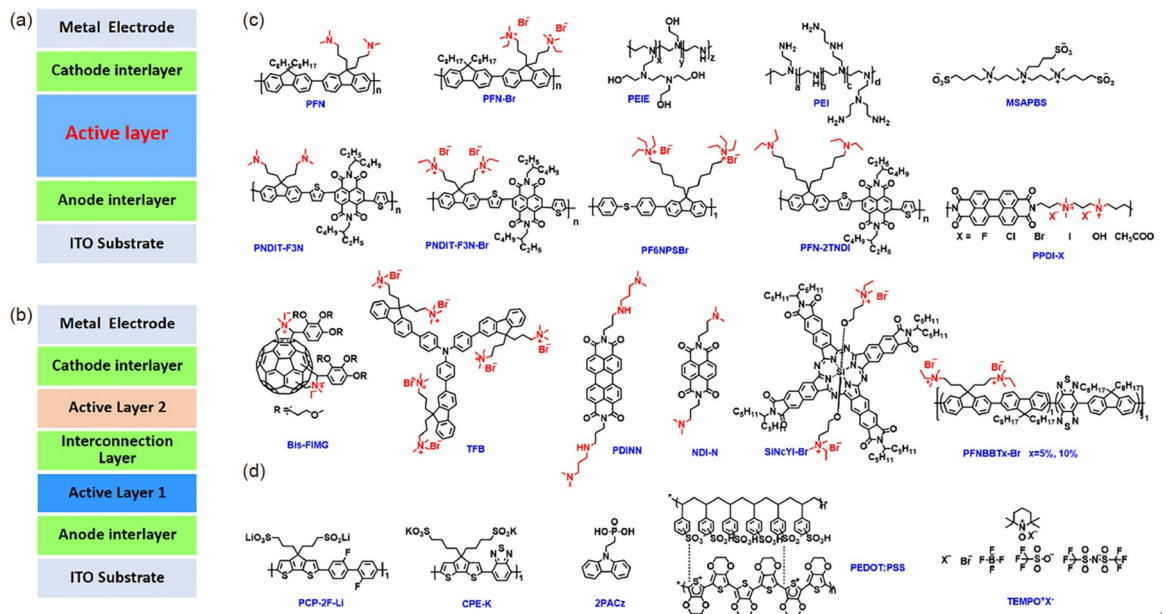


Figure 28 Device architecture of single-junction OSCs (a) and tandem OSCs (b); (c) chemical structure of interlayers for cathode modification; (d) chemical structure of interlayers for anode modification (color online).

mobilities. Thus, designing new WSCP with higher conductivities will be more compatible with the fabrication of large-scale OSC modules.

To overcome this issue, rational doping on the conjugated skeleton is proved to be an efficient strategy to enhance the charge transporting properties [378–381]. Addition of n-type dopants (such as water/alcohol soluble alkali salt) to the WSCPs exhibits a simple and efficient protocol to improve the charge transporting properties of polyfluorene-based WSCPs [382]. Xu *et al.* [383] applied a Cs₂CO₃ doping strategy to a polyfluorene-based polymer PF6NPSBr (Figure 28c) and realized a cathode interlayer with improved conductivity. It was found that Cs₂CO₃-doped PF6NPSBr showed enhanced electron transport ability and thickness-insensitive (thickness up to 50 nm) characteristic in OSCs. Tang *et al.* [384] revealed that multi-valent anions (including Ox²⁻, CO₃²⁻, and SO₃²⁻) could work as powerful electron donors to realize n-doping in multiple conjugated polymers, providing a general method to realize highly conductive cathode interlayers for OSCs.

An alternative strategy is to develop self-doped WSCPs, whose self-doping process occurs between the counterions and n-type backbones. A representative example is the naphthalene diimide-based WSCP PNDIT-F3N and its quaternized derivative PNDIT-F3N-Br (Figure 28c) [380]. The highly polar amino- or ammonium-functionalized side chains make them well-soluble in polar solvents. Compared with polyfluorene type WSCPs, the incorporation of n-type conjugated backbone in PNDIT-F3N/PNDIT-F3N-Br endow themselves with strong self-doping behaviors and high conductivity. Notable is that PNDIT-F3N/PNDIT-F3N-Br

exhibits different doping behaviors because of their different side chains. PNDIT-F3N shows a photoinduced conductivity-enhancing property, while the PNDIT-F3N-Br can be self-doped without light excitation. Resultingly, the electron mobilities of these self-doped WSCPs are much improved, enabling a large processing window for application in OSCs as cathode interlayers. OSCs with a 5 nm PNDIT-F3N-Br could achieve 10% PCE, and a 100 nm PNDIT-F3N-Br can also enable OSCs with PCE over 8% [380]. A special finding is that thick PNDIT-F3N could contribute to the exciton dissociation in the device due to the appropriate offset of energy levels between the donor and PNDIT-F3N, resulting in extra photocurrent output and improved electron collection at the cathode [385].

The high mobility of these n-type WSCPs enables the fabrication of thickness-insensitive cathode interlayer for both fullerene and nonfullerene solar cells [380,385]. Moreover, the thick n-type WSCPs could also slow down and block the diffusion of metal atoms from the cathode, thus improving the device stability [386]. In addition, these n-type WSCPs showed great potential in the application of tandem OSCs (Figure 28b) as one part of the interconnection layer (ICL) [387,388]. Zhang *et al.* [388] employed PNDIT-F3N as one component of ICL and construct a solution-processed, robust and thick (up to 140 nm) interconnection layer in combination with PEDOT:PSS. Besides the application in OSCs, WSCPs could be applied as efficient electron-transporting materials for perovskite solar cells (PVKSCs). Sun *et al.* [389] employed PFN-2TNDI (Figure 28c) as the electron transport materials to fabricate PVKSCs. It was found that PFN-2TNDI can passivate the surface in-

terface traps of the perovskite layer, resulting in reduced interface recombination and enhanced device performance of PVKSCs.

The doping behaviors of these n-type WSCPs could be further regulated by changing the counterion type and chemical structure of conjugated backbones [390]. Chen *et al.* [390] reported a series of counterion-tunable n-type WSCPs and found that the size, species and substituent groups of the counterions in WSCPs greatly affect the OSC performance. Counterions with strong electron-withdrawing substituent groups in WSCPs would preclude the self-doping behaviors from counterions to conjugated backbones, increase the work function of metal electrodes, and impede electron transport. The effect of counterions on the different doping behaviors was also verified in perylene diimide-based polyelectrolytes. Hu *et al.* [391] prepared a series of perylene diimide-based polyelectrolytes (PPDI-X, Figure 28d) with different counterions. It was found that F^- , OH^- , and CH_3COO^- in WSCPs act as strong n-type dopants, enabling stronger self-doping behaviors, while WSCPs with Cl^- , Br^- , and I^- exhibit weak self-doping properties [378]. The conjugated backbones of WSCPs also greatly impact their self-doping behaviors. Hu *et al.* [392] designed a series of tailor-made n-WSCPs with different conjugated backbones and investigate the relevance of the doping behaviors and structures of n-WSCPs. It was found that n-type backbone with better planarity and a higher affinity would promote the self-doping process and charge transport properties, resulting in improved performance in OSCs.

Self-doped molecular interlayers for OSCs were also extensively explored. For example, Yan *et al.* [393] designed a series of fullerene derivatives (FPPI, Bis-FPPI, Bis-FIMG and Bis-FITG, Figure 28c) with anion-induced n-doping behaviors between quaternary ammonium halides and adjacent π -acidic fullerene, resulting in fullerene derivatives with suitable conductivities, work-function tunability and orthogonal solution-process abilities. Wang *et al.* [394] synthesized a series of star-shaped small molecular cathode interlayer (TFB, Figure 28c) with triphenylamine unit as a core and amino-functionalized fluorene units as the arms, which could effectively lower the work function of the Al cathode, increase the built-in potential, and thus increase the PCE of OSCs. Kang *et al.* [395] reported a naphthalene diimide-based small molecular (NDI-N, Figure 28c) as a printable cathode interlayer for OSCs. It was found that NDI-N can efficiently extract electrons from both the nonfullerene acceptor and the polymer donor. Besides, NDI-N can be used for the fabrication of large-area devices due to the excellent electron transport capability and good processability. Yao *et al.* [396] synthesized aliphatic amine-functionalized perylene-diimide (PDINN, Figure 28c) as cathode interlayer, which could decrease the work function of the air-stable cathodes (Ag, Cu, etc.) and maintain good interfacial contact

with the active layer due to the hydrogen bond of the secondary amine in the side chains of PDINN. OSCs based on PM6:Y6 achieved a high PCE of 17.23% with PDINN/Ag as cathode interlayer/electrode. Cai *et al.* [397] applied naphthalocyanine derivatives (SiNcTI-N and SiNcTI-Br, Figure 28c) as an electron transport layer, and the strong self-doping properties between quaternary ammonium salt and naphthalocyanines enabled SiNcTI-Br with high electron mobility, which boosted the PCE of PM6:Y6-based OSCs to 16.71%.

The above self-doped interface materials with high conductivity usually possess stronger absorption in the visible range. N-doped WSCPs with high conductivity and great visible light transmittance is challenging but crucial to application in OSC devices. Recently, Tang *et al.* [398] introduce a diradical benzobisthiadiazole (BBT) unit into the backbones of a wide-band-gap WSCP PFNBr, resulting in new WSCPs PFNBBT5%-Br and PFNBBT10%-Br (Figure 28c). It was found that the diradical resonance of BBT units promotes the aromatic and anti-aromatic transition in the conjugated chain, thus improving the self-doping level. PFNBBT10%-Br exhibits high n-type conductivity with high transmittance in the visible region. Benefited from high visible transmittance and improved conductivity, OSC devices with PFNBBT10%-Br achieved nearly 16% PCE even when the thickness of PFNBBT10%-Br was over 50 nm.

Anode interlayers were also developed to improve the hole transport and collection in the anode of OSCs. Lu *et al.* [399] synthesized a p-doped and pH-neutral WCSP PCP-2F-Li (Figure 28d) as anode interlayer, which could effectively increase the work function of ITO electrode. OSCs based on PBDB-T-2F:IT-4F exhibited PCE of 12.7% using solution-processed PCP-2F-Li as anode interlayer. Besides, PCP-2F-Li could be used to fabricate large-area device of 1 cm² with PCE of 10.6%. Zhou *et al.* [400] synthesized a pH-neutral WSCP CPE-K (Figure 28d) as the anode interlayer for OSCs. Compared with OSCs with PEDOT:PSS as anode interlayer, p-DTS(PTTh₂)₂:PC₇₁BM-based OSCs exhibit a 60% increase in PCE with CPE-K as anode interlayer due to the elimination of interfacial protonation and energy barriers. Besides, modification on PEDOT:PSS was proved to be an efficient strategy to realize high-performance anode interlayers [367,401,402]. For example, Tang *et al.* [367] employed oxoammonium salts (TEMPO^+X^- , Figure 28d) with different counterions as secondary dopants for PEDOT:PSS, resulting in more efficient charge transfer between TEMPO^+X^- and PEDOT:PSS and thus enhanced carrier density and carrier mobility. OSCs based on secondary doped PEDOT:PSS as anode interlayer showed higher PCE than that of the pristine PEDOT:PSS. Lin *et al.* [335] reported a molecular 2PACZ (Figure 28d), which can be used as a powerful anode interlayer for OSCs. Devices with a thin layer of 2PACZ showed decreased contact resistance be-

tween anodes and active layers, reduced bimolecular recombination, and improved charge extraction in the anode. Chen *et al.* [222,335] evaluated the photovoltaic performance of OSCs based on different anode interlayers. Notably, devices based on 2PACz achieved higher PCE than that of PEDOT:PSS-based devices. Further investigation indicated that the remarkably enhanced PCE mainly originated from the improved J_{SC} due to higher average transmittance of 2PACz in the ranges of 500–800 nm. However, the PCE of 2PACz-based devices exhibited a sharply decline with only 10% of their initial PCE maintained after 90 h illumination, indicating that further exploration on transparent anode interlayers for stable OSCs is required.

9 Conclusions and outlook

Herein, we systematically summarize recent progress and development on materials science in organic solar cells field, including conjugated polymer donors, oligomer-like small molecular donors, fused ring and nonfused acceptors, polymer acceptors, single-component organic solar cells, and interface materials. We expected our review could provide valuable insight in the development of OSCs materials and promote the practical application of OSCs.

Acknowledgements This work was supported by the National Natural Science Foundation of China (51933001, 22109080, 21734009, 52173174).

Conflict of interest The authors declare no conflict of interest.

- 1 Liu Q, Jiang Y, Jin K, Qin J, Xu J, Li W, Xiong J, Liu J, Xiao Z, Sun K, Yang S, Zhang X, Ding L. *Sci Bull*, 2020, 65: 272–275
- 2 Li Y, Huang X, Ding K, Sheriff Jr HKM, Ye L, Liu H, Li CZ, Ade H, Forrest SR. *Nat Commun*, 2021, 12: 5419
- 3 Kallmann H, Pope M. *J Chem Phys*, 1959, 30: 585–586
- 4 Chamberlain GA. *Sol Cells*, 1983, 8: 47–83
- 5 Shirakawa H, Louis EJ, MacDiarmid AG, Chiang CK, Heeger AJ. *J Chem Soc Chem Commun*, 1977, 578–580
- 6 Tang CW. *Appl Phys Lett*, 1986, 48: 183–185
- 7 Sariciftci NS, Smilowitz L, Heeger AJ, Wudl F. *Science*, 1992, 258: 1474–1476
- 8 Yu G, Gao J, Hummelen JC, Wudl F, Heeger AJ. *Science*, 1995, 270: 1789–1791
- 9 Mahmood A, Wang JL. *Energy Environ Sci*, 2021, 14: 90–105
- 10 Han G, Yi Y, Shuai Z. *Adv Energy Mater*, 2018, 8: 1702743
- 11 Chow PCY, Someya T. *Adv Mater*, 2020, 32: 1902045
- 12 Park S, Heo SW, Lee W, Inoue D, Jiang Z, Yu K, Jinno H, Hashizume D, Sekino M, Yokota T, Fukuda K, Tajima K, Someya T. *Nature*, 2018, 561: 516–521
- 13 Ravishankar E, Booth RE, Saravitz C, Sederoff H, Ade HW, O'Connor BT. *Joule*, 2020, 4: 490–506
- 14 Yu G, Heeger AJ. *J Appl Phys*, 1995, 78: 4510–4515
- 15 Schilinsky P, Waldauf C, Brabec CJ. *Appl Phys Lett*, 2002, 81: 3885–3887
- 16 Li G, Shrotriya V, Huang J, Yao Y, Moriarty T, Emery K, Yang Y. *Nat Mater*, 2005, 4: 864–868
- 17 Guo X, Cui C, Zhang M, Huo L, Huang Y, Hou J, Li Y. *Energy Environ Sci*, 2012, 5: 7943
- 18 Yang C, Zhang S, Ren J, Gao M, Bi P, Ye L, Hou J. *Energy Environ Sci*, 2020, 13: 2864–2869
- 19 Svensson M, Zhang F, Veenstra SC, Verhees WJH, Hummelen JC, Kroon JM, Inganäs O, Andersson MR. *Adv Mater*, 2003, 15: 988–991
- 20 Cui C, Li Y. *Energy Environ Sci*, 2019, 12: 3225–3246
- 21 Winder C, Sariciftci NS. *J Mater Chem*, 2004, 14: 1077–1086
- 22 Günes S, Neugebauer H, Sariciftci NS. *Chem Rev*, 2007, 107: 1324–1338
- 23 Chen J, Cao Y. *Acc Chem Res*, 2009, 42: 1709–1718
- 24 Cheng YJ, Yang SH, Hsu CS. *Chem Rev*, 2009, 109: 5868–5923
- 25 Boudreault PLT, Najari A, Leclerc M. *Chem Mater*, 2011, 23: 456–469
- 26 Li G, Zhu R, Yang Y. *Nat Photon*, 2012, 6: 153–161
- 27 Li Y. *Acc Chem Res*, 2012, 45: 723–733
- 28 Xu T, Yu L. *Mater Today*, 2014, 17: 11–15
- 29 Liu C, Wang K, Gong X, Heeger AJ. *Chem Soc Rev*, 2016, 45: 4825–4846
- 30 Cai Y, Huo L, Sun Y. *Adv Mater*, 2017, 29: 1605437
- 31 Holliday S, Li Y, Luscombe CK. *Prog Polym Sci*, 2017, 70: 34–51
- 32 Li Z, Chueh CC, Jen AKY. *Prog Polym Sci*, 2019, 99: 101175
- 33 Gao K, Kan Y, Chen X, Liu F, Kan B, Nian L, Wan X, Chen Y, Peng X, Russell TP, Cao Y, Jen AKY. *Adv Mater*, 2020, 32: 1906129
- 34 An C, Zheng Z, Hou J. *Chem Commun*, 2020, 56: 4750–4760
- 35 Hou J, Inganäs O, Friend RH, Gao F. *Nat Mater*, 2018, 17: 119–128
- 36 Meng L, Zhang Y, Wan X, Li C, Zhang X, Wang Y, Ke X, Xiao Z, Ding L, Xia R, Yip HL, Cao Y, Chen Y. *Science*, 2018, 361: 1094–1098
- 37 Cui Y, Hong L, Hou J. *ACS Appl Mater Interfaces*, 2020, 12: 38815–38828
- 38 Brus VV, Lee J, Luginbuhl BR, Ko SJ, Bazan GC, Nguyen TQ. *Adv Mater*, 2019, 31: 1900904
- 39 Zhang M, Guo X, Zhang S, Hou J. *Adv Mater*, 2014, 26: 1118–1123
- 40 Grem G, Leditzky G, Ullrich B, Leising G. *Adv Mater*, 1992, 4: 36–37
- 41 Yamamoto T, Sugiyama K, Kushida T, Inoue T, Kanbara T. *J Am Chem Soc*, 1996, 118: 3930–3937
- 42 Stalder R, Mei J, Subbiah J, Grand C, Estrada LA, So F, Reynolds JR. *Macromolecules*, 2011, 44: 6303–6310
- 43 Kobayashi M, Chen J, Chung TC, Moraes F, Heeger AJ, Wudl F. *Synth Met*, 1984, 9: 77–86
- 44 Hou J, Park MH, Zhang S, Yao Y, Chen LM, Li JH, Yang Y. *Macromolecules*, 2008, 41: 6012–6018
- 45 Wang H, Lu H, Chen YN, Ran G, Zhang A, Li D, Yu N, Zhang Z, Liu Y, Xu X, Zhang W, Bao Q, Tang Z, Bo Z. *Adv Mater*, 2021, 2105483
- 46 Berrouard P, Dufresne S, Pron A, Veilleux J, Leclerc M. *J Org Chem*, 2012, 77: 8167–8173
- 47 Wang Y, Yan Z, Guo H, Uddin MA, Ling S, Zhou X, Su H, Dai J, Woo HY, Guo X. *Angew Chem Int Ed*, 2017, 56: 15304–15308
- 48 Pomerantz M, Gu X. *Synth Met*, 1997, 84: 243–244
- 49 Wudl F, Kobayashi M, Heeger AJ. *J Org Chem*, 1984, 49: 3382–3384
- 50 Pomerantz M, Chaloner-Gill B, Harding LO, Tseng JJ, Pomerantz WJ. *Synth Met*, 1993, 55: 960–965
- 51 Yao H, Ye L, Zhang H, Li S, Zhang S, Hou J. *Chem Rev*, 2016, 116: 7397–7457
- 52 Wang C, Liu F, Chen QM, Xiao CY, Wu YG, Li WW. *Chin J Polym Sci*, 2021, 39: 525–536
- 53 Liu M, Gao Y, Zhang Y, Liu Z, Zhao L. *Polym Chem*, 2017, 8: 4613–4636
- 54 Zhao C, Yang F, Xia D, Zhang Z, Zhang Y, Yan N, You S, Li W. *Chem Commun*, 2020, 56: 10394–10408
- 55 Liang Y, Wu Y, Feng D, Tsai ST, Son HJ, Li G, Yu L. *J Am Chem Soc*, 2009, 131: 56–57
- 56 Zheng Z, Yao H, Ye L, Xu Y, Zhang S, Hou J. *Mater Today*, 2020,

- 35: 115–130
- 57 Pomerantz M, Yang H, Cheng Y. *Macromolecules*, 1995, 28: 5706–5708
- 58 Murphy AR, Liu J, Luscombe C, Kavulak D, Fréchet JMJ, Kline RJ, McGehee MD. *Chem Mater*, 2005, 17: 4892–4899
- 59 Zhang M, Guo X, Yang Y, Zhang J, Zhang ZG, Li Y. *Polym Chem*, 2011, 2: 2900–2906
- 60 Zhang M, Guo X, Ma W, Ade H, Hou J. *Adv Mater*, 2014, 26: 5880–5885
- 61 Qin Y, Uddin MA, Chen Y, Jang B, Zhao K, Zheng Z, Yu R, Shin TJ, Woo HY, Hou J. *Adv Mater*, 2016, 28: 9416–9422
- 62 Wang Q, Li M, Zhang X, Qin Y, Wang J, Zhang J, Hou J, Janssen RAJ, Geng Y. *Macromolecules*, 2019, 52: 4464–4474
- 63 Yao H, Qian D, Zhang H, Qin Y, Xu B, Cui Y, Yu R, Gao F, Hou J. *Chin J Chem*, 2018, 36: 491–494
- 64 Park GE, Choi S, Park SY, Lee DH, Cho MJ, Choi DH. *Adv Energy Mater*, 2017, 7: 1700566
- 65 Liu D, Yang B, Jang B, Xu B, Zhang S, He C, Woo HY, Hou J. *Energy Environ Sci*, 2017, 10: 546–551
- 66 Li S, Ye L, Zhao W, Yan H, Yang B, Liu D, Li W, Ade H, Hou J. *J Am Chem Soc*, 2018, 140: 7159–7167
- 67 Yao H, Cui Y, Qian D, Ponseca Jr. CS, Honarfar A, Xu Y, Xin J, Chen Z, Hong L, Gao B, Yu R, Zu Y, Ma W, Chabera P, Pullerits T, Yartsev A, Gao F, Hou J. *J Am Chem Soc*, 2019, 141: 7743–7750
- 68 Wang Q, Dong X, He M, Li M, Tian H, Liu J, Geng Y. *Polymer*, 2018, 140: 89–95
- 69 Lu H, Jiang P, Wei Y, Yuan S, Liu Y, Li W, Xu X, Bo Z. *Sol RRL*, 2020, 4: 2000547
- 70 Ren J, Bi P, Zhang J, Liu J, Wang J, Xu Y, Wei Z, Zhang S, Hou J. *Natl Sci Rev*, 2021, 8: nwab031
- 71 Zhang Q, Kelly MA, Bauer N, You W. *Acc Chem Res*, 2017, 50: 2401–2409
- 72 Min J, Zhang ZG, Zhang S, Li Y. *Chem Mater*, 2012, 24: 3247–3254
- 73 Price SC, Stuart AC, Yang L, Zhou H, You W. *J Am Chem Soc*, 2011, 133: 4625–4631
- 74 Bin H, Zhang ZG, Gao L, Chen S, Zhong L, Xue L, Yang C, Li Y. *J Am Chem Soc*, 2016, 138: 4657–4664
- 75 Bin H, Gao L, Zhang ZG, Yang Y, Zhang Y, Zhang C, Chen S, Xue L, Yang C, Xiao M, Li Y. *Nat Commun*, 2016, 7: 13651
- 76 Lin Y, Zhao F, Prasad SKK, Chen JD, Cai W, Zhang Q, Chen K, Wu Y, Ma W, Gao F, Tang JX, Wang C, You W, Hodgkiss JM, Zhan X. *Adv Mater*, 2018, 30: 1706363
- 77 Lan L, Chen Z, Hu Q, Ying L, Zhu R, Liu F, Russell TP, Huang F, Cao Y. *Adv Sci*, 2016, 3: 1600032
- 78 Fan B, Zhang D, Li M, Zhong W, Zeng Z, Ying L, Huang F, Cao Y. *Sci China Chem*, 2019, 62: 746–752
- 79 Mühlbacher D, Scharber M, Morana M, Zhu Z, Waller D, Gaudiana R, Brabec C. *Adv Mater*, 2006, 18: 2884–2889
- 80 Lee JK, Ma WL, Brabec CJ, Yuen J, Moon JS, Kim JY, Lee K, Bazan GC, Heeger AJ. *J Am Chem Soc*, 2008, 130: 3619–3623
- 81 Hou J, Chen HY, Zhang S, Li G, Yang Y. *J Am Chem Soc*, 2008, 130: 16144–16145
- 82 Chen Z, Cai P, Chen J, Liu X, Zhang L, Lan L, Peng J, Ma Y, Cao Y. *Adv Mater*, 2014, 26: 2586–2591
- 83 Zhao J, Li Y, Yang G, Jiang K, Lin H, Ade H, Ma W, Yan H. *Nat Energy*, 2016, 1: 15027
- 84 Gong X, Li G, Li C, Zhang J, Bo Z. *J Mater Chem A*, 2015, 3: 20195–20200
- 85 Lu H, Zhang J, Chen J, Liu Q, Gong X, Feng S, Xu X, Ma W, Bo Z. *Adv Mater*, 2016, 28: 9559–9566
- 86 Mataka S, Takahashi K, Ikezaki Y, Hatta T, Tori-i A, Tashiro M. *Bull Chem Soc Jpn*, 1991, 64: 68–73
- 87 Wang M, Hu X, Liu P, Li W, Gong X, Huang F, Cao Y. *J Am Chem Soc*, 2011, 133: 9638–9641
- 88 Arroyave FA, Richard CA, Reynolds JR. *Org Lett*, 2012, 14: 6138–6141
- 89 Liu D, Zhao W, Zhang S, Ye L, Zheng Z, Cui Y, Chen Y, Hou J. *Macromolecules*, 2015, 48: 5172–5178
- 90 Zheng Z, Hu Q, Zhang S, Zhang D, Wang J, Xie S, Wang R, Qin Y, Li W, Hong L, Liang N, Liu F, Zhang Y, Wei Z, Tang Z, Russell TP, Hou J, Zhou H. *Adv Mater*, 2018, 30: 1801801
- 91 Yuan J, Zhang Y, Zhou L, Zhang C, Lau TK, Zhang G, Lu X, Yip HL, So SK, Beaupré S, Mainville M, Johnson PA, Leclerc M, Chen H, Peng H, Li Y, Zou Y. *Adv Mater*, 2019, 31: 1807577
- 92 Yu T, Xu X, Zhang G, Wan J, Li Y, Peng Q. *Adv Funct Mater*, 2017, 27: 1701491
- 93 Sun C, Pan F, Bin H, Zhang J, Xue L, Qiu B, Wei Z, Zhang ZG, Li Y. *Nat Commun*, 2018, 9: 743
- 94 Zheng Z, Awartani OM, Gautam B, Liu D, Qin Y, Li W, Bataller A, Gundogdu K, Ade H, Hou J. *Adv Mater*, 2017, 29: 1604241
- 95 Sun C, Qin S, Wang R, Chen S, Pan F, Qiu B, Shang Z, Meng L, Zhang C, Xiao M, Yang C, Li Y. *J Am Chem Soc*, 2020, 142: 1465–1474
- 96 Zou Y, Najari A, Berrouard P, Beaupré S, Réda Aïch B, Tao Y, Leclerc M. *J Am Chem Soc*, 2010, 132: 5330–5331
- 97 Zhang C, Li H, Wang J, Zhang Y, Qiao Y, Huang D, Di C, Zhan X, Zhu X, Zhu D. *J Mater Chem A*, 2015, 3: 11194–11198
- 98 Kim JH, Park JB, Jung IH, Grimsdale AC, Yoon SC, Yang H, Hwang DH. *Energy Environ Sci*, 2015, 8: 2352–2356
- 99 Xie Y, Huang W, Liang Q, Zhu J, Cong Z, Lin F, Yi S, Luo G, Yang T, Liu S, He Z, Liang Y, Zhan X, Gao C, Wu H, Cao Y. *ACS Energy Lett*, 2019, 4: 8–16
- 100 Zhao J, Li Q, Liu S, Cao Z, Jiao X, Cai YP, Huang F. *ACS Energy Lett*, 2020, 5: 367–375
- 101 Liang Y, Feng D, Wu Y, Tsai ST, Li G, Ray C, Yu L. *J Am Chem Soc*, 2009, 131: 7792–7799
- 102 Liang Y, Xu Z, Xia J, Tsai ST, Wu Y, Li G, Ray C, Yu L. *Adv Mater*, 2010, 22: E135–E138
- 103 Chen HY, Hou J, Zhang S, Liang Y, Yang G, Yang Y, Yu L, Wu Y, Li G. *Nat Photon*, 2009, 3: 649–653
- 104 Liao SH, Jhuo HJ, Cheng YS, Chen SA. *Adv Mater*, 2013, 25: 4766–4771
- 105 Zhang S, Ye L, Zhao W, Yang B, Wang Q, Hou J. *Sci China Chem*, 2015, 58: 248–256
- 106 Dai S, Zhan X. *Adv Energy Mater*, 2018, 8: 1800002
- 107 Zhao W, Qian D, Zhang S, Li S, Inganäs O, Gao F, Hou J. *Adv Mater*, 2016, 28: 4734–4739
- 108 Zhao W, Li S, Yao H, Zhang S, Zhang Y, Yang B, Hou J. *J Am Chem Soc*, 2017, 139: 7148–7151
- 109 Li W, Ye L, Li S, Yao H, Ade H, Hou J. *Adv Mater*, 2018, 30: 1707170
- 110 Cui Y, Yao H, Zhang J, Xian K, Zhang T, Hong L, Wang Y, Xu Y, Ma K, An C, He C, Wei Z, Gao F, Hou J. *Adv Mater*, 2020, 32: 1908205
- 111 Wu Y, An C, Shi L, Yang L, Qin Y, Liang N, He C, Wang Z, Hou J. *Angew Chem Int Ed*, 2018, 57: 12911–12915
- 112 Zhang S, Qin Y, Zhu J, Hou J. *Adv Mater*, 2018, 30: 1800868
- 113 Guo X, Fan Q, Wu J, Li G, Peng Z, Su W, Lin J, Hou L, Qin Y, Ade H, Ye L, Zhang M, Li Y. *Angew Chem Int Ed*, 2021, 60: 2322–2329
- 114 Wu J, Li G, Fang J, Guo X, Zhu L, Guo B, Wang Y, Zhang G, Arunagiri L, Liu F, Yan H, Zhang M, Li Y. *Nat Commun*, 2020, 11: 4612
- 115 Qian D, Ye L, Zhang M, Liang Y, Li L, Huang Y, Guo X, Zhang S, Tan Z'. Hou J. *Macromolecules*, 2012, 45: 9611–9617
- 116 Zhang M, Zhu L, Zhou G, Hao T, Qiu C, Zhao Z, Hu Q, Larson BW, Zhu H, Ma Z, Tang Z, Feng W, Zhang Y, Russell TP, Liu F. *Nat Commun*, 2021, 12: 309
- 117 Zhao C, Guo Y, Zhang Y, Yan N, You S, Li W. *J Mater Chem A*, 2019, 7: 10174–10199
- 118 Wang E, Mammo W, Andersson MR. *Adv Mater*, 2014, 26: 1801–1826
- 119 Mishra A, Bäuerle P. *Angew Chem Int Ed*, 2012, 51: 2020–2067
- 120 Lin Y, Li Y, Zhan X. *Chem Soc Rev*, 2012, 41: 4245–4272
- 121 Walker B, Kim C, Nguyen TQ. *Chem Mater*, 2011, 23: 470–482

- 122 Collins SD, Ran NA, Heiber MC, Nguyen TQ. *Adv Energy Mater.*, 2017, 7: 1602242
- 123 Roncali J. *Acc Chem Res.*, 2009, 42: 1719–1730
- 124 Schulze K, Uhrich C, Schüppel R, Leo K, Pfeiffer M, Brier E, Reinold E, Bäuerle P. *Adv Mater.*, 2006, 18: 2872–2875
- 125 Wan X, Li C, Zhang M, Chen Y. *Chem Soc Rev.*, 2020, 49: 2828–2842
- 126 Chen Y, Wan X, Long G. *Acc Chem Res.*, 2013, 46: 2645–2655
- 127 Liu Y, Wan X, Yin B, Zhou J, Long G, Yin S, Chen Y. *J Mater Chem.*, 2010, 20: 2464–2468
- 128 Liu Y, Wan X, Wang F, Zhou J, Long G, Tian J, You J, Yang Y, Chen Y. *Adv Energy Mater.*, 2011, 1: 771–775
- 129 Li Z, He G, Wan X, Liu Y, Zhou J, Long G, Zuo Y, Zhang M, Chen Y. *Adv Energy Mater.*, 2012, 2: 74–77
- 130 Zhang Q, Kan B, Liu F, Long G, Wan X, Chen X, Zuo Y, Ni W, Zhang H, Li M, Hu Z, Huang F, Cao Y, Liang Z, Zhang M, Russell TP, Chen Y. *Nat Photon.*, 2015, 9: 35–41
- 131 Kan B, Zhang Q, Li M, Wan X, Ni W, Long G, Wang Y, Yang X, Feng H, Chen Y. *J Am Chem Soc.*, 2014, 136: 15529–15532
- 132 Wang Y, Wang Y, Kan B, Ke X, Wan X, Li C, Chen Y. *Adv Energy Mater.*, 2018, 8: 1802021
- 133 Duan T, Gao J, Babics M, Kan Z, Zhong C, Singh R, Yu D, Lee J, Xiao Z, Lu S. *Sol RRL.*, 2020, 4: 1900472
- 134 Duan T, Tang H, Liang RZ, Lv J, Kan Z, Singh R, Kumar M, Xiao Z, Lu S, Laquai F. *J Mater Chem A.*, 2019, 7: 2541–2546
- 135 Liu Y, Wan X, Wang F, Zhou J, Long G, Tian J, Chen Y. *Adv Mater.*, 2011, 23: 5387–5391
- 136 Li M, Ni W, Wan X, Zhang Q, Kan B, Chen Y. *J Mater Chem A.*, 2015, 3: 4765–4776
- 137 Zhou J, Wan X, Liu Y, Zuo Y, Li Z, He G, Long G, Ni W, Li C, Su X, Chen Y. *J Am Chem Soc.*, 2012, 134: 16345–16351
- 138 Ni W, Li M, Wan X, Feng H, Kan B, Zuo Y, Chen Y. *RSC Adv.*, 2014, 4: 31977–31980
- 139 Zhou J, Zuo Y, Wan X, Long G, Zhang Q, Ni W, Liu Y, Li Z, He G, Li C, Kan B, Li M, Chen Y. *J Am Chem Soc.*, 2013, 135: 8484–8487
- 140 Li M, Liu F, Wan X, Ni W, Kan B, Feng H, Zhang Q, Yang X, Wang Y, Zhang Y, Shen Y, Russell TP, Chen Y. *Adv Mater.*, 2015, 27: 6296–6302
- 141 Sun K, Xiao Z, Lu S, Zajaczkowski W, Pisula W, Hanssen E, White JM, Williamson RM, Subbiah J, Ouyang J, Holmes AB, Wong WWH, Jones DJ. *Nat Commun.*, 2015, 6: 6013
- 142 Deng D, Zhang Y, Zhang J, Wang Z, Zhu L, Fang J, Xia B, Wang Z, Lu K, Ma W, Wei Z. *Nat Commun.*, 2016, 7: 13740
- 143 Ni W, Li M, Kan B, Liu F, Wan X, Zhang Q, Zhang H, Russell TP, Chen Y. *Chem Commun.*, 2016, 52: 465–468
- 144 Liang R, Zhang Y, Savikhin V, Babics M, Kan Z, Wohlfahrt M, Wehbe N, Liu S, Duan T, Toney MF, Laquai F, Beaujuge PM. *Adv Energy Mater.*, 2019, 9: 1802836
- 145 Xu C, Wang J, An Q, Ma X, Hu Z, Gao J, Zhang J, Zhang F. *Nano Energy.*, 2019, 66: 104119
- 146 Zhou Z, Xu S, Song J, Jin Y, Yue Q, Qian Y, Liu F, Zhang F, Zhu X. *Nat Energy.*, 2018, 3: 952–959
- 147 Yang L, Zhang S, He C, Zhang J, Yao H, Yang Y, Zhang Y, Zhao W, Hou J. *J Am Chem Soc.*, 2017, 139: 1958–1966
- 148 Chen H, Hu D, Yang Q, Gao J, Fu J, Yang K, He H, Chen S, Kan Z, Duan T, Yang C, Ouyang J, Xiao Z, Sun K, Lu S. *Joule*, 2019, 3: 3034–3047
- 149 Hu D, Yang Q, Chen H, Wobben F, Le Corre VM, Singh R, Liu T, Ma R, Tang H, Koster LJA, Duan T, Yan H, Kan Z, Xiao Z, Lu S. *Energy Environ Sci.*, 2020, 13: 2134–2141
- 150 Qin J, An C, Zhang J, Ma K, Yang Y, Zhang T, Li S, Xian K, Cui Y, Tang Y, Ma W, Yao H, Zhang S, Xu B, He C, Hou J. *Sci China Mater.*, 2020, 63: 1142–1150
- 151 Zhou R, Jiang Z, Yang C, Yu J, Feng J, Adil MA, Deng D, Zou W, Zhang J, Lu K, Ma W, Gao F, Wei Z. *Nat Commun.*, 2019, 10: 5393
- 152 Gao K, Li L, Lai T, Xiao L, Huang Y, Huang F, Peng J, Cao Y, Liu F, Russell TP, Janssen RAJ, Peng X. *J Am Chem Soc.*, 2015, 137: 7282–7285
- 153 Gao K, Miao J, Xiao L, Deng W, Kan Y, Liang T, Wang C, Huang F, Peng J, Cao Y, Liu F, Russell TP, Wu H, Peng X. *Adv Mater.*, 2016, 28: 4727–4733
- 154 Nian L, Gao K, Jiang Y, Rong Q, Hu X, Yuan D, Liu F, Peng X, Russell TP, Zhou G. *Adv Mater.*, 2017, 29: 1700616
- 155 Li M, Gao K, Wan X, Zhang Q, Kan B, Xia R, Liu F, Yang X, Feng H, Ni W, Wang Y, Peng J, Zhang H, Liang Z, Yip HL, Peng X, Cao Y, Chen Y. *Nat Photon.*, 2017, 11: 85–90
- 156 Gao K, Jo SB, Shi X, Nian L, Zhang M, Kan Y, Lin F, Kan B, Xu B, Rong Q, Shui L, Liu F, Peng X, Zhou G, Cao Y, Jen AKY. *Adv Mater.*, 2019, 31: 1807842
- 157 Coughlin JE, Henson ZB, Welch GC, Bazan GC. *Acc Chem Res.*, 2014, 47: 257–270
- 158 Sun Y, Welch GC, Leong WL, Takacs CJ, Bazan GC, Heeger AJ. *Nat Mater.*, 2012, 11: 44–48
- 159 Takacs CJ, Sun Y, Welch GC, Perez LA, Liu X, Wen W, Bazan GC, Heeger AJ. *J Am Chem Soc.*, 2012, 134: 16597–16606
- 160 van der Poll TS, Love JA, Nguyen TQ, Bazan GC. *Adv Mater.*, 2012, 24: 3646–3649
- 161 Gupta V, Kyaw AKK, Wang DH, Chand S, Bazan GC, Heeger AJ. *Sci Rep.*, 2013, 3: 1965
- 162 Zhou J, Wan X, Liu Y, Long G, Wang F, Li Z, Zuo Y, Li C, Chen Y. *Chem Mater.*, 2011, 23: 4666–4668
- 163 Kwon OK, Park JH, Kim DW, Park SK, Park SY. *Adv Mater.*, 2015, 27: 1951–1956
- 164 Scharber MC. *Adv Mater.*, 2016, 28: 1994–2001
- 165 Schmidt-Mende L, Fechtenkotter A, Mullen K, Moons E, Friend RH, MacKenzie JD. *Science*, 2001, 293: 1119–1122
- 166 Lin Y, Wang J, Zhang ZG, Bai H, Li Y, Zhu D, Zhan X. *Adv Mater.*, 2015, 27: 1170–1174
- 167 Feng L, Yuan J, Zhang Z, Peng H, Zhang ZG, Xu S, Liu Y, Li Y, Zou Y. *ACS Appl Mater Interfaces.*, 2017, 9: 31985–31992
- 168 Gao B, Yao H, Hou J, Yu R, Hong L, Xu Y, Hou J. *J Mater Chem A.*, 2018, 6: 23644–23649
- 169 Zhang H, Yao H, Hou J, Zhu J, Zhang J, Li W, Yu R, Gao B, Zhang S, Hou J. *Adv Mater.*, 2018, 30: 1800613
- 170 Zhang Z, Guang S, Yu J, Wang H, Cao J, Du F, Wang X, Tang W. *Sci Bull.*, 2020, 65: 1533–1536
- 171 Lin Y, Li T, Zhao F, Han L, Wang Z, Wu Y, He Q, Wang J, Huo L, Sun Y, Wang C, Ma W, Zhan X. *Adv Energy Mater.*, 2016, 6: 1600854
- 172 Cai G, Xue P, Chen Z, Li T, Liu K, Ma W, Lian J, Zeng P, Wang Y, Han RPS, Zhan X. *Chem Mater.*, 2018, 31: 6484–6490
- 173 Kan B, Feng H, Wan X, Liu F, Ke X, Wang Y, Wang Y, Zhang H, Li C, Hou J, Chen Y. *J Am Chem Soc.*, 2017, 139: 4929–4934
- 174 Shi X, Chen J, Gao K, Zuo L, Yao Z, Liu F, Tang J, Jen AKY. *Adv Energy Mater.*, 2018, 8: 1702831
- 175 Dai S, Xiao Y, Xue P, James Rech J, Liu K, Li Z, Lu X, You W, Zhan X. *Chem Mater.*, 2018, 30: 5390–5396
- 176 Dai S, Li T, Wang W, Xiao Y, Lau TK, Li Z, Liu K, Lu X, Zhan X. *Adv Mater.*, 2018, 30: 1706571
- 177 Wang W, Lu H, Chen Z, Jia B, Li K, Ma W, Zhan X. *J Mater Chem A.*, 2020, 8: 3011–3017
- 178 Gao W, Zhang M, Liu T, Ming R, An Q, Wu K, Xie D, Luo Z, Zhong C, Liu F, Zhang F, Yan H, Yang C. *Adv Mater.*, 2018, 30: 1800052
- 179 Gao W, Liu T, Zhong C, Zhang G, Zhang Y, Ming R, Zhang L, Xin J, Wu K, Guo Y, Ma W, Yan H, Liu Y, Yang C. *ACS Energy Lett.*, 2018, 3: 1760–1768
- 180 Lu B, Chen Z, Jia B, Wang J, Ma W, Lian J, Zeng P, Qu J, Zhan X. *ACS Appl Mater Interfaces.*, 2020, 12: 14029–14036
- 181 Xiao Z, Jia X, Li D, Wang S, Geng X, Liu F, Chen J, Yang S, Russell TP, Ding L. *Sci Bull.*, 2017, 62: 1494–1496
- 182 Yang F, Li C, Lai W, Zhang A, Huang H, Li W. *Mater Chem Front.*, 2017, 1: 1389–1395
- 183 Li S, Ye L, Zhao W, Zhang S, Mukherjee S, Ade H, Hou J. *Adv Mater.*, 2016, 28: 9423–9429

- 184 Hao M, Liu T, Xiao Y, Ma LK, Zhang G, Zhong C, Chen Z, Luo Z, Lu X, Yan H, Wang L, Yang C. *Chem Mater*, 2019, 31: 1752–1760
- 185 Zhu J, Li S, Liu X, Yao H, Wang F, Zhang S, Sun M, Hou J. *J Mater Chem A*, 2017, 5: 15175–15182
- 186 Zhang Z, Feng L, Xu S, Yuan J, Zhang ZG, Peng H, Li Y, Zou Y. *J Mater Chem A*, 2017, 5: 11286–11293
- 187 Luo Z, Bin H, Liu T, Zhang ZG, Yang Y, Zhong C, Qiu B, Li G, Gao W, Xie D, Wu K, Sun Y, Liu F, Li Y, Yang C. *Adv Mater*, 2018, 30: 1706124
- 188 Yan D, Liu W, Yao J, Zhan C. *Adv Energy Mater*, 2018, 8: 1800204
- 189 Yao H, Ye L, Hou J, Jang B, Han G, Cui Y, Su GM, Wang C, Gao B, Yu R, Zhang H, Yi Y, Woo HY, Ade H, Hou J. *Adv Mater*, 2017, 29: 1700254
- 190 Yang Y, Zhang ZG, Bin H, Chen S, Gao L, Xue L, Yang C, Li Y. *J Am Chem Soc*, 2016, 138: 15011–15018
- 191 Lin Y, Zhao F, He Q, Huo L, Wu Y, Parker TC, Ma W, Sun Y, Wang C, Zhu D, Heeger AJ, Marder SR, Zhan X. *J Am Chem Soc*, 2016, 138: 4955–4961
- 192 Fei Z, Eisner FD, Jiao X, Azzouzi M, Röhr JA, Han Y, Shahid M, Chesman ASR, Easton CD, McNeill CR, Anthopoulos TD, Nelson J, Heeney M. *Adv Mater*, 2018, 30: 1705209
- 193 Wang J, Wang W, Wang X, Wu Y, Zhang Q, Yan C, Ma W, You W, Zhan X. *Adv Mater*, 2017, 29: 1702125
- 194 Kan B, Zhang J, Liu F, Wan X, Li C, Ke X, Wang Y, Feng H, Zhang Y, Long G, Friend RH, Bakulin AA, Chen Y. *Adv Mater*, 2018, 30: 1704904
- 195 Zhang Y, Kan B, Sun Y, Wang Y, Xia R, Ke X, Yi YQQ, Li C, Yip HL, Wan X, Cao Y, Chen Y. *Adv Mater*, 2018, 30: 1707508
- 196 Zhang Z, Yu J, Yin X, Hu Z, Jiang Y, Sun J, Zhou J, Zhang F, Russell TP, Liu F, Tang W. *Adv Funct Mater*, 2018, 28: 1705095
- 197 Yuan J, Huang T, Cheng P, Zou Y, Zhang H, Yang JL, Chang SY, Zhang Z, Huang W, Wang R, Meng D, Gao F, Yang Y. *Nat Commun*, 2019, 10: 570
- 198 Lin F, Jiang K, Kaminsky W, Zhu Z, Jen AKY. *J Am Chem Soc*, 2020, 142: 15246–15251
- 199 Cai F, Zhu C, Yuan J, Li Z, Meng L, Liu W, Peng H, Jiang L, Li Y, Zou Y. *Chem Commun*, 2020, 56: 4340–4343
- 200 Gao W, Fu H, Li Y, Lin F, Sun R, Wu Z, Wu X, Zhong C, Min J, Luo J, Woo HY, Zhu Z, Jen AKY. *Adv Energy Mater*, 2021, 11: 2003177
- 201 Gao W, Fan B, Qi F, Lin F, Sun R, Xia X, Gao J, Zhong C, Lu X, Min J, Zhang F, Zhu Z, Luo J, Jen AKY. *Adv Funct Mater*, 2021, 31: 2104369
- 202 Luo M, Zhou L, Yuan J, Zhu C, Cai F, Hai J, Zou Y. *J Energy Chem*, 2020, 42: 169–173
- 203 Zhou Z, Liu W, Zhou G, Zhang M, Qian D, Zhang J, Chen S, Xu S, Yang C, Gao F, Zhu H, Liu F, Zhu X. *Adv Mater*, 2020, 32: 1906324
- 204 Zhang Z, Li Y, Cai G, Zhang Y, Lu X, Lin Y. *J Am Chem Soc*, 2020, 142: 18741–18745
- 205 Yuan J, Zhang Y, Zhou L, Zhang G, Yip HL, Lau TK, Lu X, Zhu C, Peng H, Johnson PA, Leclerc M, Cao Y, Ulanski J, Li Y, Zou Y. *Joule*, 2019, 3: 1140–1151
- 206 Cui Y, Yao H, Zhang J, Zhang T, Wang Y, Hong L, Xian K, Xu B, Zhang S, Peng J, Wei Z, Gao F, Hou J. *Nat Commun*, 2019, 10: 2515
- 207 Wang H, Liu T, Zhou J, Mo D, Han L, Lai H, Chen H, Zheng N, Zhu Y, Xie Z, He F. *Adv Sci*, 2020, 7: 1903784
- 208 Xu Y, Yao H, Ma L, Hong L, Li J, Liao Q, Zu Y, Wang J, Gao M, Ye L, Hou J. *Angew Chem Int Ed*, 2020, 59: 9004–9010
- 209 Lai H, Zhao Q, Chen Z, Chen H, Chao P, Zhu Y, Lang Y, Zhen N, Mo D, Zhang Y, He F. *Joule*, 2020, 4: 688–700
- 210 An Q, Wang J, Gao W, Ma X, Hu Z, Gao J, Xu C, Hao M, Zhang X, Yang C, Zhang F. *Sci Bull*, 2020, 65: 538–545
- 211 Zhang Y, Cai F, Yuan J, Wei Q, Zhou L, Qiu B, Hu Y, Li Y, Peng H, Zou Y. *Phys Chem Chem Phys*, 2019, 21: 26557–26563
- 212 Cao C, Lai H, Chen H, Zhu Y, Pu M, Zheng N, He F. *J Mater Chem A*, 2021, 9: 16418–16426
- 213 Yang W, Luo Z, Sun R, Guo J, Wang T, Wu Y, Wang W, Guo J, Wu Q, Shi M, Li H, Yang C, Min J. *Nat Commun*, 2020, 11: 1218
- 214 Tao L, Liu X, Deng C, Zhang W, Song W. *ACS Appl Mater Interfaces*, 2020, 12: 49659–49665
- 215 Qin R, Wang D, Zhou G, Yu ZP, Li S, Li Y, Liu ZX, Zhu H, Shi M, Lu X, Li CZ, Chen H. *J Mater Chem A*, 2019, 7: 27632–27639
- 216 Luo Z, Ma R, Liu T, Yu J, Xiao Y, Sun R, Xie G, Yuan J, Chen Y, Chen K, Chai G, Sun H, Min J, Zhang J, Zou Y, Yang C, Lu X, Gao F, Yan H. *Joule*, 2020, 4: 1236–1247
- 217 Lai H, Chen H, Zhu Y, Chen L, Huang HH, He F. *J Mater Chem A*, 2020, 8: 9670–9676
- 218 Liu T, Zhang Y, Shao Y, Ma R, Luo Z, Xiao Y, Yang T, Lu X, Yuan Z, Yan H, Chen Y, Li Y. *Adv Funct Mater*, 2020, 30: 2000456
- 219 Jiang K, Wei Q, Lai JYL, Peng Z, Kim HK, Yuan J, Ye L, Ade H, Zou Y, Yan H. *Joule*, 2019, 3: 3020–3033
- 220 Cui Y, Yao H, Hong L, Zhang T, Tang Y, Lin B, Xian K, Gao B, An C, Bi P, Ma W, Hou J. *Natl Sci Rev*, 2020, 7: 1239–1246
- 221 Hong L, Yao H, Wu Z, Cui Y, Zhang T, Xu Y, Yu R, Liao Q, Gao B, Xian K, Woo HY, Ge Z, Hou J. *Adv Mater*, 2019, 31: 1903441
- 222 Chen S, Feng L, Jia T, Jing J, Hu Z, Zhang K, Huang F. *Sci China Chem*, 2021, 64: 1192–1199
- 223 Qi F, Jiang K, Lin F, Wu Z, Zhang H, Gao W, Li Y, Cai Z, Woo HY, Zhu Z, Jen AKY. *ACS Energy Lett*, 2020, 6: 9–15
- 224 Yuan J, Zhang C, Chen H, Zhu C, Cheung SH, Qiu B, Cai F, Wei Q, Liu W, Yin H, Zhang R, Zhang J, Liu Y, Zhang H, Liu W, Peng H, Yang J, Meng L, Gao F, So S, Li Y, Zou Y. *Sci China Chem*, 2020, 63: 1159–1168
- 225 Li C, Zhou J, Song J, Xu J, Zhang H, Zhang X, Guo J, Zhu L, Wei D, Han G, Min J, Zhang Y, Xie Z, Yi Y, Yan H, Gao F, Liu F, Sun Y. *Nat Energy*, 2021, 6: 605–613
- 226 Chai G, Chang Y, Peng Z, Jia Y, Zou X, Yu D, Yu H, Chen Y, Chow PCY, Wong KS, Zhang J, Ade H, Yang L, Zhan C. *Nano Energy*, 2020, 76: 105087
- 227 Chen Y, Bai F, Peng Z, Zhu L, Zhang J, Zou X, Qin Y, Kim HK, Yuan J, Ma LK, Zhang J, Yu H, Chow PCY, Huang F, Zou Y, Ade H, Liu F, Yan H. *Adv Energy Mater*, 2021, 11: 2003141
- 228 Liu Y, Song J, Bo Z. *Chem Commun*, 2021, 57: 302–314
- 229 Li Y, Gu M, Pan Z, Zhang B, Yang X, Gu J, Chen Y. *J Mater Chem A*, 2017, 5: 10798–10814
- 230 Liu Y, Zhang Z, Feng S, Li M, Wu L, Hou R, Xu X, Chen X, Bo Z. *J Am Chem Soc*, 2017, 139: 3356–3359
- 231 Liu Y, Zhang C, Hao D, Zhang Z, Wu L, Li M, Feng S, Xu X, Liu F, Chen X, Bo Z. *Chem Mater*, 2018, 30: 4307–4312
- 232 Jiang P, Ming S, Jia QQ, Liu Y, Lu H, Li M, Xu X, Li HB, Bo Z. *J Mater Chem A*, 2018, 6: 21335–21340
- 233 Zhang C, Jiang P, Zhou X, Feng S, Bi Z, Xu X, Li C, Tang Z, Ma W, Bo Z. *ACS Appl Mater Interfaces*, 2020, 12: 40590–40598
- 234 Yao H, Chen Y, Qin Y, Yu R, Cui Y, Yang B, Li S, Zhang K, Hou J. *Adv Mater*, 2016, 28: 8283–8287
- 235 Lin Y, Zhang ZG, Bai H, Wang J, Yao Y, Li Y, Zhu D, Zhan X. *Energy Environ Sci*, 2015, 8: 610–616
- 236 Yao H, Cui Y, Yu R, Gao B, Zhang H, Hou J. *Angew Chem Int Ed*, 2017, 56: 3045–3049
- 237 Cui Y, Yang C, Yao H, Zhu J, Wang Y, Jia G, Gao F, Hou J. *Adv Mater*, 2017, 29: 1703080
- 238 Liu Y, Li M, Zhou X, Jia QQ, Feng S, Jiang P, Xu X, Ma W, Li HB, Bo Z. *ACS Energy Lett*, 2018, 3: 1832–1839
- 239 Liu D, Kan B, Ke X, Zheng N, Xie Z, Lu D, Liu Y. *Adv Energy Mater*, 2018, 8: 1801618
- 240 Lee J, Song S, Huang J, Du Z, Lee H, Zhu Z, Ko SJ, Nguyen TQ, Kim JY, Cho K, Bazan GC. *ACS Mater Lett*, 2020, 2: 395–402
- 241 Li S, Zhan L, Zhao W, Zhang S, Ali B, Fu Z, Lau TK, Lu X, Shi M, Li CZ, Hou J, Chen H. *J Mater Chem A*, 2018, 6: 12132–12141
- 242 Huang H, Guo Q, Feng S, Zhang C', Bi Z, Xue W, Yang J, Song J, Li C, Xu X, Tang Z, Ma W, Bo Z. *Nat Commun*, 2019, 10: 3038
- 243 Hou R, Li M, Ma X, Huang H, Lu H, Jia Q, Liu Y, Xu X, Li HB, Bo Z. *ACS Appl Mater Interfaces*, 2020, 12: 46220–46230
- 244 Feng S, Li M, Tang N, Wang X, Huang H, Ran G, Liu Y, Xie Z, Zhang W, Bo Z. *ACS Appl Mater Interfaces*, 2020, 12: 4638–4648

- 245 Qin R, Yang W, Li S, Lau TK, Yu Z, Liu Z, Shi M, Lu X, Li CZ, Chen H. *Mater Chem Front*, 2019, 3: 513–519
- 246 Li S, Zhan L, Lau TK, Yu ZP, Yang W, Andersen TR, Fu Z, Li CZ, Lu X, Shi M, Chen H. *Small Methods*, 2019, 3: 1900531
- 247 Wang Y, Liu Z, Cui X, Wang C, Lu H, Liu Y, Fei Z, Ma Z, Bo Z. *J Mater Chem A*, 2020, 8: 12495–12501
- 248 Liu X, Wei Y, Zhang X, Qin L, Wei Z, Huang H. *Sci China Chem*, 2021, 64: 228–231
- 249 Zhang Z, Zhang S, Liu Z, Zhang Z, Li Y, Li C, Chen H. *Acta Physico-Chim Sin*, 2019, 35: 394–400
- 250 Yu ZP, Liu ZX, Chen FX, Qin R, Lau TK, Yin JL, Kong X, Lu X, Shi M, Li CZ, Chen H. *Nat Commun*, 2019, 10: 2152
- 251 Chen YN, Li M, Wang Y, Wang J, Zhang M, Zhou Y, Yang J, Liu Y, Liu F, Tang Z, Bao Q, Bo Z. *Angew Chem Int Ed*, 2020, 59: 22714–22720
- 252 Zhou Y, Li M, Lu H, Jin H, Wang X, Zhang Y, Shen S, Ma Z, Song J, Bo Z. *Adv Funct Mater*, 2021, 31: 2101742
- 253 Ma L, Zhang S, Zhu J, Wang J, Ren J, Zhang J, Hou J. *Nat Commun*, 2021, 12: 5093
- 254 Wang X, Cui X, Lu H, Chen YN, Liu Y, Zhou Y, Zhang C, Song J, Li C, Zhang Z, Bo Z. *Org Electron*, 2021, 89: 106029
- 255 Wang X, Lu H, Zhou J, Xu X, Zhang C, Huang H, Song J, Liu Y, Xu X, Xie Z, Tang Z, Bo Z. *ACS Appl Mater Interfaces*, 2021, 13: 39652–39659
- 256 Wang X, Lu H, Liu Y, Zhang A, Yu N, Wang H, Li S, Zhou Y, Xu X, Tang Z, Bo Z. *Adv Energy Mater*, 2021, 11: 2102591
- 257 Li S, Zhan L, Sun C, Zhu H, Zhou G, Yang W, Shi M, Li CZ, Hou J, Li Y, Chen H. *J Am Chem Soc*, 2019, 141: 3073–3082
- 258 Wang N, Zhan L, Li S, Shi M, Lau TK, Lu X, Shikler R, Li CZ, Chen H. *Mater Chem Front*, 2018, 2: 2006–2012
- 259 Yu S, Chen Y, Yang L, Ye P, Wu J, Yu J, Zhang S, Gao Y, Huang H. *J Mater Chem A*, 2017, 5: 21674–21678
- 260 Park SH, Park GE, Choi S, Kim YU, Park SY, Park CG, Cho MJ, Choi DH. *J Mater Chem C*, 2018, 6: 7549–7556
- 261 Wu J, Xu Y, Yang Z, Chen Y, Sui X, Yang L, Ye P, Zhu T, Wu X, Liu X, Cao H, Peng A, Huang H. *Adv Energy Mater*, 2019, 9: 1803012
- 262 Li S, Zhan L, Liu F, Ren J, Shi M, Li CZ, Russell TP, Chen H. *Adv Mater*, 2018, 30: 1705208
- 263 He C, Li Y, Li S, Yu ZP, Li Y, Lu X, Shi M, Li CZ, Chen H. *ACS Appl Mater Interfaces*, 2020, 12: 16700–16706
- 264 Zheng R, Guo Q, Hao D, Zhang C, Xue W, Huang H, Li C, Ma W, Bo Z. *J Mater Chem C*, 2019, 7: 15141–15147
- 265 Yi YQQ, Feng H, Zheng N, Ke X, Kan B, Chang M, Xie Z, Wan X, Li C, Chen Y. *Chem Mater*, 2019, 31: 904–911
- 266 Zhang X, Li C, Qin L, Chen H, Yu J, Wei Y, Liu X, Zhang J, Wei Z, Gao F, Peng Q, Huang H. *Angew Chem Int Ed*, 2021, 60: 17720–17725
- 267 Zhang X, Qin L, Yu J, Li Y, Wei Y, Liu X, Lu X, Gao F, Huang H. *Angew Chem Int Ed*, 2021, 60: 12475–12481
- 268 Wen TJ, Liu ZX, Chen Z, Zhou J, Shen Z, Xiao Y, Lu X, Xie Z, Zhu H, Li CZ, Chen H. *Angew Chem Int Ed*, 2021, 60: 12964–12970
- 269 Halls JJM, Walsh CA, Greenham NC, Marseglia EA, Friend RH, Moratti SC, Holmes AB. *Nature*, 1995, 376: 498–500
- 270 Zou Y, Hou J, Yang C, Li Y. *Macromolecules*, 2006, 39: 8889–8891
- 271 Sang G, Zou Y, Huang Y, Zhao G, Yang Y, Li Y. *Appl Phys Lett*, 2009, 94: 193302
- 272 Flesch HG, Resel R, McNeill CR. *Org Electron*, 2009, 10: 1549–1555
- 273 Mori D, Benten H, Ohkita H, Ito S. *Adv Energy Mater*, 2015, 5: 1500304
- 274 Kang H, Lee W, Oh J, Kim T, Lee C, Kim BJ. *Acc Chem Res*, 2016, 49: 2424–2434
- 275 Zhan X, Tan Z, Domercq B, An Z, Zhang X, Barlow S, Li Y, Zhu D, Kippelen B, Marder SR. *J Am Chem Soc*, 2007, 129: 7246–7247
- 276 Zhou E, Cong J, Wei Q, Tajima K, Yang C, Hashimoto K. *Angew Chem Int Ed*, 2011, 50: 2799–2803
- 277 Lee C, Lee S, Kim GU, Lee W, Kim BJ. *Chem Rev*, 2019, 119: 8028–8086
- 278 Hwang YJ, Earmme T, Courtright BAE, Eberle FN, Jenekhe SA. *J Am Chem Soc*, 2015, 137: 4424–4434
- 279 Cheng P, Ye L, Zhao X, Hou J, Li Y, Zhan X. *Energy Environ Sci*, 2014, 7: 1351–1356
- 280 Yu R, Zhang S, Yao H, Guo B, Li S, Zhang H, Zhang M, Hou J. *Adv Mater*, 2017, 29: 1700437
- 281 Liu M, Yang J, Lang C, Zhang Y, Zhou E, Liu Z, Guo F, Zhao L. *Macromolecules*, 2017, 50: 7559–7566
- 282 Guo Y, Li Y, Awartani O, Han H, Zhao J, Ade H, Yan H, Zhao D. *Adv Mater*, 2017, 29: 1700309
- 283 Guo X, Watson MD. *Org Lett*, 2008, 10: 5333–5336
- 284 Yan H, Chen Z, Zheng Y, Newman C, Quinn JR, Dötz F, Kastler M, Facchetti A. *Nature*, 2009, 457: 679–686
- 285 Zhou N, Facchetti A. *Mater Today*, 2018, 21: 377–390
- 286 Moore JR, Albert-Seifried S, Rao A, Massip S, Watts B, Morgan DJ, Friend RH, McNeill CR, Sirringhaus H. *Adv Energy Mater*, 2011, 1: 230–240
- 287 Fabiano S, Chen Z, Vahedi S, Facchetti A, Pignataro B, Loi MA. *J Mater Chem*, 2011, 21: 5891–5896
- 288 Mori D, Benten H, Okada I, Ohkita H, Ito S. *Energy Environ Sci*, 2014, 7: 2939
- 289 Kang H, Uddin MA, Lee C, Kim KH, Nguyen TL, Lee W, Li Y, Wang C, Woo HY, Kim BJ. *J Am Chem Soc*, 2015, 137: 2359–2365
- 290 Mu C, Liu P, Ma W, Jiang K, Zhao J, Zhang K, Chen Z, Wei Z, Yi Y, Wang J, Yang S, Huang F, Facchetti A, Ade H, Yan H. *Adv Mater*, 2014, 26: 7224–7230
- 291 Gao L, Zhang ZG, Xue L, Min J, Zhang J, Wei Z, Li Y. *Adv Mater*, 2016, 28: 1884–1890
- 292 Li Z, Zhong W, Ying L, Liu F, Li N, Huang F, Cao Y. *Nano Energy*, 2019, 64: 103931
- 293 Zhu L, Zhong W, Qiu C, Lyu B, Zhou Z, Zhang M, Song J, Xu J, Wang J, Ali J, Feng W, Shi Z, Gu X, Ying L, Zhang Y, Liu F. *Adv Mater*, 2019, 31: 1902899
- 294 Fan B, Ying L, Zhu P, Pan F, Liu F, Chen J, Huang F, Cao Y. *Adv Mater*, 2017, 29: 1703906
- 295 Li W, Roelofs WSC, Turbiez M, Wienk MM, Janssen RAJ. *Adv Mater*, 2014, 26: 3304–3309
- 296 Liu S, Kan Z, Thomas S, Cruciani F, Brédas JL, Beaujuge PM. *Angew Chem Int Ed*, 2016, 55: 12996–13000
- 297 Sun H, Tang Y, Koh CW, Ling S, Wang R, Yang K, Yu J, Shi Y, Wang Y, Woo HY, Guo X. *Adv Mater*, 2019, 31: 1807220
- 298 Zhao R, Liu J, Wang L. *Acc Chem Res*, 2020, 53: 1557–1567
- 299 Dou C, Ding Z, Zhang Z, Xie Z, Liu J, Wang L. *Angew Chem Int Ed*, 2015, 54: 3648–3652
- 300 Long X, Ding Z, Dou C, Zhang J, Liu J, Wang L. *Adv Mater*, 2016, 28: 6504–6508
- 301 Shi S, Chen P, Chen Y, Feng K, Liu B, Chen J, Liao Q, Tu B, Luo J, Su M, Guo H, Kim MG, Facchetti A, Guo X. *Adv Mater*, 2019, 31: 1905161
- 302 Feng K, Huang J, Zhang X, Wu Z, Shi S, Thomsen L, Tian Y, Woo HY, McNeill CR, Guo X. *Adv Mater*, 2020, 32: 2001476
- 303 Zhao R, Wang N, Yu Y, Liu J. *Chem Mater*, 2020, 32: 1308–1314
- 304 Zhang ZG, Yang Y, Yao J, Xue L, Chen S, Li X, Morrison W, Yang C, Li Y. *Angew Chem Int Ed*, 2017, 56: 13503–13507
- 305 Zhang ZG, Li Y. *Angew Chem Int Ed*, 2021, 60: 4422–4433
- 306 Meng Y, Wu J, Guo X, Su W, Zhu L, Fang J, Zhang ZG, Liu F, Zhang M, Russell TP, Li Y. *Sci China Chem*, 2019, 62: 845–850
- 307 Fan Q, Su W, Meng X, Guo X, Li G, Ma W, Zhang M, Li Y. *Sol RRL*, 2017, 1: 1700020
- 308 Wu J, Meng Y, Guo X, Zhu L, Liu F, Zhang M. *J Mater Chem A*, 2019, 7: 16190–16196
- 309 Li Y, Jia Z, Zhang Q, Wu Z, Qin H, Yang J, Wen S, Woo HY, Ma W, Yang R, Yuan J. *ACS Appl Mater Interfaces*, 2020, 12: 33028–33038
- 310 Fan Q, Su W, Chen S, Kim W, Chen X, Lee B, Liu T, Méndez-Romero UA, Ma R, Yang T, Zhuang W, Li Y, Kim TS, Hou L,

- Yang C, Yan H, Yu D, Wang E. *Joule*, 2020, 4: 658–672
- 311 Fan Q, Su W, Chen S, Liu T, Zhuang W, Ma R, Wen X, Yin Z, Luo Z, Guo X, Hou L, Moth-Poulsen K, Li Y, Zhang Z, Yang C, Yu D, Yan H, Zhang M, Wang E. *Angew Chem Int Ed*, 2020, 59: 19835–19840
- 312 Yao H, Bai F, Hu H, Arunagiri L, Zhang J, Chen Y, Yu H, Chen S, Liu T, Lai JYL, Zou Y, Ade H, Yan H. *ACS Energy Lett*, 2019, 4: 417–422
- 313 Huang S, Wu F, Liu Z, Cui Y, Chen L, Chen Y. *J Energy Chem*, 2021, 53: 63–68
- 314 Jia T, Zhang J, Zhong W, Liang Y, Zhang K, Dong S, Ying L, Liu F, Wang X, Huang F, Cao Y. *Nano Energy*, 2020, 72: 104718
- 315 Wang W, Wu Q, Sun R, Guo J, Wu Y, Shi M, Yang W, Li H, Min J. *Joule*, 2020, 4: 1070–1086
- 316 Du J, Hu K, Meng L, Angunawela I, Zhang J, Qin S, Liebman-Pelaez A, Zhu C, Zhang Z, Ade H, Li Y. *Angew Chem Int Ed*, 2020, 59: 15181–15185
- 317 Wu Q, Wang W, Wang T, Sun R, Guo J, Wu Y, Jiao X, Brabec CJ, Li Y, Min J. *Sci China Chem*, 2020, 63: 1449–1460
- 318 Tang A, Li J, Zhang B, Peng J, Zhou E. *ACS Macro Lett*, 2020, 9: 706–712
- 319 Su N, Ma R, Li G, Liu T, Feng LW, Lin C, Chen J, Song J, Xiao Y, Qu J, Lu X, Sangwan VK, Hersam MC, Yan H, Facchetti A, Marks TJ. *ACS Energy Lett*, 2021, 6: 728–738
- 320 Fan Q, An Q, Lin Y, Xia Y, Li Q, Zhang M, Su W, Peng W, Zhang C, Liu F, Hou L, Zhu W, Yu D, Xiao M, Moons E, Zhang F, Anthopoulos TD, Inganäs O, Wang E. *Energy Environ Sci*, 2020, 13: 5017–5027
- 321 Du J, Hu K, Zhang J, Meng L, Yue J, Angunawela I, Yan H, Qin S, Kong X, Zhang Z, Guan B, Ade H, Li Y. *Nat Commun*, 2021, 12: 5264
- 322 Sun H, Yu H, Shi Y, Yu J, Peng Z, Zhang X, Liu B, Wang J, Singh R, Lee J, Li Y, Wei Z, Liao Q, Kan Z, Ye L, Yan H, Gao F, Guo X. *Adv Mater*, 2020, 32: 2004183
- 323 Wang R, Xu J, Fu L, Zhang C, Li Q, Yao J, Li X, Sun C, Zhang ZG, Wang X, Li Y, Ma J, Xiao M. *J Am Chem Soc*, 2021, 143: 4359–4366
- 324 Yang H, Fan H, Wang Z, Yan H, Dong Y, Cui C, Ade H, Li Y. *Macromolecules*, 2020, 53: 9026–9033
- 325 Wang T, Sun R, Wang W, Li H, Wu Y, Min J. *Chem Mater*, 2021, 33: 761–773
- 326 Luo Z, Liu T, Ma R, Xiao Y, Zhan L, Zhang G, Sun H, Ni F, Chai G, Wang J, Zhong C, Zou Y, Guo X, Lu X, Chen H, Yan H, Yang C. *Adv Mater*, 2020, 32: 2005942
- 327 Yu H, Pan M, Sun R, Agunawela I, Zhang J, Li Y, Qi Z, Han H, Zou X, Zhou W, Chen S, Lai JYL, Luo S, Luo Z, Zhao D, Lu X, Ade H, Huang F, Min J, Yan H. *Angew Chem Int Ed*, 2021, 60: 10137–10146
- 328 Fu H, Li Y, Yu J, Wu Z, Fan Q, Lin F, Woo HY, Gao F, Zhu Z, Jen AKY. *J Am Chem Soc*, 2021, 143: 2665–2670
- 329 Zhu C, Li Z, Zhong W, Peng F, Zeng Z, Ying L, Huang F, Cao Y. *Chem Commun*, 2021, 57: 935–938
- 330 Zhang L, Jia T, Pan L, Wu B, Wang Z, Gao K, Liu F, Duan C, Huang F, Cao Y. *Sci China Chem*, 2021, 64: 408–412
- 331 Wu Q, Wang W, Wu Y, Chen Z, Guo J, Sun R, Guo J, Yang YM, Min J. *Adv Funct Mater*, 2021, 31: 2010411
- 332 Xu Y, Yuan J, Liang S, Chen JD, Xia Y, Larson BW, Wang Y, Su GM, Zhang Y, Cui C, Wang M, Zhao H, Ma W. *ACS Energy Lett*, 2019, 4: 2277–2286
- 333 Liu T, Yang T, Ma R, Zhan L, Luo Z, Zhang G, Li Y, Gao K, Xiao Y, Yu J, Zou X, Sun H, Zhang M, Dela Peña TA, Xing Z, Liu H, Li X, Li G, Huang J, Duan C, Wong KS, Lu X, Guo X, Gao F, Chen H, Huang F, Li Y, Li Y, Cao Y, Tang B, Yan H. *Joule*, 2021, 5: 914–930
- 334 Liang S, Jiang X, Xiao C, Li C, Chen Q, Li W. *Acc Chem Res*, 2021, 54: 2227–2237
- 335 Lin Y, Firdaus Y, Isikgor FH, Nugraha MI, Yengel E, Harrison GT, Hallani R, El-Labban A, Faber H, Ma C, Zheng X, Subbiah A, Howells CT, Bakr OM, McCulloch I, Wolf SD, Tsetseris L, Anthopoulos TD. *ACS Energy Lett*, 2020, 5: 2935–2944
- 336 Roncali J. *Adv Energy Mater*, 2011, 1: 146
- 337 Li W. *Acta Polym Sin*, 2019, 50: 209–218
- 338 Lucas S, Kammerer J, Pfannmöller M, Schröder RR, He Y, Li N, Brabec CJ, Leydecker T, Samori P, Marszalek T, Pisula W, Mena-Osteritz E, Bäuerle P. *Sol RRL*, 2021, 5: 2000653
- 339 Roncali J, Grosu I. *Adv Sci*, 2019, 6: 1801026
- 340 Bu L, Guo X, Yu B, Qu Y, Xie Z, Yan D, Geng Y, Wang F. *J Am Chem Soc*, 2009, 131: 13242–13243
- 341 Bu L, Guo X, Yu B, Fu Y, Qu Y, Xie Z, Yan D, Geng Y, Wang F. *Polymer*, 2011, 52: 4253–4260
- 342 Qu J, Gao B, Tian H, Zhang X, Wang Y, Xie Z, Wang H, Geng Y, Wang F. *J Mater Chem A*, 2014, 2: 3632–3640
- 343 He Y, Li N, Brabec CJ. *Org Mater*, 2021, 03: 228–244
- 344 Guo C, Lin YH, Witman MD, Smith KA, Wang C, Hexemer A, Strzalka J, Gomez ED, Verduzco R. *Nano Lett*, 2013, 13: 2957–2963
- 345 Chen S, An Y, Dutta GK, Kim Y, Zhang ZG, Li Y, Yang C. *Adv Funct Mater*, 2017, 27: 1603564
- 346 Zhou N, Dudnik AS, Li TING, Manley EF, Aldrich TJ, Guo P, Liao HC, Chen Z, Chen LX, Chang RPH, Facchetti A, Olvera de la Cruz M, Marks TJ. *J Am Chem Soc*, 2016, 138: 1240–1251
- 347 Yan Y, Liu Y, Zhang Q, Han Y. *Front Chem*, 2020, 8: 394
- 348 Zhao Z, Xu C, Niu L, Zhang X, Zhang F. *Laser Photonics Rev*, 2020, 14: 2000262
- 349 Zhong Z, Li K, Zhang J, Ying L, Xie R, Yu G, Huang F, Cao Y. *ACS Appl Mater Interfaces*, 2019, 11: 14208–14214
- 350 Nakabayashi K, Mori H. *Macromolecules*, 2012, 45: 9618–9625
- 351 Park CG, Park SH, Kim Y, Nguyen TL, Woo HY, Kang H, Yoon HJ, Park S, Cho MJ, Choi DH. *J Mater Chem A*, 2019, 7: 21280–21289
- 352 Lee JH, Park CG, Kim A, Kim HJ, Kim Y, Park S, Cho MJ, Choi DH. *ACS Appl Mater Interfaces*, 2018, 10: 18974–18983
- 353 Lee DH, Lee JH, Kim HJ, Choi S, Park GE, Cho MJ, Choi DH. *J Mater Chem A*, 2017, 5: 9745–9751
- 354 Park SH, Kim Y, Kwon NY, Lee YW, Woo HY, Chae WS, Park S, Cho MJ, Choi DH. *Adv Sci*, 2020, 7: 1902470
- 355 Benincori T, Brenna E, Sannicola F, Trimarco L, Sozzani P, Zotti G. *Angew Chem Int Ed*, 1996, 35: 648–651
- 356 Ramos AM, Rispen MT, van Duren JKJ, Hummelen JC, Janssen RAJ. *J Am Chem Soc*, 2001, 123: 6714–6715
- 357 Zhang F, Svensson M, Andersson MR, Maggini M, Bucella S, Menna E, Inganäs O. *Adv Mater*, 2001, 13: 1871–1874
- 358 Feng G, Li J, Colberts FJM, Li M, Zhang J, Yang F, Jin Y, Zhang F, Janssen RAJ, Li C, Li W. *J Am Chem Soc*, 2017, 139: 18647–18656
- 359 Feng G, Li J, He Y, Zheng W, Wang J, Li C, Tang Z, Osvet A, Li N, Brabec CJ, Yi Y, Yan H, Li W. *Joule*, 2019, 3: 1765–1781
- 360 Jiang X, Yang J, Karuthedath S, Li J, Lai W, Li C, Xiao C, Ye L, Ma Z, Tang Z, Laquai F, Li W. *Angew Chem Int Ed*, 2020, 59: 21683–21692
- 361 He Y, Heumüller T, Lai W, Feng G, Classen A, Du X, Liu C, Li W, Li N, Brabec CJ. *Adv Energy Mater*, 2019, 9: 1900409
- 362 Duan C, Zhang K, Zhong C, Huang F, Cao Y. *Chem Soc Rev*, 2013, 42: 9071–9104
- 363 Chueh CC, Li CZ, Jen AKY. *Energy Environ Sci*, 2015, 8: 1160–1189
- 364 Hu Z, Ying L, Huang F, Cao Y. *Sci China Chem*, 2017, 60: 571–582
- 365 Roman LS, Mammo W, Petersson LAA, Andersson MR, Inganäs O. *Adv Mater*, 1998, 10: 774–777
- 366 Xia Y, Sun K, Ouyang J. *Adv Mater*, 2012, 24: 2436–2440
- 367 Tang H, Liu Z, Hu Z, Liang Y, Huang F, Cao Y. *Sci China Chem*, 2020, 63: 802–809
- 368 Cui Q, Bazan GC. *Acc Chem Res*, 2018, 51: 202–211
- 369 Xu B, Hou J. *Adv Energy Mater*, 2018, 8: 1800022
- 370 Wang F, Tan Z, Li Y. *Energy Environ Sci*, 2015, 8: 1059–1091
- 371 Zhou Y, Fuentes-Hernandez C, Shim J, Meyer J, Giordano AJ, Li H, Winget P, Papadopoulos T, Cheun H, Kim J, Fenoll M, Dindar A, Haske W, Najafabadi E, Khan TM, Sojoudi H, Barlow S, Graham S, Brédas JL, Marder SR, Kahn A, Kippelen B. *Science*, 2012, 336:

- 327–332
- 372 Ouyang X, Peng R, Ai L, Zhang X, Ge Z. *Nat Photon*, 2015, 9: 520–524
- 373 Xie Z, Würthner F. *Adv Energy Mater*, 2017, 7: 1602573
- 374 Huang F, Wu H, Wang D, Yang W, Cao Y. *Chem Mater*, 2004, 16: 708–716
- 375 He Z, Zhong C, Su S, Xu M, Wu H, Cao Y. *Nat Photon*, 2012, 6: 591–595
- 376 Zhang K, Zhong C, Liu S, Mu C, Li Z, Yan H, Huang F, Cao Y. *ACS Appl Mater Interfaces*, 2014, 6: 10429–10435
- 377 Wang J, Lin K, Zhang K, Jiang XF, Mahmood K, Ying L, Huang F, Cao Y. *Adv Energy Mater*, 2016, 6: 1502563
- 378 Li CZ, Chueh CC, Ding F, Yip HL, Liang PW, Li X, Jen AKY. *Adv Mater*, 2013, 25: 4425–4430
- 379 Schlitz RA, Brunetti FG, Glaudell AM, Miller PL, Brady MA, Takacs CJ, Hawker CJ, Chabiny ML. *Adv Mater*, 2014, 26: 2825–2830
- 380 Wu Z, Sun C, Dong S, Jiang XF, Wu S, Wu H, Yip HL, Huang F, Cao Y. *J Am Chem Soc*, 2016, 138: 2004–2013
- 381 Liu H, Huang L, Cheng X, Hu A, Xu H, Chen L, Chen Y. *ACS Appl Mater Interfaces*, 2017, 9: 1145–1153
- 382 Huang F, Shih PI, Shu CF, Chi Y, Jen AKY. *Adv Mater*, 2009, 21: 361–365
- 383 Xu R, Zhang K, Liu X, Jin Y, Jiang XF, Xu QH, Huang F, Cao Y. *ACS Appl Mater Interfaces*, 2018, 10: 1939–1947
- 384 Tang CG, Syafiqah MN, Koh QM, Zhao C, Zaini J, Seah QJ, Cass MJ, Humphries MJ, Grizzi I, Burroughes JH, Png RQ, Chua LL, Ho PKH. *Nature*, 2019, 573: 519–525
- 385 Sun C, Wu Z, Hu Z, Xiao J, Zhao W, Li HW, Li QY, Tsang SW, Xu YX, Zhang K, Yip HL, Hou J, Huang F, Cao Y. *Energy Environ Sci*, 2017, 10: 1784–1791
- 386 Zhang K, Fan B, Xia R, Liu X, Hu Z, Gu H, Liu S, Yip HL, Ying L, Huang F, Cao Y. *Adv Energy Mater*, 2018, 8: 1703180
- 387 Zhang K, Gao K, Xia R, Wu Z, Sun C, Cao J, Qian L, Li W, Liu S, Huang F, Peng X, Ding L, Yip HL, Cao Y. *Adv Mater*, 2016, 28: 4817–4823
- 388 Liu G, Jia J, Zhang K, Jia X, Yin Q, Zhong W, Li L, Huang F, Cao Y. *Adv Energy Mater*, 2019, 9: 1803657
- 389 Sun C, Wu Z, Yip HL, Zhang H, Jiang XF, Xue Q, Hu Z, Hu Z, Shen Y, Wang M, Huang F, Cao Y. *Adv Energy Mater*, 2016, 6: 1501534
- 390 Chen Z, Hu Z, Wu Z, Liu X, Jin Y, Xiao M, Huang F, Cao Y. *J Mater Chem A*, 2017, 5: 19447–19455
- 391 Hu Z, Xu R, Dong S, Lin K, Liu J, Huang F, Cao Y. *Mater Horiz*, 2017, 4: 88–97
- 392 Hu Z, Chen Z, Zhang K, Zheng N, Xie R, Liu X, Yang X, Huang F, Cao Y. *Sol RRL*, 2017, 1: 1700055
- 393 Yan K, Liu ZX, Li X, Chen J, Chen H, Li CZ. *Org Chem Front*, 2018, 5: 2845–2851
- 394 Wang Z, Li Z, Xu X, Li Y, Li K, Peng Q. *Adv Funct Mater*, 2016, 26: 4643–4652
- 395 Kang Q, Ye L, Xu B, An C, Stuard SJ, Zhang S, Yao H, Ade H, Hou J. *Joule*, 2019, 3: 227–239
- 396 Yao J, Qiu B, Zhang ZG, Xue L, Wang R, Zhang C, Chen S, Zhou Q, Sun C, Yang C, Xiao M, Meng L, Li Y. *Nat Commun*, 2020, 11: 2726
- 397 Cai C, Yao J, Chen L, Yuan Z, Zhang ZG, Hu Y, Zhao X, Zhang Y, Chen Y, Li Y. *Angew Chem Int Ed*, 2021, 60: 19053–19057
- 398 Tang H, Liu Z, Tang Y, Du Z, Liang Y, Hu Z, Zhang K, Huang F, Cao Y. *Giant*, 2021, 6: 100053
- 399 Lu L, Liao Q, Zu Y, Xu Y, Xu B, Hou J. *Adv Energy Mater*, 2019, 9: 1803826
- 400 Zhou H, Zhang Y, Mai CK, Seifert J, Nguyen TQ, Bazan GC, Heeger AJ. *ACS Nano*, 2015, 9: 371–377
- 401 Zeng M, Wang X, Ma R, Zhu W, Li Y, Chen Z, Zhou J, Li W, Liu T, He Z, Yan H, Huang F, Cao Y. *Adv Energy Mater*, 2020, 10: 2000743
- 402 Zeng M, Zhu W, Luo J, Song N, Li Y, Chen Z, Zhang Y, Wang Z, Liang W, Guo B, Zhang K, Huang F, Cao Y. *Sol RRL*, 2021, 5: 2000625